Mechanism Methodology for Structural Health Monitoring of Arch Bridges

BY

CHAD FISCHER
B.S., University of Illinois at Urbana-Champaign, 1999
M.S., University of Illinois at Urbana-Champaign, 2000

THESIS

Submitted as partial fulfillment of the requirements
for the degree of Doctor of Philosophy in Civil Engineering
in the Graduate College of the
University of Illinois at Chicago, 2011

Chicago, Illinois

Defense Committee:

Dr. Farhad Ansari, Chair and Advisor
Dr. Michael McNallan
Dr. Eduard Karpov
Dr. Didem Ozevin
Dr. Aftab Mufti, University of Manitoba, Winnipeg, Manitoba, Canada

This thesis is dedicated to my wife, Lisa, and son, Jake, who provided never ending encouragement of my research. They made numerous sacrifices to allow me the time to complete this work as I spent many hours at the library and in the laboratory. Their motivation and never ending love made this possible.

ACKNOWLEDGEMENTS

I would like to acknowledge Dr. Farhad Ansari for without him, this study and research would not have been possible. His passion for structural health monitoring research was contagious and made this study exciting and successful. Dr. Ansari is a leader in the industry of structural health monitoring. His insights and ideas for monitoring plans and analysis provided a great foundation for developing new ideas.

My thesis committee and fellow researchers provided many hours of their time reviewing my work and helping refining my research focus. Dr. Aftab Mufti, Dr. Michael McNallan, Dr. Eduard Karpov, Dr. Didem Ozevin, and Dr. Ernesto Indocochea all took time from their busy schedules to review my thesis work and encourage future development. Fellow researcher, Iman Talebinejad, was an invaluable resource and friend during all of our field monitoring and laboratory testing. Asad Bassam, Amir Iranmanish, and Ali Zarafshan also spent countless hours listening to ideas and assisting with laboratory test setups.

Also, I would like to recognize the New York City Department of Transportation and in particular, the work of Dr. Bojidar Yanev and Kevin McAnulty. Dr. Sreenivas Alampalli of the State of New York Department of Transportation was also instrumental in making this study a success. Dr. Yanev and Dr. Allampalli have a great vision toward bridge

management and maintenance. They have an eye toward the future of bridge maintenance and inspection.

Finally, I would also like to acknowledge Engineering Systems Inc. for their support and freedom in allowing me to complete this work. Dr. August Domel and Dr. Daniel Wojnowski were instrumental in assisting with the resources needed for my PhD work.

CRF

TABLE OF CONTENTS

LIST OF TABLES

TABLE PAGE

LIST OF FIGURES

FIGURE PAGE

SUMMARY

There are numerous in-service masonry arch bridges across Europe, India, and North America. As these bridges age and deteriorate, it is important to be able to safely evaluate them for the allowable loads that they can support. Structural health monitoring systems using fiber optic sensors are valuable tools that can provide real-time feedback about the movement and performance of the arch structures under railway and traffic loads. Sensors can measure parameters such as crack opening displacements, bridge deflections, support movements, thermal fluctuations, and vibrations. However, monitoring systems are only successful if there is proven baseline against which to compare the measured data.

Many theories and methodologies have been previously developed to calculate the ultimate strength, or load carrying capacity of masonry arch bridges. However, none of these analysis methods were able to provide estimates of real-time bridge performance under service loading conditions. In order to address these concerns, a new methodology for analyzing masonry arches is proposed using a combination of rigid block analysis and finite element modeling. There is a need for simplified methods for rapid analysis of masonry arches using generic finite element programs. Such methods provide the opportunity for interpretation of data from structural health monitoring systems. To fill this gap, a methodology has been proposed in this dissertation for accurate, yet simple analysis of masonry arches.

The proposed methodology was validated with a series of scaled masonry arch tests in the laboratory. It was then implemented to understand data from a structural health monitoring system installed on the masonry approach arches of the Brooklyn Bridge.

1. INTRODUCTION

The ultimate question that the owner of any bridge wants to know is how much weight can my bridge support. This can be a sophisticated question to answer for any bridge engineer due to the complexity of structural interactions with the numerous structural components, the foundations and various materials. The types of loading the bridge may experiences and the amount of traffic also has an effect on the answer to this question along with environmental factors and deterioration considerations. In the case of masonry arch brides, this question is further complicated since the material is an orthotropic combination of bricks and mortar. Moreover, in comparison to other structural materials, masonry arch bridges do not behave in a linear elastic manner.

Since the 1600s, researchers and engineers have studied masonry arches and have attempted to answer the question of how much weight can the bridge hold. Several influential theories have been developed which come from a variety of theoretical backgrounds. Some were developed from lines of thrust and pressure, and then elastic calculations. More recently, the focus has been more on plastic or mechanism based methods.

Much of the recent research and analysis techniques for masonry arches have added numerical complexity, very detailed parameters, and sophisticated computational

methods that at the end do not add any significant accuracy. Additionally, these analyses techniques are of little help to the engineer trying to interpret the output of sensor data from a structural health monitoring setup.

Sensor and computer advances have now made it more practical in recent years to instrument a bridge and study its behavior over time. The performance of the bridge can be continuously monitored in real time under service load conditions. Structural health monitoring of this type can provide invaluable data for determining the ultimate load capacity of the bridge while monitoring for deteriorating conditions and changes in the structural performance. However, a numerical model of the bridge is needed to estimate real-time service load deflections and crack openings so that the monitoring data can be compared against a predicted benchmark.

Currently, all of the state-of-the-art masonry arch assessment methods only predict the ultimate load capacity of an arch bridge and do not provide any information regarding the expected deflections and crack opening displacement of the bridge. In addition, most of the existing assessment methods require time consuming programming and analysis or the purchase of costly software programs.

The study enumerated in this dissertation pertains to the development of a novel numerical methodology in order to assist engineers in understanding and interpreting

the results from a masonry arch structural health monitoring (SHM) program. At the same time, the methodology provides an easy to use method for calculating the ultimate load capacity of a masonry arch of any geometric shape, with any loading conditions, and with varying amounts of support settlements. The method does not require sophisticated numerical algorithms and can be employed by implementing this approach with any off-the-shelf finite element software program.

1.1. Motivation for Research

The Brooklyn Bridge is one of the iconic bridge structures in the United States. Constructed between 1880 and 1887, the bridge is still in use today. The Brooklyn Bridge was the concept of John A. Roebling. Roebling was a renowned bridge builder in the United States and had already constructed a number of significant bridge structures such as those at Cincinnati, Niagara Falls, and Waco, Texas. At the time, the only method of passage between Brooklyn and New York City was across the East River via ferry or other boats. Travel during the winter months became difficult to nearly impossible as sections of the East River would freeze over. This challenged commerce and business relationships between the two cities. Roebling envisioned a monumental bridge to span the East River. His plan included roadways for horse carriage and pedestrian use along with a center railroad track.

Roebling initially designed the bridge and began to secure financing for the project. However, during the early stages of the project, he was injured during surveying of the bridge which eventually led to his death shortly thereafter. His son, Washington Roebling, took over construction of the bridge and saw it through to completion. Needless to say, Washington Roebling faced his own challenges as he was struck with caissons disease and confined to his house during much of the project.

The Brooklyn Bridge is known for a number of its unique structural characteristics. The bridge is a hybrid cable stay and suspension bridge with deep truss girders. The two main stone towers are supported on deep caissons. The caisson themselves were a unique project as they had to be excavated by hand to depths of over 45'. The men excavating the caissons worked in a chamber filled with compressed air in order to keep the river water out. This led to cases of nitrogen poisoning more commonly known as caisson's disease the "bends".

The key elements of the monumental bridge span tend to overshadow other impressive elements of the bridge construction at the approach ramps. In order to meet the high clearance requirements of the bridge over the East River to allow for passage of large ships underneath, long approach spans were constructed at both the Brooklyn and New York ends of the bridge. In fact, the approach span at the New York side is 1562' long which is nearly as long as the main 1595' span over the river (Figure 1). The approach

spans were constructed of masonry arches of increasing height and span as they approach the river (Figure 2 Figure 3). The arch spans allowed for traffic to pass beneath the approach ramp and also to provide a usable space for shops and markets underneath the bridge.

Construction of the Brooklyn Bridge was instrumental in merging Brooklyn and New York and ultimately led them combining into one city. The bridge is still of significant need to the city. Due to continued maintenance and regular inspections over the years, the Brooklyn Bridge and approach spans have been kept in good working condition and continuous service. Occasional maintenance and repairs are made to the structure, but very few significant structural repairs have been needed.

The use of the bridge has changed over the years. The bridge no longer is used as a railway, but it is used for vehicular traffic and pedestrian use. Nonetheless, it is still a major corridor and access route between Brooklyn and Manhattan Island. The bridge condition has been regularly monitored primarily through visual inspection similar to other transportation structures in the United States.

During recent visual inspections of the bridge, large longitudinal cracks were observed at the crowns of two brick arch spans. These cracks were observed in Arch Spans 3 and 4 on the Manhattan side of the bridge (Figure 4). Spans 3 and 4 are the longest of

masonry arches in the approach ramps. They are located adjacent to the anchorage assembly at the Manhattan abutment. Arch Span 3 has a span of 36 feet. Arch Span 4 has a span of 32 feet but has a skew and tapers down to a span of 20 feet at the north end. Both of the arches are semi-circular in cross section.

As noted, the longitudinal cracks were located at the underside of the arch at the peak. They were continuous along the length of the entire arch width for both spans. Spray paint markings noted their existence at least since 1996. Recent bridge inspection reports also noted their existence. Other than documenting their presence in inspection reports and with photographs, it was difficult to monitor if they were actively moving or widening. At one point, nails had been installed at the opposing sides of the cracks in order to take measurements of the crack width. However, it was difficult to access the top of the arches so measurements could only be taken at select times and such measurements could not be correlated to cracks and movements at other parts of the structure. In addition to the longitudinal cracks at the top of the arch, there were vertical cracks throughout the walls and foundation of the approach structure. These cracks were indicative of past differential soil settlements.

A major bridge retrofit plan was developed and designed for the Brooklyn Bridge. This included grouting and reinforcement repairs to the cracks of the two subject approach spans. However, due to funding and planning reasons, these repairs were not scheduled

to be undertaken for several years. In order to insure the safety and operation of the bridge, the New York City Department of Transportation decided to monitor the cracks in real time until such repairs could be made.

Figure 1. Satellite view of lower Manhattan and Brooklyn. Brooklyn Bridge main span in red and Manhattan approach spans in yellow (from Google Earth).

Figure 2. Brooklyn Bridge looking south, area of investigation highlighted (from Google Earth)

Figure 3. Brooklyn Bridge looking north, area of investigation highlighted (from Google Earth).

Figure 4. South elevation of Brooklyn Bridge masonry arch approach spans.

1.2. Structural Health Monitoring

Field testing of bridges is not a new activity. In fact, bridges have been load tested for centuries (Mufti 1996). There are several different categories of bridge tests. The most commonly known test is the ultimate load test. Essentially, the bridge is cumulatively loaded until it fails. While a great deal of information can be learned from such tests, the bridge is obviously no longer usable afterwards. Proof tests are similar to an ultimate load test in which case the bridge is cumulatively loaded but only to a point for confirmation of a previously estimated load carrying capacity. Behavior and diagnostic load tests are carried out at lower stress levels to investigate certain methods of analysis or the interaction of different components of the bridge structure (Mufti 1996). Such loads tests have provided invaluable information about how bridges react to specific sets of loads and have increased our knowledge of design equations and analysis methods.

Structural health monitoring (SHM) is the application of using sensors and computer equipment to monitor the performance and condition of a structure over its life. While the sensors of a SHM system may be used during a load test of the bridge, structural health monitoring typically refers to monitoring a bridge over a portion of its life under normal daily service loads. In contrast to bridge load tests, the intent of a SHM program is to understand how the structure behaves and reacts with the environment and

applied loadings in real time over its lifespan and also to detect and predict any significant damage to the structure. Also, SHM programs are conducted without disruption to traffic flow.

SHM has been studied rigorously over the last 20 years. Within the last decade, the cost of sensors and advancement in computing technologies has made SHM of large scale bridge structures economically feasible. SHM systems can be installed on bridge structures and monitored remotely over wireless and cellular networks. Real time updates of a structure's condition can be reviewed on remote computers in an engineer's office and critical updates and condition assessments can be sent immediately to mobile cell phones and tablets.

SHM plans can be implemented in two ways; at a global or local level. Global SHM includes monitoring the overall structure. By detecting changes in the movements, natural frequencies, or mode shapes of the structure, the presence of damage can be identified and ideally the approximate location of the damage can determined. Sensors used for global SHM include accelerometers, strain gauges, and tiltmeters.

Local SHM consists of monitoring individual or localized components of a bridge. Such individualized components could include individual bolts or structural members. It could also include focusing on an existing crack or area of deterioration. Yet another

example of local SHM would be focusing sensors on a particular bridge bearing or support. Sensors used for local SHM include strain gauges, displacement sensors, and tiltmeters.

Past studies of techniques using global SHM has shown some promise and success. However, a better overall bridge maintenance performance can be had by integrating a local SHM plan with a global SHM plan. Such an integrated plan combines the benefits of each and provides the bridge owner with better data.

In order to monitor the cracks for the approach spans in the Brooklyn Bridge, a combined global and local SHM plan was developed. The global plan focused on the overall performance and movement of the approach structure. The global plan also monitored how the approach structure reacted with and was affected by the adjacent bridge anchorage to the east and steel roadway truss to the west. The local plan concentrated monitoring efforts on the already known cracks. It monitored how much the cracks moved in real time. Temperature measurements and roadway vibration measurements supplemented the data for both the global and the local monitoring parts of the plan.

1.3. History of Masonry Arch Design and Construction

Masonry arches have been constructed for many centuries. They were found to be an economical method of constructing long spans with the construction materials available at the time. Additionally, masonry arches were considered to be a pleasing architectural form. Today, many masonry arch bridges are still in use today for both highway and railway bridges. Reports have noted approximately 1,000 in service arch bridges in the United States (Boothby 1995). Numerous more masonry arch bridges are still in use in England for highway and railway passage. Historical arch bridge construction is also very prevalent in India, while numerous other masonry arch bridges are being used throughout other countries in Europe, the Americas, and Asia. Also, a new masonry arch bridge will be occasionally constructed today because of historical or architectural reasons. These new arch bridges are based on similar construction methods and materials as older masonry bridges and continue to add to the number of in service arch bridges.

The structural theory of masonry arch bridges has been studied for centuries. The analysis and published techniques have ranged from work by Hooke in the late 1600s and Castigliano in the 1870s to Pippard (1930s) and Heyman (1970s) in more recent times. The initial theories were based on assumptions of elastic stress analysis and later

derived into plastic and mechanism based methods. One of the earliest forms of arch analysis, thrust line analysis, is still used as a major stay of arch bridge analysis today.

1.4. Statement of Need and Importance

Historically, many of the analysis theories and equations for masonry arches have made the assumption that the supports, or abutments, of the arch do not translate or rotate. This assumption accompanies other such assumptions that the masonry has no tensile strength or that the individual voussoirs do not slip in relation to one anther. These assumptions are typically needed in order to make the equations solvable and limit the number of unknowns.

For a newly constructed arch, the assumption that the supports do not translate or rotate may be a reasonable one. It would be assumed that the soil supporting the abutment would be properly graded and compacted. The abutment should be large enough to distribute the load over a wider area of soil to minimize settlement and the masonry of the arch should be in generally sound condition. However, as is the case with many older arch bridges, the abutments will settle and rotate over time. This may be due to soil issues such as long term soil settlement, scour, and changes in the water table. The movement of the abutment could also have been caused by structural issues such as thrust changes from bridge overloads, axial force changes from cyclical

temperature cycles, deterioration of the abutment, and thrust changes from unequal arch spans on multi-span bridges.

Translational and rotational movements of the abutments typically occur slowly over a period of time and are not sudden movements. Because of the long term nature of the movements, they are difficult to measure and quantify. It has been acknowledged through visual bridge inspections that foundation settlements and movements can be a cause of arch cracking and bridge distress, but in the past it has never been possible to accurately quantify the amount of foundation movement. In the recent past, it may have been possible to obtain some rough measurements of long term foundation movements with laser survey equipment, but even this type of monitoring introduces a large potential for measurement error over time.

Recent advances in structural health monitoring systems and fiber optic sensors now make it possible to record changes due to the movements of arch bridge abutments over long periods of time. Monitoring and recording the amount of movement is an important step in understanding the effects of support movement on the condition, lifespan and load capacity of the arch. However, when monitoring the movements of an abutment, it is important to have an analytical model to understand and estimate the safe limits of movement. Such an analytical model should be able to provide accurate estimate of load capacity and real time deflections without requiring extensive

computational time. In summary, the analytical model to accompany a SHM test plan for masonry arches should be able to provide estimated deflections and crack openings under service load conditions.

To date, there has been no such analytical model or equation based approach for determining the real-time effects of abutment movement on the performance of arch bridges. The analytical models to date only provide the output of the maximum load capacity of the arch and the estimated hinge locations at failure.

One of the most widespread masonry arch analysis methods in use today is the MEXE method. The method was developed during WWII to analyze arch bridges to determine their adequacy for supporting heavy tank loads. It is based on a two-hinge elastic arch model. The method has provided reasonable results for a typical subset of bridges. The output from the MEXE method is a single allowable load value for the bridge. In order to handle the effects of support movement, the allowable bridge load, is divided by a factor of 1.2 or 1.4 depending on the severity of the support movement. Little guidance is given as to what qualifies as severe support movement and this method is of little help to the engineer evaluating the bridge for movement and cracking under service loads.

The traditional elastic based hand calculation methods of Castigliano and the adapted three-hinged arch models allow for some calculation of the effects of support movement.

The downfalls of such methods are that they are iterative and time consuming methods and they require a comprehensive understanding of the subject of arch bridges or a specially written computer program. Other downfalls are that they make assumptions that are not always realistic in a service load situation. Again, these methods do not provide a real time analysis of what can be expected of the structure as it experiences support movement.

Within the last 30 years, the focus of masonry arch analysis has been on rigid block analysis; otherwise know as limit state methods. These methods have furthered the analysis capabilities for masonry arch bridges and some of them have been developed into sophisticated software programs such as Ring 2.0. However, none of the methodologies to date have much capacity to handle the issue of support movement. Block and Ochsendorf are some of the few researchers to address the issue of support movement (Block 2006 and Ochsendorf 2006). Their analysis and research has focused on the collapse of cathedral and building arches due to support movements. However, like so many of the other analysis methods, these methods are based on the ultimate collapse limits from support movement. For example, results of his semi-circular arch analysis show the collapse state to occur only at a support movement of over 15% of the arch span length. For a 30 foot arch span, this translates to a support translation of over 4 feet. While it is true, that the arch may be able to withstand this much support movement before collapsing under its own weight, there are many service and

maintenance concerns for a bridge that undergoes this much deformation. Also, this analysis requires individualized computer programming and cannot be easily adapted to various sizes and shapes of arch structures or changing vehicle loads.

1.5. Thesis Statement

Arch structures are structurally stable only when they have a horizontal support to restrain them. These horizontal supports are typically a concrete or masonry abutment which distributes the thrust load from the arch into the supporting soil. Ideally, these abutments are designed to be completely rigid and do not allow for any movement. However, in practice, effects such as differential settlement, tall and slender abutments, soil erosion, scour, poor soil conditions, and temperature changes, can cause the abutments to spread over time. As the abutments spread, the performance of the arch and its ability to safely carry loads is diminished.

Understanding the effects of abutment spread is important to the understanding of overall masonry arch strength and performance. However, only brief attention has been given to the calculation of abutment spread and its effects on the performance of masonry arches.

In order to address the above concerns and analysis needs, a new methodology is proposed using a combination of rigid block analysis and finite element modeling. The

method, which can be used to analyze masonry arch bridges in nearly any finite element code, will allow the user a real-time understanding of masonry arch deflections and movements under service loads. This will be an invaluable tool for interpreting the results from a structural health monitoring program.

From construction to failure, a masonry arch goes through a number of steps. The failure method is not simply that the material is overstressed and then yields or buckles as it approaches failure. Instead, masonry arches develop areas of high stresses and as a result develop hinge points. These hinge points can open and close and even change locations depending on the variability of moving loads and temperature changes over time. Typically arches are considered stable until a fourth hinge develops. A formulation is proposed in this dissertation that gives a more complete understanding of horizontal arch spread. By combining fixed arch analysis methods with one, two, and three hinges arch methods, a more universal formulation can be developed.

As a validation to this modeling, the method will be compared to the lateral support movement test results obtained at the UIC lab. For further comparison, the method will be used to model historical load tests of actual bridges from the literature. The results will show good confirmation with the proposed analytical model. As a final case study of the analytical model, it will be applied to the structural health monitoring program completed to the masonry arch bridge spans of the Brooklyn Bridge.

2. BACKGROUND AND LITERATURE REVIEW

2.1. Structural Life of a Masonry Arch

A masonry arch is initially constructed and a hingeless structure with fixed support conditions. As it is loaded and subjected to outside forces, cracks form in the masonry cross section creating hinge points in the structure.

2.1.1. Hingeless Arch

Most 19th century masonry arches were constructed with the intent that they were going to be a fixed-fixed or hingeless arch. However, in reality, it has been seen that few arches actually behave in this manner.

In order for arch to remain without hinges, the thrust line must never touch the exterior limits of the arch. Furthermore, in order to prevent any cracking in the arch and insure that the arch is fully in compression, the thrust line at all point must remain within the center 1/3 of the arch for all loading conditions (Figure 5).

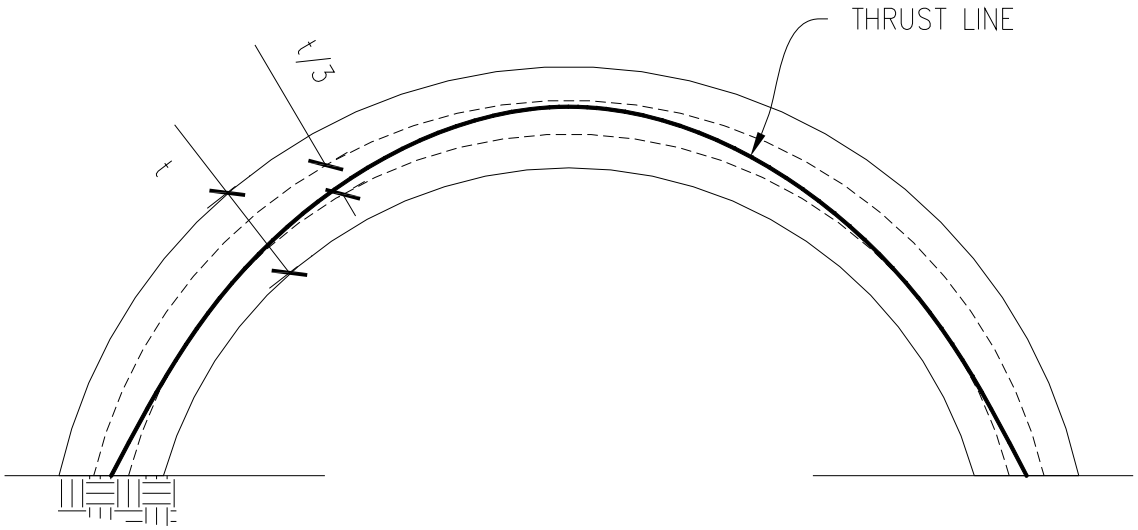

Figure 5. Hingeless arch with thrust line shown within the limits of the middle third cross section.

2.1.2. Two Hinge Arch

A two-hinge arch is typically assumed to have hinge points at the two support abutments (Figure 6). In the case of a semi-circular hinge, these points may occur slightly higher up the arch. A two-hinged arch is one-degree statically indeterminate.

As will be discussed later, studies by Pippard found that any slight movement of the abutment will cause the two hinges at the supports to occur. This hinge formation typically even occurs when the centering is removed after the arch construction.

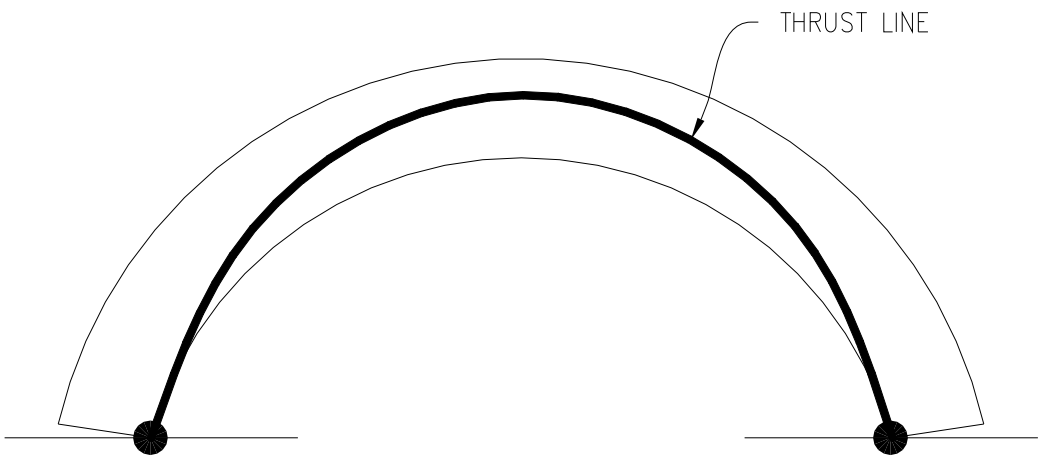

Figure 6. Two hinged arch with hinges at supports.

2.1.3. Three Hinge Arch

A three hinge arch is a well know structural form. It is normally studied in structural analysis curriculum and is statically determinate.

As discussed earlier, a masonry arch typically takes the form of a two-hinged arch shortly after construction when the centering has been removed. Any length increase due to a temperature increase or support spread causes a significant increase in the bending stress at the peak of the arch. This will quickly cause an overstress in the masonry material which has a very low tensile strength. For a uniformly loaded arch, a third hinge will form at the crown of the arch. Once the third hinge forms, the structure becomes statically determinate (Figure 7).

The horizontal and vertical reactions for the statically determinate three-hinged arch can be determined from a series of four equations and four unknowns (Equations (1)-(4)). Figure 8 Figure 9 pertain to the nomenclature used in the equations. At that point, the moment and thrust equations of equilibrium can be applied at the hinges and subsequently at any point along the arch. A unique thrust line can be drawn for the three hinged arch since it must pass through all three hinges.

At the time of the third hinge formation, additional support movements do not significantly change the thrust or vertical reactions of the arch. However, as the support movements begin to exceed a certain amount, the thrust line changes due to the changes of the arch geometry. The addition of a vertical point load on the arch can also change the three hinge arch behavior. At this point, either the hinge will move from the crown or an additional hinge will form.

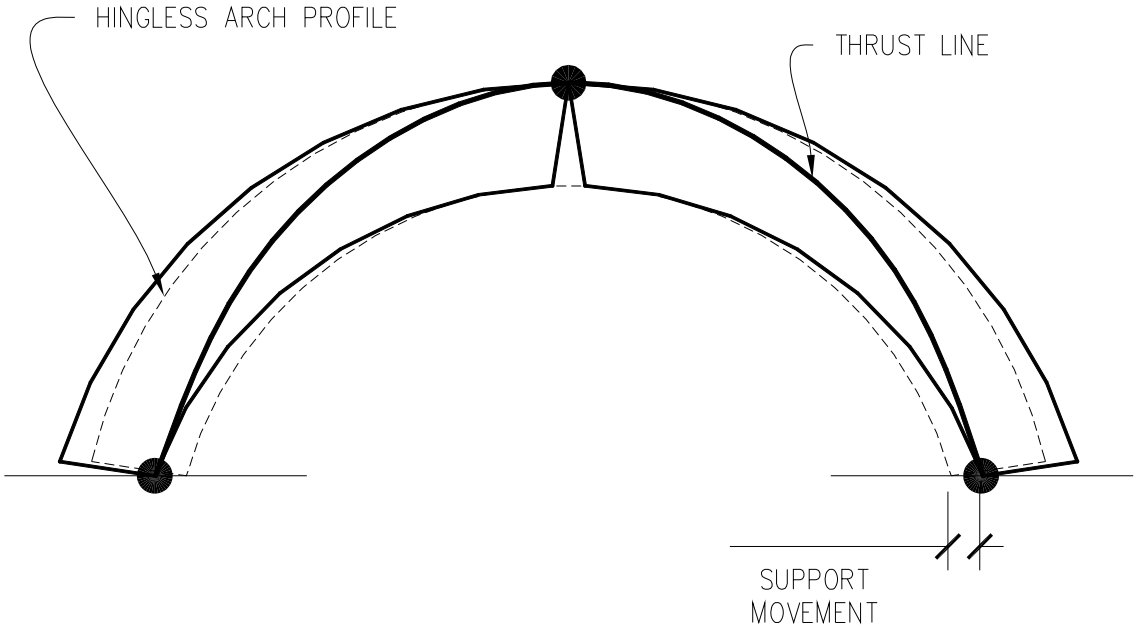

Figure 7. Three-hinged arch with support movement.

$$\begin{aligned} &\sum F_x = 0 \\ &H_A - H_B = 0 \\ &H_A = H_B \end{aligned} \tag{1}$$

$$\begin{aligned} &\sum F_y = 0 \\ &V_A + V_B - P - w \cdot L = 0 \\ &V_A = P + w \cdot L - V_B \end{aligned} \tag{2}$$

$$\begin{aligned} &\sum M_A = 0 \\ &-P \cdot x - w \cdot L \cdot \frac{L}{2} + V_B \cdot L = 0 \\ &V_B = \frac{P \cdot x}{L} + \frac{w \cdot L}{2} \\ &V_A = P \cdot (1 - \frac{x}{L}) + \frac{w \cdot L}{2} \end{aligned} \tag{3}$$

$$\sum M_C = 0$$

$$P \cdot (X_{hinge} - x) + w \cdot \left(\frac{X_{hinge}}{L} \right) \cdot \left(\frac{X_{hinge}}{2} \right) + H_A \cdot Z_{hinge} - V_A \cdot X_{hinge} = 0 \qquad (4)$$

$$H_A = P \cdot x \cdot \left(\frac{1 - \frac{X_{hinge}}{L}}{Z_{hinge}} \right) + \frac{w \cdot X_{hinge}}{2 \cdot L \cdot Z_{hinge}} \cdot (X_{hinge} - L)$$

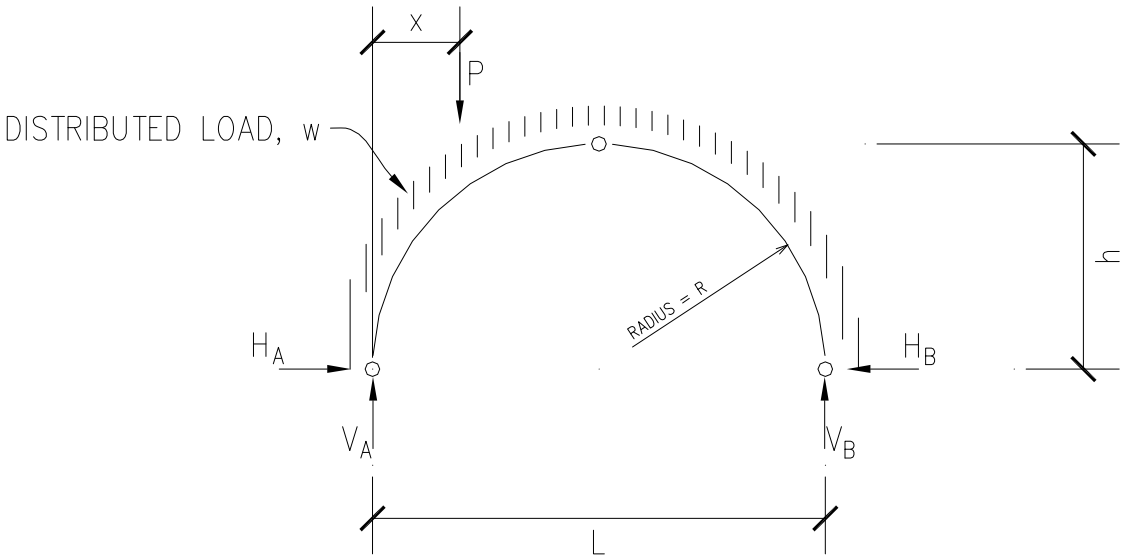

Figure 8. Nomenclature for three hinge arch analysis.

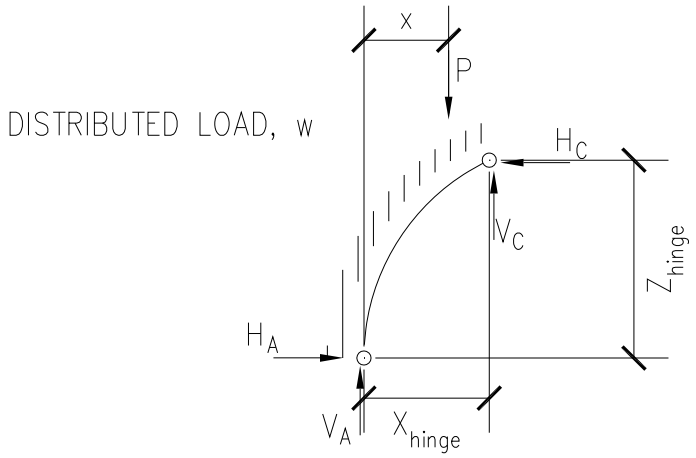

Figure 9. Free body diagram for three hinge arch analysis.

2.2. Masonry Arch Analysis - Pre 1900

2.2.1. Rule of Thumb Design equations

Several engineers and builders published on rules of thumb methods for determining the thickness of masonry arches. Many of these were based off of historical studies of existing bridges that withstood the test of time while others had some limited background analysis as the premise for their output. One of the more popular empirical design equations proposed by Rankine in 1877 (Corradi 1996) follows:

$$\begin{aligned} d &= 0.19\sqrt{R} \text{ for single span bridges} \\ d &= 0.26\sqrt{R} \text{ for multi-span bridges} \end{aligned} \tag{5}$$

where,

d = barrel thickness

R = segmental arch radius

Other published equations of the time were similar in that they were based on ratios between the radius of the arch and the thickness of the arch barrel. As can be seen from the Rankine equation, the empirical equation used the arch shape as input for the design and does not take into account the arch loadings. While this may have been relevant at the time of their development, serious concerns exist for using such equation to evaluate existing bridge structures which may be subjected to heavier traffic loads or railway loads. However, they are none the less a good starting point for evaluating an older arch bridge and understanding the historical basis for their design.

2.2.2. Navier 1826

Navier had demonstrated that for linear elastic arch structures in which plane sections remained plane, tension could be avoided by ensuring that the thrust line lay within the middle third of the section (ICE 2008). However, it was shown later that this led to very over conservative arch designs.

2.2.3. Castigliano 1879

Castigliano applied the theories of strain energy to masonry arch analysis. The underlying premise for this model is a two-hinged elastic arch.

The forces of a two hinged arch may be solved using Castigliano's theorem which shows that the partial derivative of the strain energy, U, with respect to force is equal to the displacement in the direction of the force. The strain energy is made up of three components:

$$U = U_B + U_T + U_S \tag{6}$$

where,

U_B = strain energy due to bending = $\int_A^B (M^2 ds) / 2EI$

U_T = strain energy due to axial thrust = $\int_A^B (T^2 ds) / 2AE$

U_S = strain energy due to shearing force $\int_A^B (S^2 ds) / 2GA$

For most arch rib analyses it is acceptable to ignore the components of axial thrust and shearing force. The partial derivative of the bending strain energy to force yields the following:

$$\frac{dU}{dH} = \int_A^B M \frac{dM}{dH} \frac{ds}{EI} \tag{7}$$

where,

U = strain energy

H = horiztonal reaction at the abutment

M = total bending moment at x

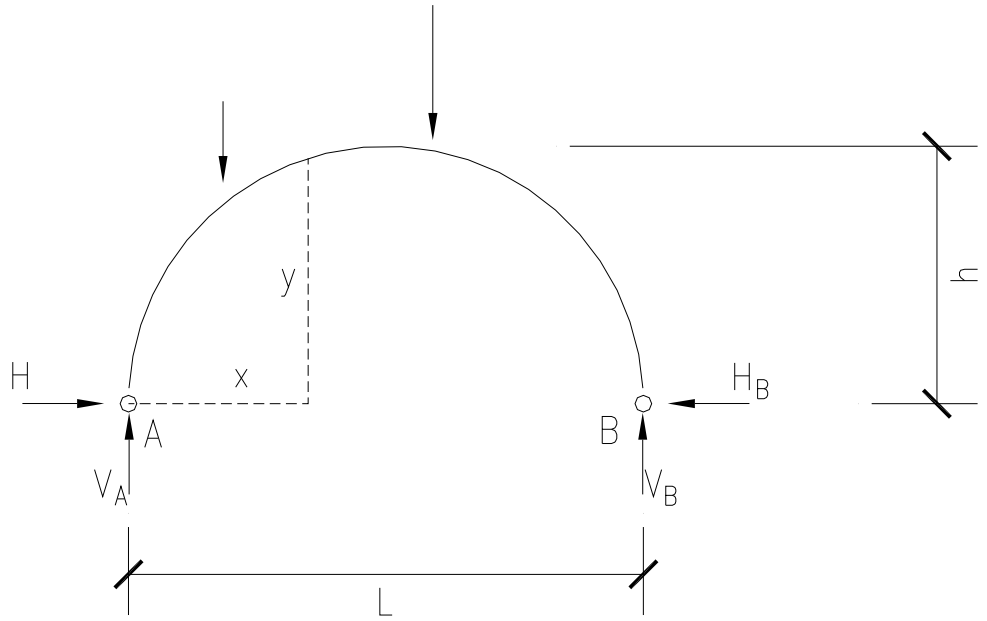

Figure 10. Castigliano arch diagram.

When the case of no support movement as shown in Figure 10 is considered, $dU / dH = \delta_H = 0$. The bending moment in a generic arch may be considered as the sum of that arising from two loading cases:

a) externally applied loading with the arch on a roller at one of the supports, and
b) the arch with a roller at the same support and an unknown horizontal thrust applied to the roller.

The total bending moment at x is then given by,

$$M = M_s - Hy \tag{8}$$

where M_s is the statically determinate bending moment and therefore, $\frac{dM}{dH} = -y$ and:

$$\int_A^B (M_s - Hy)(-y)\frac{ds}{EI} = 0 \tag{9}$$

which leads to:

$$H = \frac{\int_A^B M_s y \frac{ds}{EI}}{\int_A^B y^2 \frac{ds}{EI}} \tag{10}$$

Spreadsheet based computer programs (Hughes 2002) have utilized the Castigliano approach. The programs calculate the position of the thrust line. At any point where the thrust line lies outside of the middle third of the section, the tension zone is removed and the arch re-analyzed. The arch is iteratively analyzed until there are no longer any tension sections left.

2.2.4. Brooklyn Bridge

Francis Collingwood, one of the on-site engineers during construction of the Brooklyn Bridge, noted that a careful analysis of the masonry arches was made for the Brooklyn Bridge construction. He reported that analyses were performed by calculating the arch thrust lines (Collingwood 1876). The analyses were made under the various conditions of load in which they would be subjected. The intent was to keep the line of pressure within the center one-third of the thickness. Other than this limited information, the only other known design details for the masonry arches of Brooklyn Bridge are those which are found in the original project drawings (NYC Dept. of Records 1867)

2.3. Masonry Arch Analysis - Post 1900

The following is a review of some of the prominent arch analysis research approaches and analysis techniques developed for masonry arches during the 20th century.

2.3.1. Pippard Elastic Analysis

The background for Pippard's analysis was based on a series of scale model load tests which he ran to understand the failure mechanisms of arches and explain his elastic analysis. The generally accepted procedure at the time made the following assumptions:

- Mortar joints are very weak in tension
- Necessary to confine the thrust line to the middle-third of the arch to ensure compressive stresses only are present

Pippard observed that larger eccentricities led to a development of a plastic hinge. His experiments also revealed that the initial settlement of the supports create hinges at or near the supports (Boothby 2001). Thus, he concluded that a starting point for arch analysis should be a two-hinge model. Pippard's analysis of the two hinged arch was solved by Castigliano's theorem by choosing the horizontal thrust as the redundant quantity.

The bridge considered by Pippard is shown in Figure 11 and the nomenclature for his analysis is shown in Figure 12. Pippard used the horizontal thrust equation from Castigliano's stain energy derivation as the starting point for his analysis (Equation (11).

$$H = \frac{\int_A^B M_s y \frac{ds}{EI}}{\int_A^B y^2 \frac{ds}{EI}} \tag{11}$$

From this point, he made a series of assumption in order to simplify the analysis (Pippard 1948 and summarized by Wang 2010):

1. The arch is assumed to be parabolic, with a span-to-rise ratio of 4 and with a secant variation in second moment of area, namely $I = I_0 \sec\alpha$
2. The arch is assumed to be pinned at the abutments, i.e. two-hinged arch.
3. The dispersal of loading applied at the surface of the fill was assumed to occur only in the transverse direction with a 45° load spread angle. Because this is least at the crown, Pippard considered the case of a single point load applied at the mid-span, with strength assessments being made at the crown.
4. The effective width of the arch was taken as twice the fill thickness at the crown, $b = 2h$
5. The fill was assumed to have no structural strength and to only impose vertical loads on the arch. The fill was assumed to be of the same density as the arch ring, which was 125 lb/ft^3.

6. The limiting compressive stress was taken to be f_c = 200 psi and the limiting tensile stress was taken to be f_t = 100 psi.
7. It was assumed, for arches of standard width with standard fill depth, that two wheel loads could exist side by side corresponding to an axle loading.

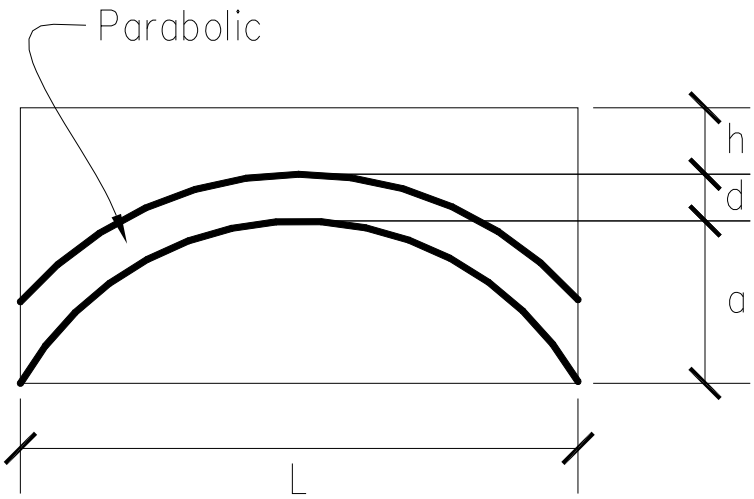

Figure 11. Bridge considered by Pippard, where *h* = fill thickness at crown and *d* = arch barrel thickness at crown.

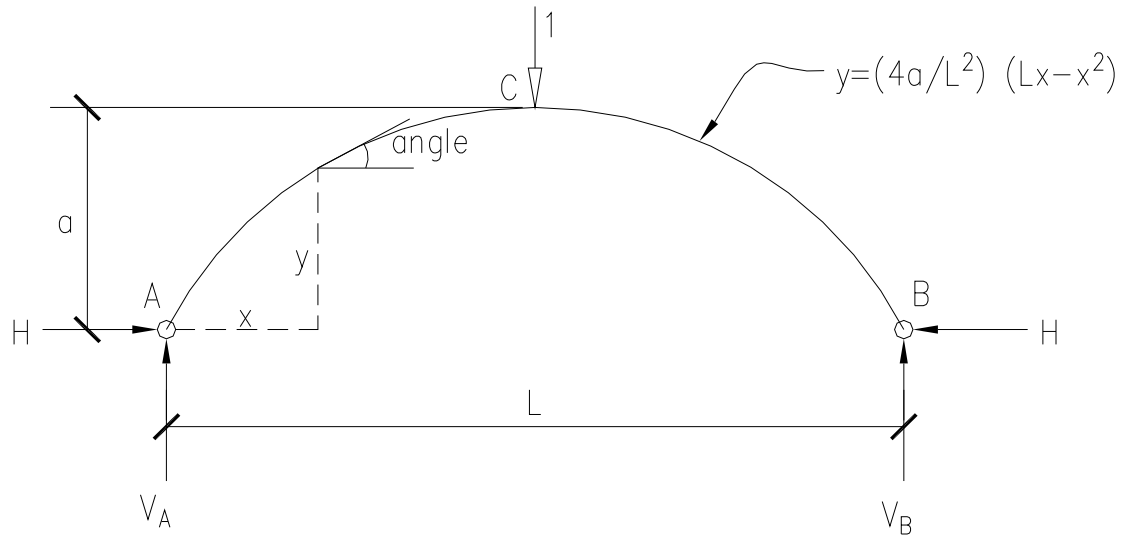

Figure 12. Nomenclature for Pippard analysis.

With a unit load at the crown of the arch as shown in Figure 12, Equation (11) can be solved for the horizontal thrust and bending moment at the crown; Equations (12) and (13) , respectively. At this point, the axial and bending stresses at any other location along the statically indeterminate arch can be calculated.

$$H_L = \frac{25}{128}\frac{L}{a} \tag{12}$$

$$M_L = \frac{7}{128}L \tag{13}$$

When the combined dead and live load stresses in the arch are compared to the maximum permitted compressive stress, the maximum point load at the crown can be solved for. This yields the following equation (Figure 12):

$$W_A = 2W = 2\left[\frac{\frac{256 f_c hd}{L} - 128\rho Lh\left(\frac{1}{21} + \frac{h+d}{4a} - \frac{a}{28d}\right)}{\left(\frac{25}{a} + \frac{42}{d}\right)}\right] \qquad (14)$$

where $\rho =$ density of masonry and fill. See Wang and Melbourne (Wang 2010) for full derivation of Equation (14).

Pippard's work also noted that as a concentrated point load is increased, the thrust line will reach the edge of the voussoir indicating the formation of the third hinge. At this point, the arch becomes statically determinate.

Pippard was the first to explain that structures can support loads producing large eccentricities of thrust. This was a deviation from the previous complete reliance on elastic analysis (Pippard 1936, Boothby 2001). He explained the behavior of an arch in regards to the formation of the hinges as the loads increased and progressed. However, Pippard's load analyses were based on elastic methods and he never fully expanded his observations on the hinge formations as a mechanism based failure analysis.

Pippard's elastic analysis work would later be used as the computational basis for the MEXE method.

2.3.2. MEXE (Military Engineering Experimental Establishment) Method

This method was based on the two-hinged elastic analysis work by Pippard that was then calibrated with both field and laboratory tests from the 1930s. The method was most predominately used in World War II as a way to quickly classify the load carrying capacity of older masonry arch bridges. However, since that time, the MEXE method has still been used as a way to load rate masonry arch bridges. Recently, some concerns have been raised over the accuracy of the load rating for short span bridges (ICE 2008).

The method comprises of the primary calculation of:

$$PAL = 740(d + h)^2 / L^{1.3} \quad (15)$$

where,

$PAL =$ provisional axle load, metric tonnes

$L =$ span, m

$d =$ thickness of arch barrel adjacent to the keystone, m

$h =$ average depth of fill at the quarter points of the transverse road profile, between the road surface and the arch barrel at the crown, including road surfacing, m

as applicable for bridges with the following dimensions:

1.5 m (4.9 ft) < L < 18 m (60 ft), and

0.25 m (0.8 ft) < d < 1.8 m (5.9 ft)

Once the PAL has been calculated, it should be modified by a number of various load factors as presented by the method. Such factors include modifications for the effects of:

- Arch profile (semi-circular, elliptical, parabolic, other)

- Material (masonry type and condition of barrel and backfill)
- Joint (condition and size of mortar joints)
- Condition of arch (existence of longitudinal, transverse, and diagonal cracks)

Upon evaluation of these factors, the PAL is to be modified per the following equation:

$$MAL = F_{sr}F_pF_mF_jF_{cm}(PAL) \quad (16)$$

where,

MAL = modified axle load (metric tonnes)

F_{sr} = span/rise factor

F_p = profile factor

F_m = material factor

F_j = joint factor

F_{cm} = condition factor

Explanation of each of these factors can be found in many references (ICE 2008).

The MEXE method is based on the assumption that the arch is supported on stable abutments. Other sources had suggested factors of 0.9 and 0.8 if the bridge is supported on one or two piers, respectively, instead of abutments.

As can be seen from the above formulations, the MEXE calculation is very user friendly, but does not allow for many inputs to be changed. Also, arbitrary assumptions must be made about the condition factors with little quantitative basis. Some guidance is given in the Advice Note BA 16/97 (Department of Transport 1997), but it is primarily left to the interpretation of the user. Also, upon studying some of the background and

underlying theories to the development of the method, an allowable tensile stress of 0.7 N/mm^2 (101 psi) was used in tension and 1.4 N/mm^2 (202 psi) in compression (ICE 2008). This 2:1 compressive to tensile strength ratio is quite low for a masonry arch and overestimates the allowable tensile strength in most cases.

Advantages

- Quick calculation of maximum allowable load.
- No complex computer modeling required.

Disadvantages

- Based on point load at crown. Mechanism may form with point load at 1/4 or 1/3 point prior to overstress of masonry.
- Allowable axle load is arbitrarily modified by factors to account for material condition and existing arch cracking.
- No clear guidance on how to handle conditions of support movement or slender piers
- User does not readily understand the background of the formulation.
- Effects of support movement are only modeled with a single modification factor.
- Changes in hinge location and points of maximum stress can not be determined.
- Assumes a relatively high allowable tensile strength of the arch.

2.3.3. Heyman

Heyman authored several books and articles on the topic of masonry analyses. His methodologies revolved around plastic analysis techniques. Heyman, who had also previously researched the development of plastic hinges in steel structures, expanded and refined the ideas of Pippard (Boothby 2001). He applied the idea of hinge formation in unreinforced masonry structures. As part of his studies and analysis, he outlined the following simplifying assumptions (Heyman 1966):

- Masonry units are infinitely rigid
- Masonry unites are infinitely strong
- Masonry units do not slide at the joints
- Joints transmit no tension

From these assumptions, Heyman considered a yield locus in the axial force and the bending moment with an associated flow rule in the coordinates representing the axial and rotational displacements (Boothby 2001). As a result of the assumptions, the bounding theorems of plasticity can be applied to determine the ultimate load of a masonry arch. Plasticity theories incorporate two theorems: a lower bound, or equilibrium solution, and an upper bound, or mechanism solution.

The lower bound solution can also be described as the yielding solution. For an arch, the yield condition can be modeled by superimposing the thrust line onto the shape of the arch. The point of yield is the limit where the thrust line stays just within edges of the arch.

The upper bound theorem is a mechanism based approach. A mechanism, or deformed hinge model, is drawn of the arch. Then virtual work can be used to assess the failure load of the arch. The collapse load factor is the spot at which both the upper and lower bound solutions are satisfied by a specified load factor.

Heyman introduced two primary concepts to masonry arch analysis. The first was fact that masonry arch collapse loads can be determined by analyzing the arch as a mechanism instead of an elastic structure. Pippard's studies identified how hinges form in arches and their effects on collapse. However, his analysis still relied on elastic methods. Heyman realized the effects of hinges on the collapse load of masonry arches. He suggested that the researcher should indentify the possible hinge point locations. Then calculate the forces and stresses in the indeterminate structure. The locations of the hinges should then be adjusted based on the calculations and the process continued iteratively until the location of the hinges stabilizes.

The second concept introduced by Heyman was that of the geometric factor of safety (Heyman 1995). Heyman recommended determining the smallest possible arch thickness of which the thrust line with assumed hinge locations would fit within. That thickness was then compared to the actual arch thickness. He considered the ratio of the two values to be the geometric factor of safety for the arch.

From his work, he developed the "quick analysis" method. It is based on an arch with inputs of dimensionless parameters and a point load P. The equation is based on a failure occurring with hinges at each of the springings, under the live load, and at the crown (ICE 2008).

$$P = 16\frac{W_2 x_2 \left\{\alpha + (1-\tfrac{1}{4}k)\tau\right\} - (W_1 x_1 + \tfrac{1}{4}W_2)\left\{(1-\alpha) - (1+\tfrac{1}{4}k)\tau\right\}}{(3-2\alpha) - (2+k)\tau} \qquad (17)$$

where,

parameters per Figure 13, and

$h_q / h_c = \alpha$

$h_0 / h_c = \beta$

$t / h_c = \tau$

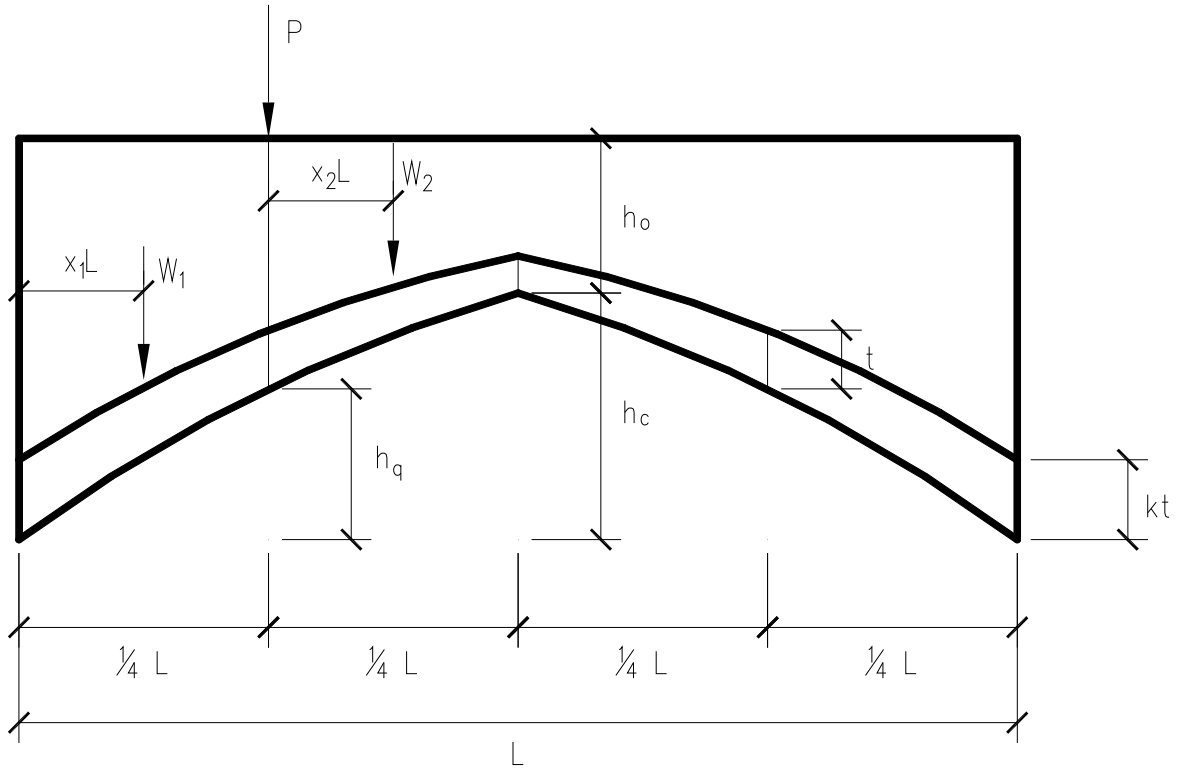

Figure 13. Nomenclature for Heyman method.

The 'quick analysis' method is based on two assumptions. The first is that the failure load occurs at the quarter point of the arch span. The second is that the failure hinge points occur at each of the abutments, at the quarter point underneath the live load, and at the crown. However, for most arches, the fourth hinge will occur between the crown and the opposite abutment. This difference in hinge location is attributed to the inaccuracies that may result from using this method. However, this analysis technique is particular helpful for quickly checking computer output results by hand.

Advantages

- Began the concept of mechanism based failures in masonry arch structures and noted the benefits of understanding hinge locations.
- Heyman's work provided the foundation for many future analysis works and methods.

Disadvantages

- No commercially developed software of specific industry wide analysis technique was directly derived from Heyman's work.
- To calculate failure load, hinge locations must be assumed and the problem solved through iteration. This can result in a time consuming computation.

2.3.4. Limit State Analysis

Livesley was able to take Heyman's assumptions and ideas about mechanism based methods and solve them with linear programming methods (Livesley 1978). Livesley modeled the stresses between the blocks of a stone arch by simplifying them to reactions at the intrados and extrados only. Then, by applying the four assumptions made by Heyman, he was able to calculate the collapse load solution and the collapse load mechanism with a linear programming algorithm.

In 1978, Livesley published a paper with equilibrium and mechanism formulations for a masonry arch that was formulated as a series of rigid blocks (Livesley 1978). Using the same general assumptions as those described by Heyman, Livesley developed a set of equations that could be solved using linear programming, where the objective function is the maximization of the collapse load factor subject to the constraints of the first order equilibrium equations (Boothby 2001). Livesley's work was motivated by Heyman's research which showed that the collapse load of a masonry arch could be formulated into a mechanism based model.

In Livesley's discrete model, the masonry arch bridge is idealized into a series of rigid blocks (Figure 14). The blocks are typically modeled as geometrically larger than the individual voussoirs to account for the size of the mortar joints since they are not modeled explicitly. Individual voussoirs can also be combined into larger 'macroblocks' to decrease the required computational effort. However, care must be taken to ensure that the larger discretization does not significantly affect the response of the failure mode (Gilbert 2007).

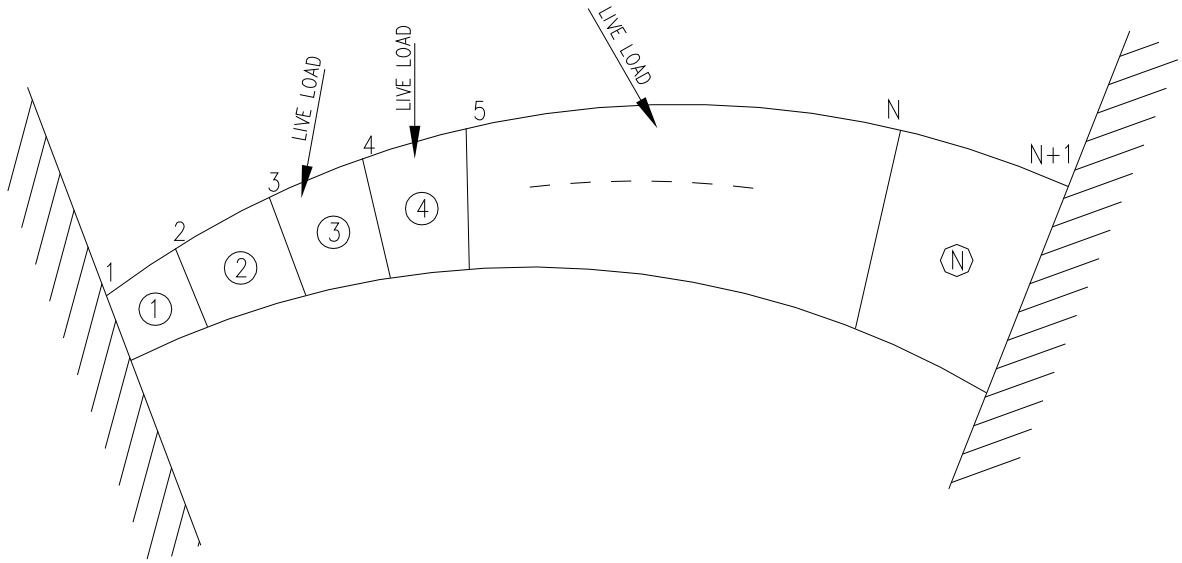

Figure 14. Plane of N rigid arch blocks at described by Livesley for limit analysis.

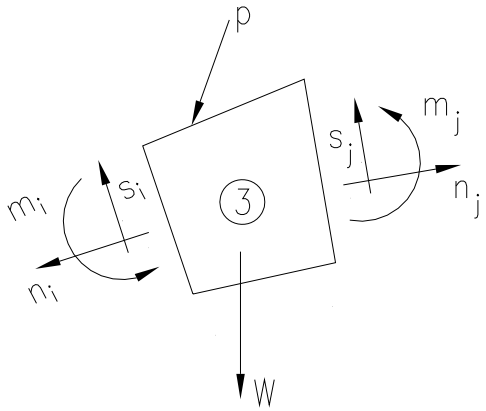

Figure 15. Free body diagram of element 3 from Figure 14.

For each block, or element, the equilibrium equations for force equilibrium in the x and y directions and moment about G_j are developed (Figure 15) and then written in the following form:

$$w_j + p_j = G_j r_j + H_j r_{j+1} \tag{18}$$

for $j = 1, \ldots\ldots, N$ where,

$w_j =$ vector of block weights

$p_j =$ vector of applied live loads on the blocks

$G_j, H_j =$ angular conversion to principle force directions of normal and shear

$r_j, r_{j+1} =$ vector of stress resultants between blocks

Equation (18) may be expressed in matrix form as

$$\begin{bmatrix} w_1 \\ . \\ . \\ w_N \end{bmatrix} + \begin{bmatrix} p_1 \\ . \\ . \\ p_N \end{bmatrix} = \begin{bmatrix} G_1 & H_1 & & & 0 \\ & G_2 & H_2 & & \\ & & G_{\cdots} & H_{\cdots} & \\ 0 & & & G_N & H_N \end{bmatrix} \begin{bmatrix} r_1 \\ . \\ . \\ r_{N+1} \end{bmatrix} \tag{19}$$

The maximum arch loads are solved by maximizing the scalar load factor, λ, subject to the equilibrium equation as follows,

$$\lambda p + w = Hr \tag{20}$$

Livesley is the first to attempt to relax the assumption that the blocks do not slide at the joints, but there are several computational difficulties with this assumption (Boothby 2001). This difficulty has been continued to be addressed by other researchers

The limit state method developed by Livesley was never developed into a commercially available analysis code, and hence, was never itself widely used by researchers and consulting engineers. However, it has been used as the basis for the development and implementation of other similar methods.

2.3.5. Rigid Block Analysis

The rigid block analysis has been popularized by Gilbert (Gilbert 1994). He developed his modeling into a software program, 'Ring' (Gilbert 2001). The software program has been continuously developed through today. Other than the MEXE method, the Ring software program is probably one of the most used methods of arch bridge analysis today.

A joint equilibrium formulation is used similar to that which was proposed by Livesley. The joint equilibrium equations are set up for sliding forces, normal forces, and moments at each of the contact surfaces. This series of equations is then solved by maximizing the scalar factor, λ, subject to a set of equilibrium constraints.

Assuming there are 'b' blocks and 'c' contact surfaces, the problems is stated as:

$$\text{Max } \lambda \tag{21}$$

subject to equilibrium constraints:

$$Bq - \lambda f_L = f_D \tag{22}$$

where,

$\lambda =$ load factor

B = directional equilibrium matrix

q = vector of contact forces

f_L, f_D = vector of block load, live and dead

and no tension ('rocking') yield constraints:

$$\left.\begin{array}{r} m_i \le 0.5 n_i t_i \\ m_i \ge -0.5 n_i t_i \end{array}\right\} \text{for each contact } i = 1, \ldots, c \qquad (23)$$

and sliding yield constraints:

$$\left.\begin{array}{r} s_i \le \mu_i n_i \\ s_i \ge -\mu_i n_i \end{array}\right\} \text{for each contact } i = 1, \ldots, c \qquad (24)$$

where,

μ = coefficient of friction

Contact and block forces, dimensions, and friction properties are shown in Figure 16. The linear programming variables are the contact forces, n_i, s_i, m_i, and the unknown load factor, λ. (LimitState Ltd. and Gilbert 2007)

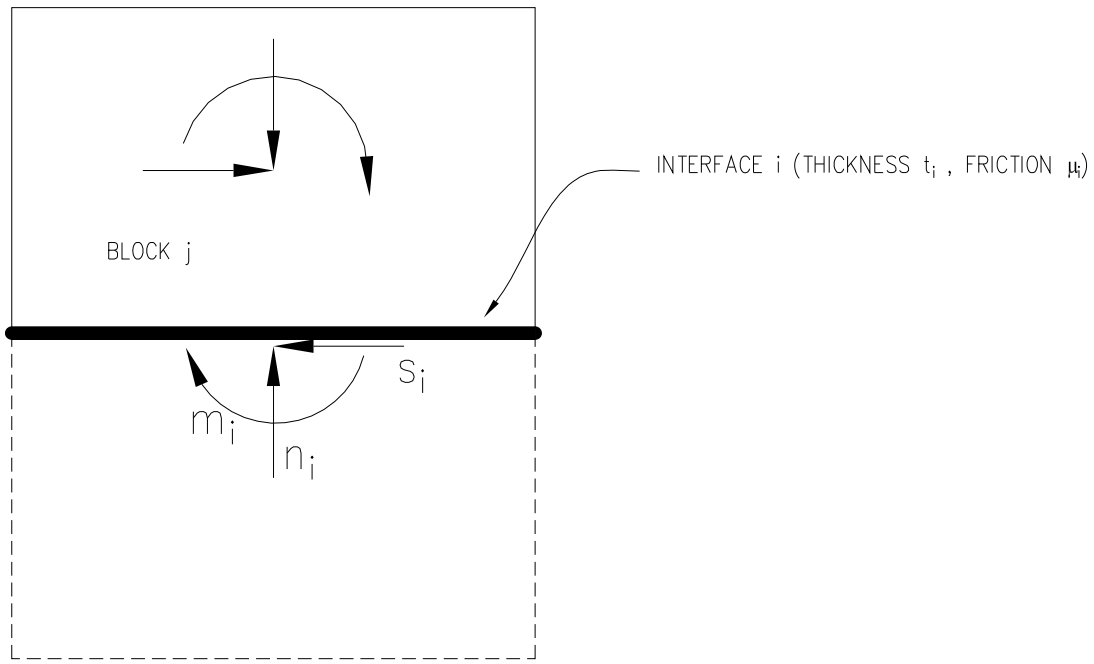

Figure 16. Block *j* and contact forces for interface *i* for rigid block formulation.

Additional constraints can be set to model the effects of finite compressive strength and sliding between blocks.

A methodology is also proposed in the computer programming to adjust for the condition of support movement. Using a formulation similar to that above with the following changes:

$$\text{Min } E \tag{25}$$

subject to equilibrium constraints:

$$Bq - f_{SUP} = f_D \tag{26}$$

and a constraint specifying the support movements:

$$d_{SUP}^T f_{SUP} - E = 0 \tag{27}$$

where,

E = support movement energy
d_{SUP} = vector of pre-defined block support movement
f_{SUP} = unknown block support reactions

The solution identifies the hinge points and location of the thrust line as a result of the support movement. However, it does not provide information regarding the effects of the support movement on the future load-displacement behavior of the arch.

Advantages

- Quick calculation of maximum allowable load for various locations of loading points.
- Shows location of thrust line and hinge formations under various location combinations.

- Output has been calibrated against several different laboratory and in-situ bridge loads tests.
- Can analyze other failure mechanisms besides hinge formations such as sliding, multi-ring separation, and localized crushing.

Disadvantages

- Only arch geometry preprogrammed into the software can be used for analysis. Analysis of a non-uniform cross section would require the user to develop an independent software code to complete the analysis. In the case of the Brooklyn Bridge with a stepped cross section, both a 3' or 2' cross sections would need to be analyzed, where neither of which completely accurately model the exact structural configuration.
- Purchasing proprietary software is required for analysis.
- The real time effects of support movement can not be modeled. The effects of support movement are shown by changes in the hinge locations and an energy based output is provided. However, there are currently no capabilities for crack opening displacements to assist with a structural health monitoring program.

2.3.6. Finite Element Modeling

Finite element modeling has been widely adopted as a procedure of choice when analyzing bridge and building structures. And the application of finite element modeling to masonry arch structures has also been widely used.

Finite element models are dependent on several factors. Two inputs in particular can have consequential effects on the results. The first is the effect of the Young's modulus. In the case of modern structural material such as steel and concrete, the material properties are readily known or can be estimated with reasonable accuracy. However, in the case of masonry materials, there is much more uncertainty. One problem is that masonry is made up of two individual components, brick or stone blocks and mortar joints. The Young's modulus is a combination of a weighted average of these two materials. Also, the properties of mortar and bricks can vary widely from structure to structure as there is no set formulation for their manufacture. Page (Page 1993) gives some typical values for brick and stone work that can be used as a starting point in a finite element analysis.

The second concern is the modeling of support conditions. Modeling an end connection as fixed, partially fixed, or pinned can cause wide ranges of analysis results.

As a starting point for a finite element analysis, the ICE Manual of Bridge Engineering (ICE 2008) provides some guidance on geometrically modeling arches in a finite element program:

1. Arch ring idealization should consist of at least 12 elements with pinned supports.

2. The load should be applied at the road level and dispersed through the backfill at slope of 2 vertical to 1 horizontal.
3. If analysis assumes a unit width of 1m of arch, the effective width of the axle load should be computed based on:

$$w = h + 1.5 \quad (28)$$

where,

$w =$ effective transverse width of arch barrel for axle loading, in meters
$h =$ fill depth at point under consideration, in meters

Advantages

- Any arch shape can be modeled.
- Any load pattern can be analyzed.
- Software widely available.
- Temperature changes of arch materials can easily be incorporated into the model.

Disadvantages

- User can vary the output greatly by changes in support conditions and material modulus.
- Special modeling required to address no tension in units.
- Viewing stresses is difficult due to changing orientation of arch shell elements.
- No standardized method on how to handle support movement.

2.4. Comparison of Masonry Arch Bridge Analysis Methods

The United Kingdom's Bridge Engineering Division of the Highways Agency completed a study to compare the results of three masonry arch analysis methods with ten full scale bridges which had been tested by the Transportation Research Laboratory (TRL) (Department of Transport 2001a). The assessment methods compared were:

1. Mechanism/ Line of Thrust method (computer program ARCHIE)
2. Castigliano Elastic method (computer package CTAP)
3. Pippard/MEXE method (using computer program MNIPOINT)
4. Finite Element based method developed by British Rail Research
5. Mechanism method (computer program ARCH)

Only the ARCHIE computer program is still available for use today. However, the results of the study show the variability that can be expected between different analysis methods.

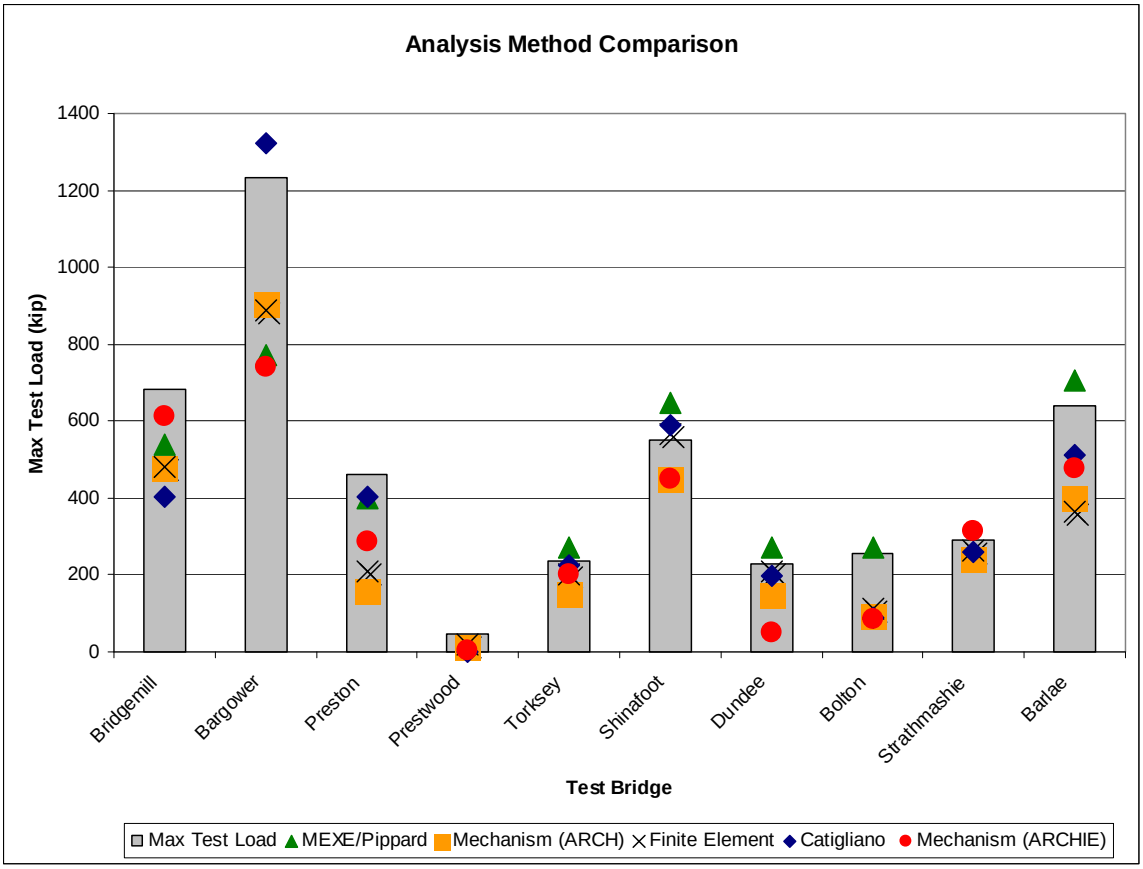

Figure 17. UK Department of Transport Analysis Method comparison.

Test Bridge	Castigliano	Mechanism	MEXE/Pippard	Mechanism	Finite Element
Bridgemill	59%	90%	79%	70%	71%
Bargower	107%	60%	63%	73%	72%
Preston	88%	62%	86%	35%	45%
Prestwood	0%	9%	32%	27%	36%
Torksey	95%	84%	115%	64%	84%
Shinafoot	107%	82%	118%	82%	103%
Dundee	87%	22%	118%	64%	92%
Bolton	35%	33%	106%	37%	44%
Strathmashie	89%	108%	85%	83%	91%
Barlae	80%	74%	110%	63%	57%
Average	75%	62%	91%	60%	70%
	(CTAP)	(Archie)	(Minipoint)	(Arch)	(MAFEA)

Table 1. Summary of Department of Transport Analysis Method Comparison.

The results of the study are shown in Figure 17. All of the methods with the exception of the Castigliano method were modified by an arbitrary Condition Factor, F_{cM}, as determined by the TRL. It was concluded by the authors of the study that all methods seem to give fairly reasonable safe estimates of collapse loads. A summary of the percent differences of the analysis from the collapse loads is shown in Table 1. Note that most of the analysis methods conservatively underestimated the collapse loads. This is due to the fact that actual bridges have individual features such as interior spandrel walls and haunching near the springings which the analysis methods cannot account for (Department of Transport 2001a). It is accepted that masonry arch bridge assessment methods will typically yield results of +/- 20% due to these variables and other factors of material properties which can vary greatly across masonry structures.

3. FIELD TESTING: SHM OF BROOKLYN BRIDGE APPROACH STRUCTURE

The main intent of the Brooklyn Bridge structural health monitoring program was to monitor the condition of the two largest masonry arch approach spans to insure that the bridge could be operated safely until the schedule permanent repairs could be implemented. Secondary goals included understanding the cause of the masonry cracks and how active they were. The monitoring program was in place for over a year's time.

The structural health monitoring program consisted of three phases:

1. Visual inspection and study of existing bridge documentation,
2. Sensor layout plan and instrumentation, and
3. Long term monitoring over remote data network.

3.1. Visual Inspection and Study of Existing Bridge Documentation

Figure 18 is a photograph of the masonry arch approach spans. The arches spanned 36 feet and 34 feet respectively. The western arch had a skew and tapered down to a span of 20 feet at the north end while maintaining the semicircular profile. Both of the arches were supported on masonry walls. The masonry walls were approximately 6' at the base and stepped down to 3' at the top. The two arches shared bearing on the center wall.

The original structural drawings for the Brooklyn Bridge are maintained by the New York City Department of Records. The drawings available for the arches show the dimensions which match the structure in the field. Detailed stone facade drawings existed but there was little details on the construction specification of the masonry other than it was to be of brick construction. The stone facade was made entirely of limestone. The backfill above the arch consisted of large granite rubble. This was confirmed by an inspection opening that was made in the east arch (Figure 21). The backfill above the tapered arch would have been quite heavy at the smaller end. As an alternative, a series of spandrel jack arches of increasing size were constructed over this end. The arch thickness stepped from 3' to 2' at approximately 1/3 points of the arch span.

An article published by Collingwood (Collingwood 1876) noted that the mortar used for the masonry construction was mixed at a bulk ratio of: one part cement : two part sand. No lime was reportedly used for the mortar. This mortar is comparable to a Type N mortar of masonry cement by today's standards. Inspection of the mortar joints in the brick arches found them to be in relatively good condition. There was some mortar joint erosion due to long term water infiltration, but this was at relatively isolated locations in the brick arches. The City of New York uses a special ice melting solution over the Brooklyn Bridge which has less corrosive properties than salt. This has no doubt reduced the wear and deterioration on the mortar joints.

A large longitudinal crack was observed running down the length of each arch at the crown (Figure 19). Paint marks indicated that this crack had occurred to at least some extent in 1996. Whether it had widened or grew since that point was unknown.

A number of vertical cracks were also noted in the support walls of the arches (Figure 20). Some of these cracks could be traced the entire height of the wall through to the stone foundation. Other cracks stair stepped to the arched door openings. These cracks were clearly evident of past differential settlements. Again, paint marks dated some of the cracks to 1996, but there was no historical record of their existence or behavior.

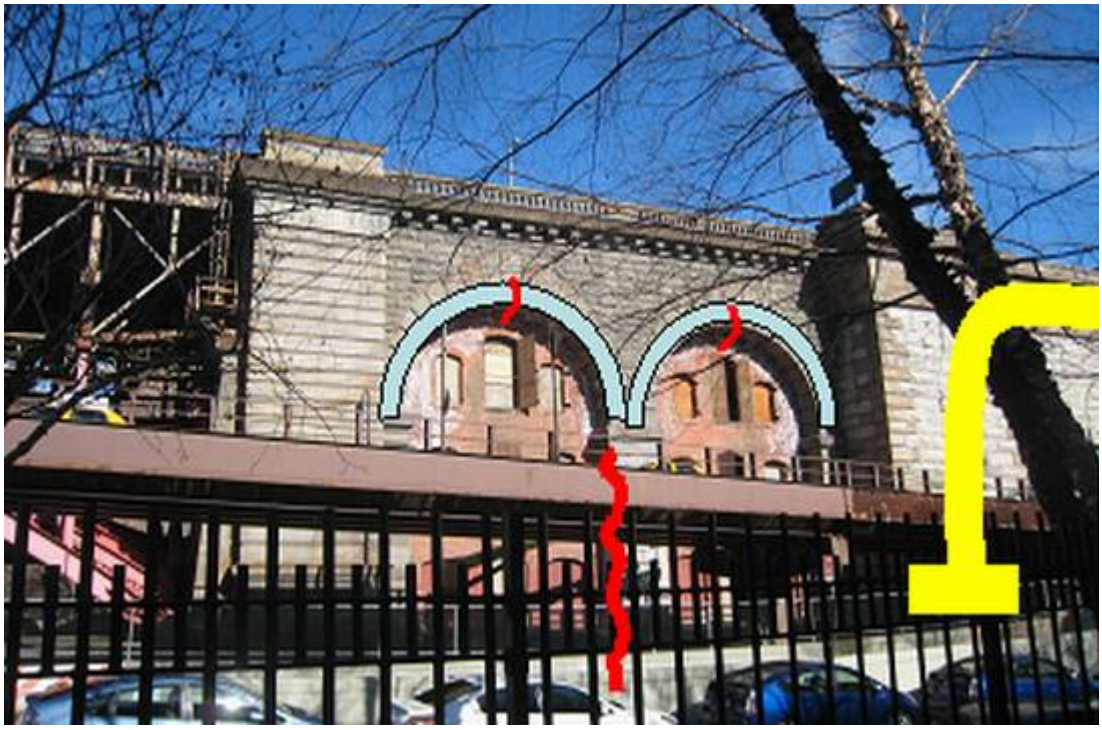

Figure 18. Diagram of arches and crack locations.

Figure 19. Longitudinal crack at the crown of the arch.

Figure 20. Vertical masonry cracks indicating past differential settlement.

Figure 21. Inspection opening in arch showing 2' brick thickness and granite rubble fill.

3.2. SHM System

It was decided to use a fiber optic based structural health monitoring system for the Brooklyn Bridge. The most significant advantage of this type of system was that sensors could be connected in series, thereby eliminating excessive amounts of wiring. Also, since the sensors were going to be in place for well over a year with the possibility that they could be in place for five years or longer, a robust, but low cost wiring system was needed.

Electrical sensor lines are typically run inside of metal or plastic conduit. On a project such as this with over 40 sensors to be installed, the conduit material and installation

costs would have been a burden on the project. Instead, an armored cable fiber optic lead line system was utilized. The fiber cable line was protected by a ribbon of flexible metal tubing, Kevlar yarn, and braided wire sheathing (Figure 22). This gave the fiber as much, if not more, protection as if it had been installed in a metal conduit or plastic innerduct. The total diameter of the line was less than 3/16" diameter. It was installed by attaching it to the brick with plastic cable clips at approximately 3' on center.

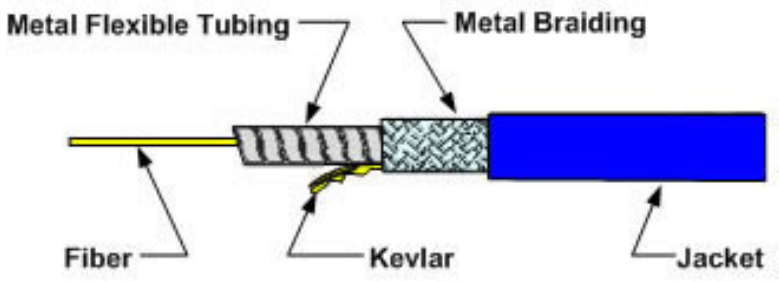

Figure 22. Detail of armored cable used on Brooklyn Bridge.

In order to minimize the light loss in the system and maximize the number of sensors that could be installed, all of the splices in the fiber were fusion spliced with a core alignment splicer. The splicer automatically aligns the fiber optic core of the two lines to be connected and then welds them together. Each of the splices is then back checked for signal loss. Finally, a plastic tube with a steel spline is secured around the splice to reinforce it and a piece of heat shrink tube covers the entire assembly to make it water tight.

The alternative to fusion splicing the connections is to attach them with mechanical screw connectors. This type of installation is typically faster in the field, but because of signal loss across the connectors, less than half as many sensors can be installed per channel.

After installation and final inspection of the sensors, all 40 sensors were operational throughout the duration of the project.

Figure 23. Core alignment fusion splicer.

Figure 24. Mechanical fiber optic connector.

In order to read and record the change in wavelengths of the sensors, an interrogator and data collector were required as part of the system. The Micron Optics' sm130 sensing module was chosen for the interrogator (Figure 25). The interrogator has 4 channels and can record at up to 1000 Hz. It has a wavelength range of 1510nm to

1590nm which when configured with sensors as for the Brooklyn Bridge project can accommodate up to 20 sensors per channel. The repeatability accuracy of the interrogator is 1pm per NIST Technical Note 1297.

The interrogator was supplemented with a 4x8 multiplexer. The multiplexer was static only as all fibers were scanned instantaneously. It was installed only for wiring management to reduce the length of lead lines.

The companion Micron Optic computer, sp130, was chosen as the data collector. The computer is constructed per military specifications for operating over a wide range of temperature and humidity ranges. It also has low power consumption.

The entire data collection system was housed in a NEMA enclosure at the bridge site (Figure 26). The enclosure had a temperature and humidity controls to moderate the environmental conditions within the box. The onsite computer module was accessed remotely through a dedicated cellular internet connection. Due to the thick masonry walls of the Brooklyn Bridge structure and interference from surrounding buildings, internet service was occasionally spotty. This was remedied by the installation of an external antenna (Figure 27).

Figure 25. Micron Optics' sm130 interrogator unit.

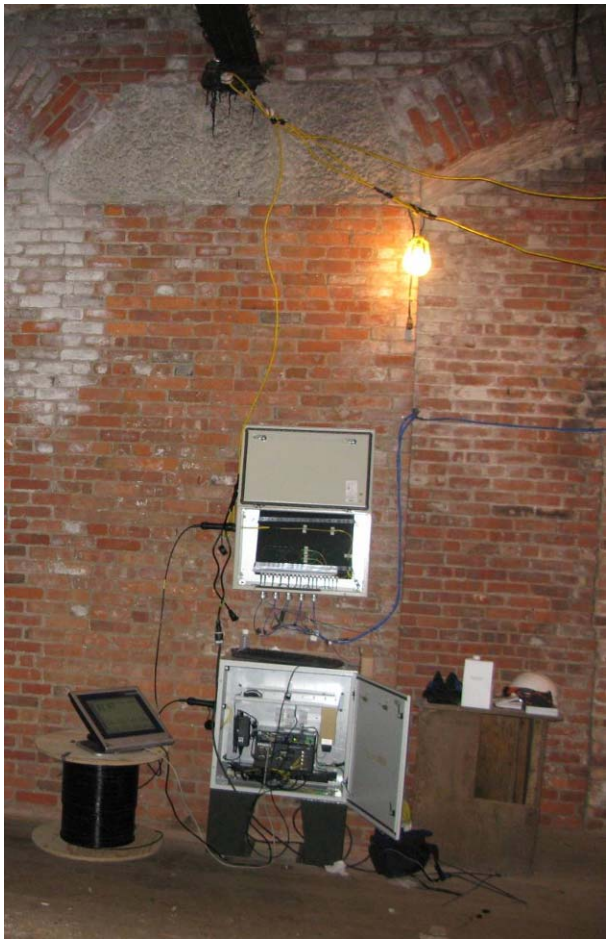

Figure 26. Interrogator and data collection system at the Brooklyn Bridge.

Figure 27. Cellular antenna installation.

3.2.1. Sensor Instrumentation

The sensor layout plan was developed with several initiatives in mind. The masonry approach structure had obvious evidence of prior differential settlement. There was a large volume of traffic using the roadway with particularly heavy usage during rush hour commutes. Also, temperature effects on the structure were to be studied. And finally, the effect, if any, of the adjacent cable anchorage structure to the east and the steel roadway truss and masonry buttress to the west were of interest.

The primary concern was to monitor the cracks to determine if they were widening, closing, or actively moving. This was achieved by using a fiber optic crack sensor. The crack sensor was originally used for monitoring cracks in the concrete structures, but with some connection modifications was adapted for use in a masonry structure. The

crack sensor is advantageous because it can measure cyclical crack movement of +/- 1/4" with repeatable accuracy and can measure unidirectional crack opening up to well over 1/2".

Figure 28 shows one of the installed crack sensors. An integral FBG (fiber Bragg grating) can correlate change in wavelength to crack opening. Each of the sensors was calibrated and the conversion to crack opening can be made with the following equation:

$$\Delta_{crack} = \frac{\lambda - \lambda_{initial}}{GF} \tag{29}$$

where,

Δ_{crack} = crack opening displacement
λ = recorded wavelength
$\lambda_{initial}$ = initial, or reference, wavelength
GF = gauge factor for wavelength to displacement conversion, calibrated for each sensor

The crack sensor could be modified with a second FBG on each sensor so that they were internally temperature compensated. However, testing and observation of data records found that applying the typical temperature compensation for an FBG was adequate and doubling the number of FBGs for the crack sensors was not warranted. The following temperature compensation formula was used for the crack sensors.

$$\Delta' = \frac{(\Delta\lambda) - (\Delta\lambda_{temp})}{GF} \tag{30}$$

where,

Δ' = temperature adjusted crack opening displacement

$\Delta\lambda$ = change in sensor wavelength

$\Delta\lambda_{temp}$ = change in recorded wavelength of nearby temperature sensor

GF = gauge factor for wavelength to displacement conversion, calibrated for each sensor

With the heavy volume of traffic on the bridge and the large crack at the crown, it was of interest to discern whether there were any differential movements on opposite sides of the crack. An accelerometer was mounted on each side of the longitudinal crack to measure any differential vibration or movements across the crack (Figure 28). These accelerometers would also be able to detect any slippage at the crack.

The accelerometers used were a custom fabricated uni-axial device with an internal FBG. The accelerometer had a measured frequency detection range of 0.2 Hz to 25 Hz with a sensitivity of 0.2 nm/g and a resolution of 0.015 g.

The acceleration records were temperature compensated and calculated using the following equation:

$$a' = \left[(\lambda - \lambda_{initial}) - (\Delta\lambda_{temp}) \right] \cdot GF \qquad (31)$$

where,

a' = temperature adjusted acceleration

λ = recorded wavelength

$\lambda_{initial}$ = initial, or reference, wavelength

$\Delta\lambda_{temp}$ = change in recorded wavelength of nearby temperature sensor

GF = gauge factor for wavelength to acceleration conversion, calibrated for each sensor

In addition to mounting accelerometers at the crown, they were mounted on the east exterior wall near the tower anchorage. This was to study if there were any structural movements that could be recorded as a result of the adjacent anchorage.

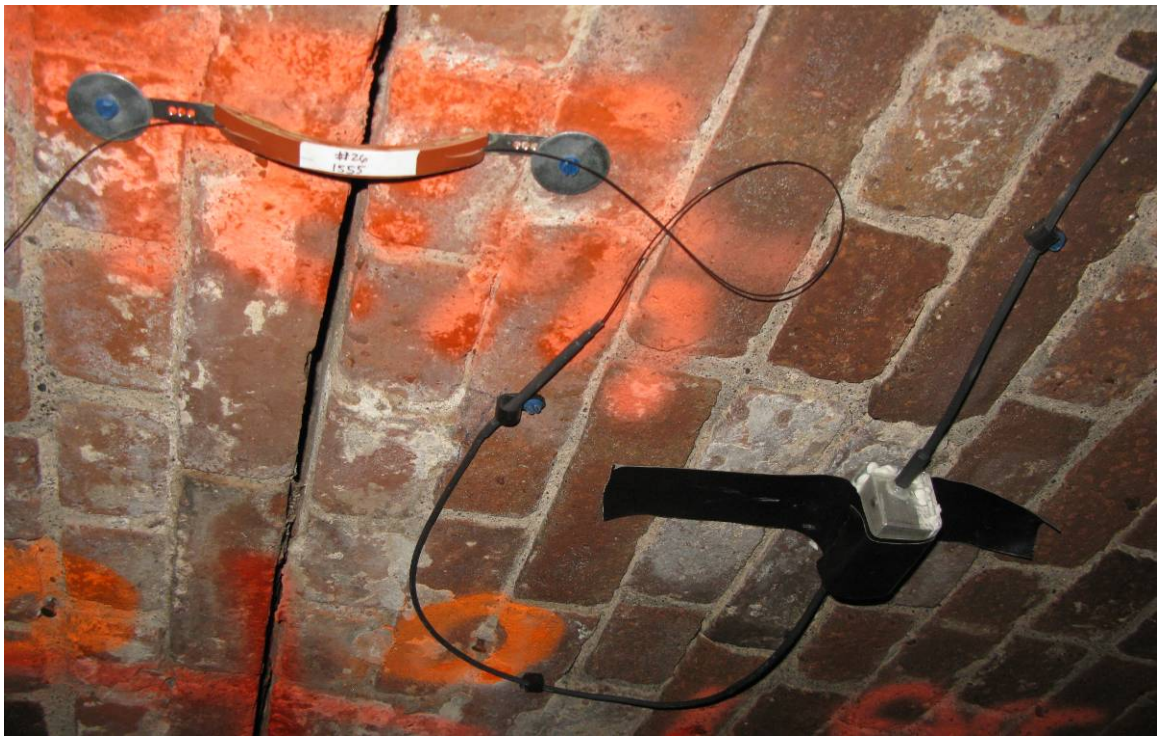

Figure 28. Fiber optic crack gauge and accelerometer.

Tiltmeters were installed to monitor the rotation of the walls (Figure 29). The tiltmeters used were a commercially available device with internal temperature compensation.

The tiltmeters had a measurement range of 6 degrees with a sensitivity of 486 picometers/degree. The tiltmeters were strategically placed at each floor level on the supporting masonry walls. Additional tiltmeters were installed on the walls of the upper floor level on opposing sides of the vertical wall cracks.

The angle of wall rotation was calculated using the following:

$$A = \frac{\left[(WL_2 - CWL_2) - (WL_1 - CWL_1)\right]}{S} \tag{32}$$

where,

A = tilt towards vertical (deg)
$WL_{1,2}$ = measured wavelength (nm) related to each FBG
$CWL_{1,2}$ = center, or reference, wavelength (nm) related to each FBG
S = sensor specific sensitivity (deg/nm), ≈ 0.48 for sensors on this project

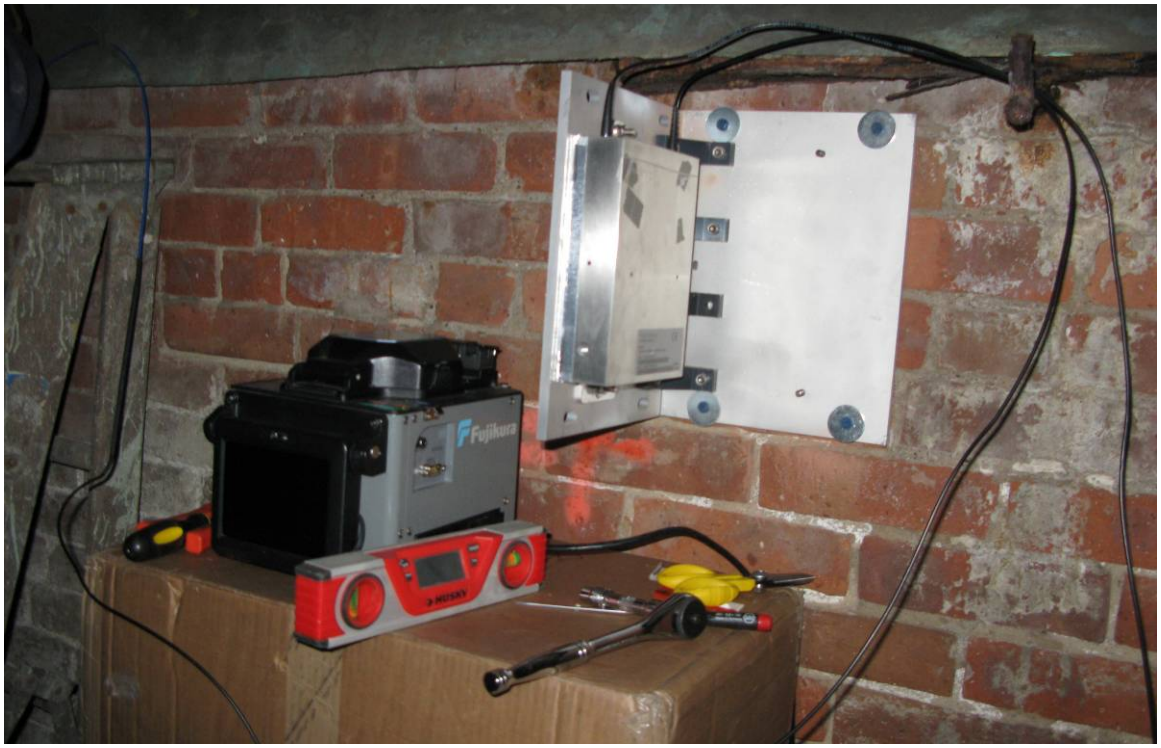

Figure 29. Fiber optic tiltmeter.

Temperature sensors were used throughout the structure to calibrate the measurement sensors and document the outdoor ambient temperatures. The temperature gauges used were commercially available sensors with identical gauge factors.

3.2.2. Sensor Layout Plan

A total of 40 fiber optic sensors were used for the Brooklyn Bridge monitoring project which consisted of 16 crack sensors, 5 displacement sensors, 5 accelerometers, and 8 tiltmeters, 6 temperature sensors. Figure 30 through Figure 35 show a layout of the sensors within the arch approach structure.

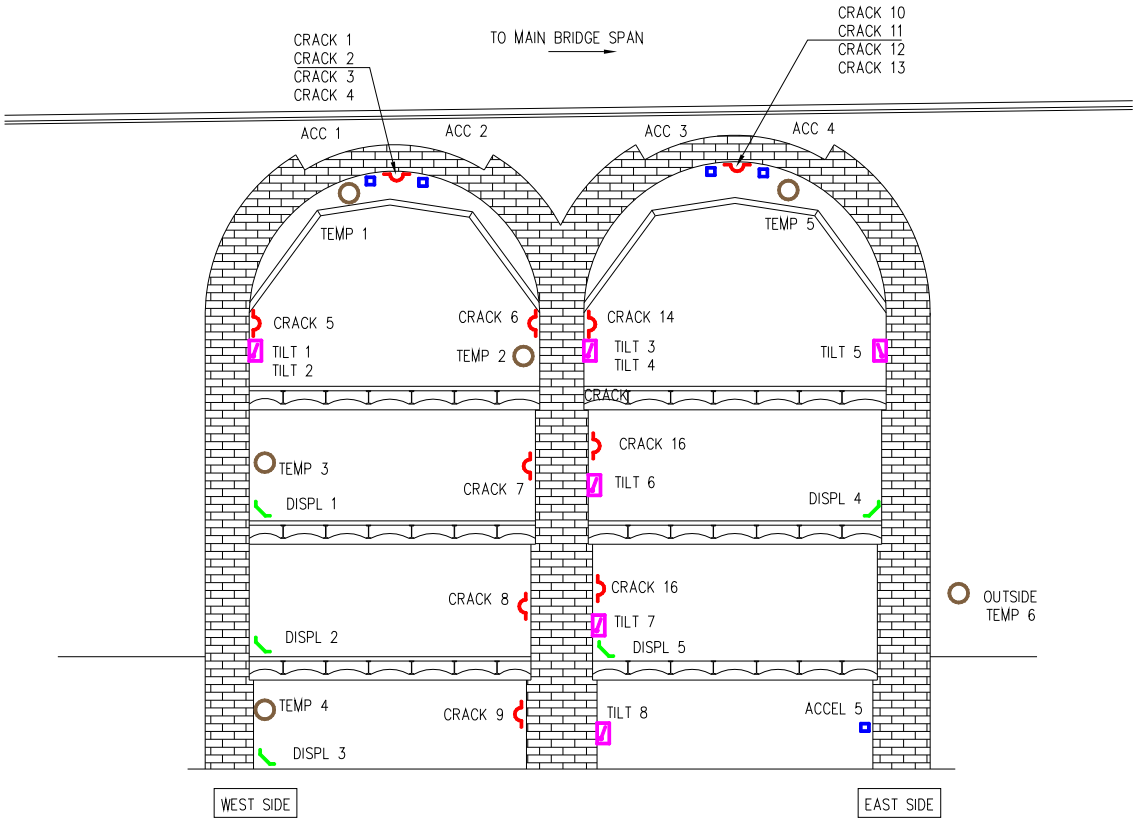

Figure 30. Section view of arch approach structure with sensor layout.

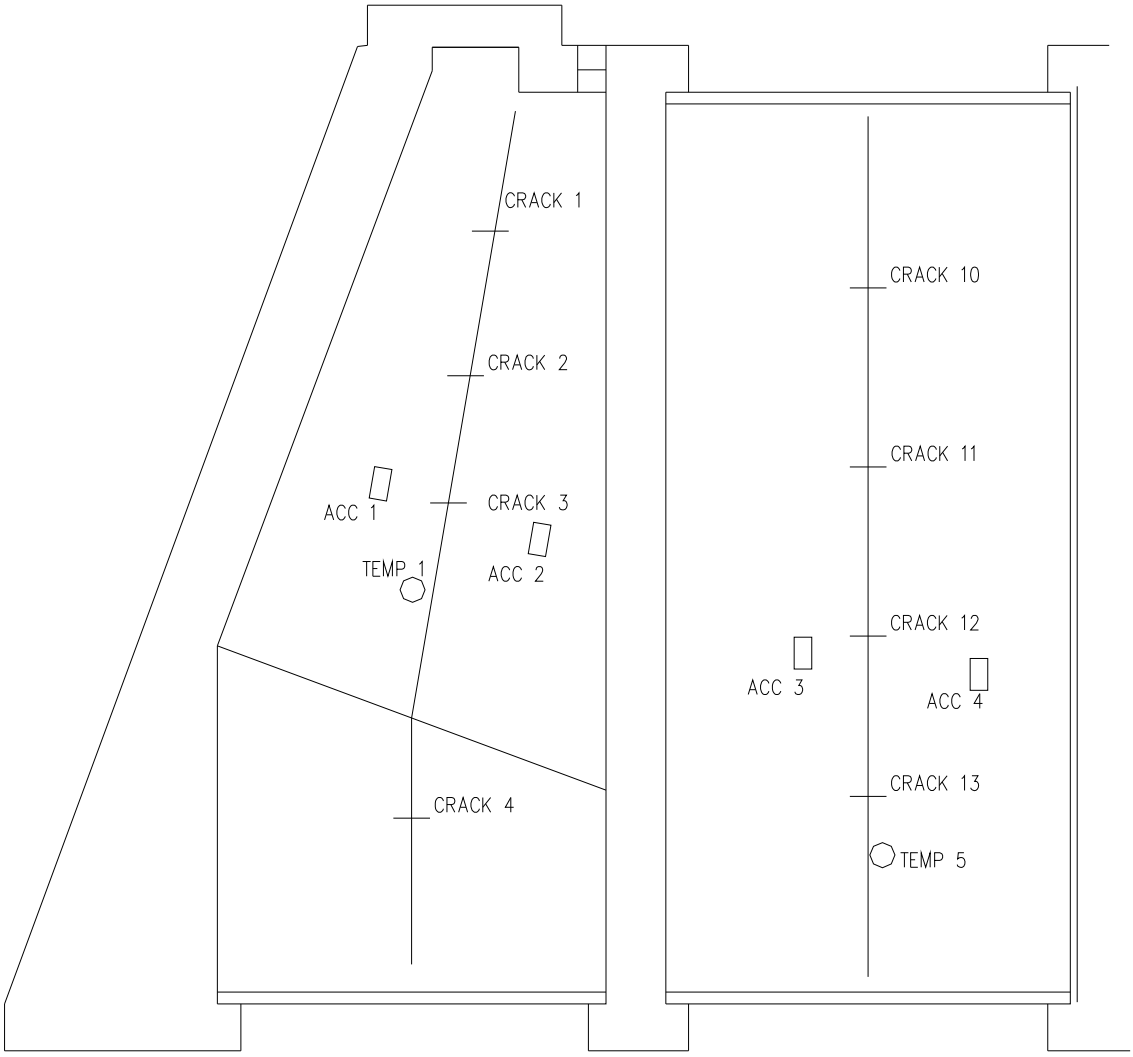

Figure 31. Sensor layout at arch intrados.

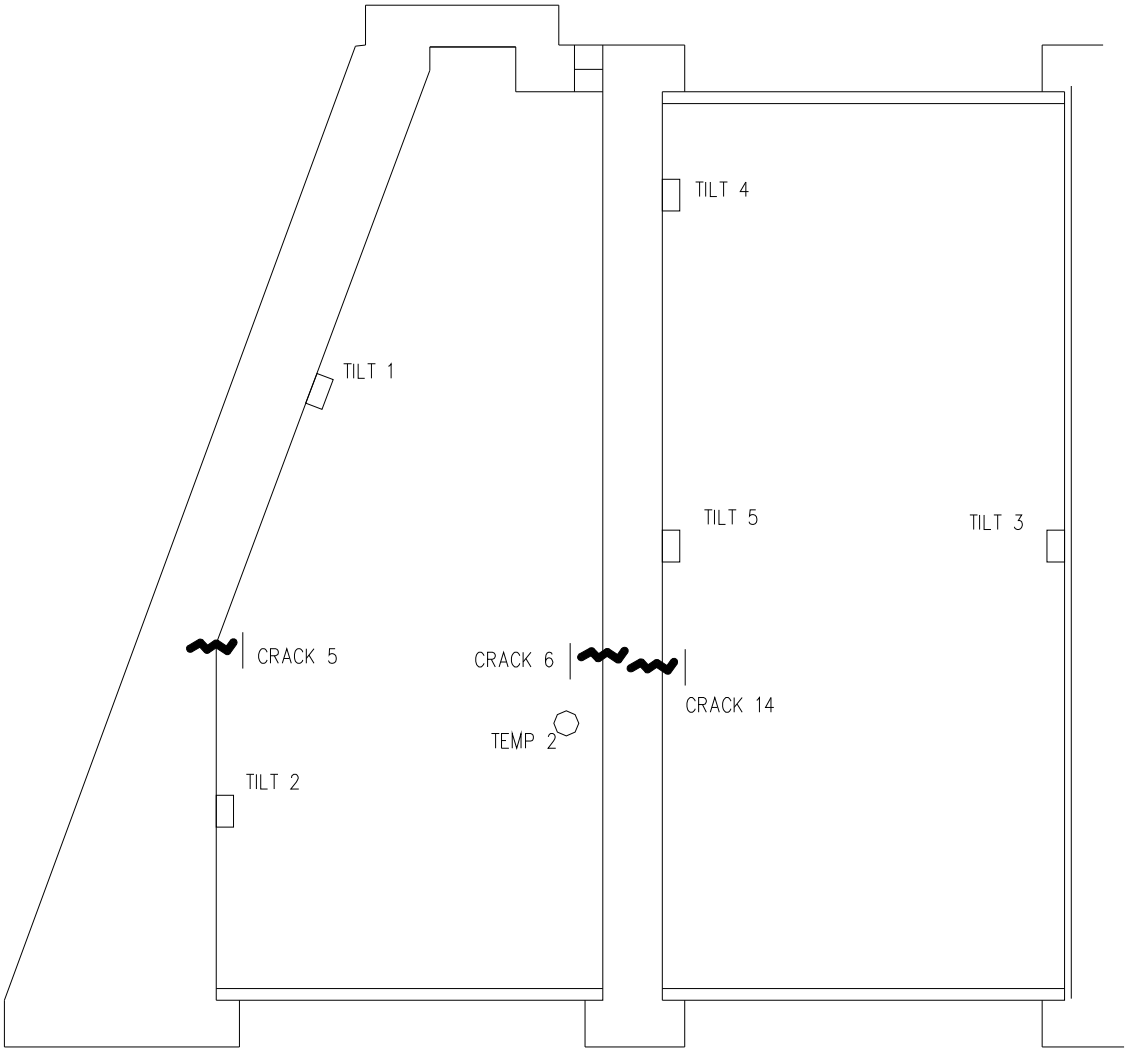

Figure 32. Sensor layout at third floor.

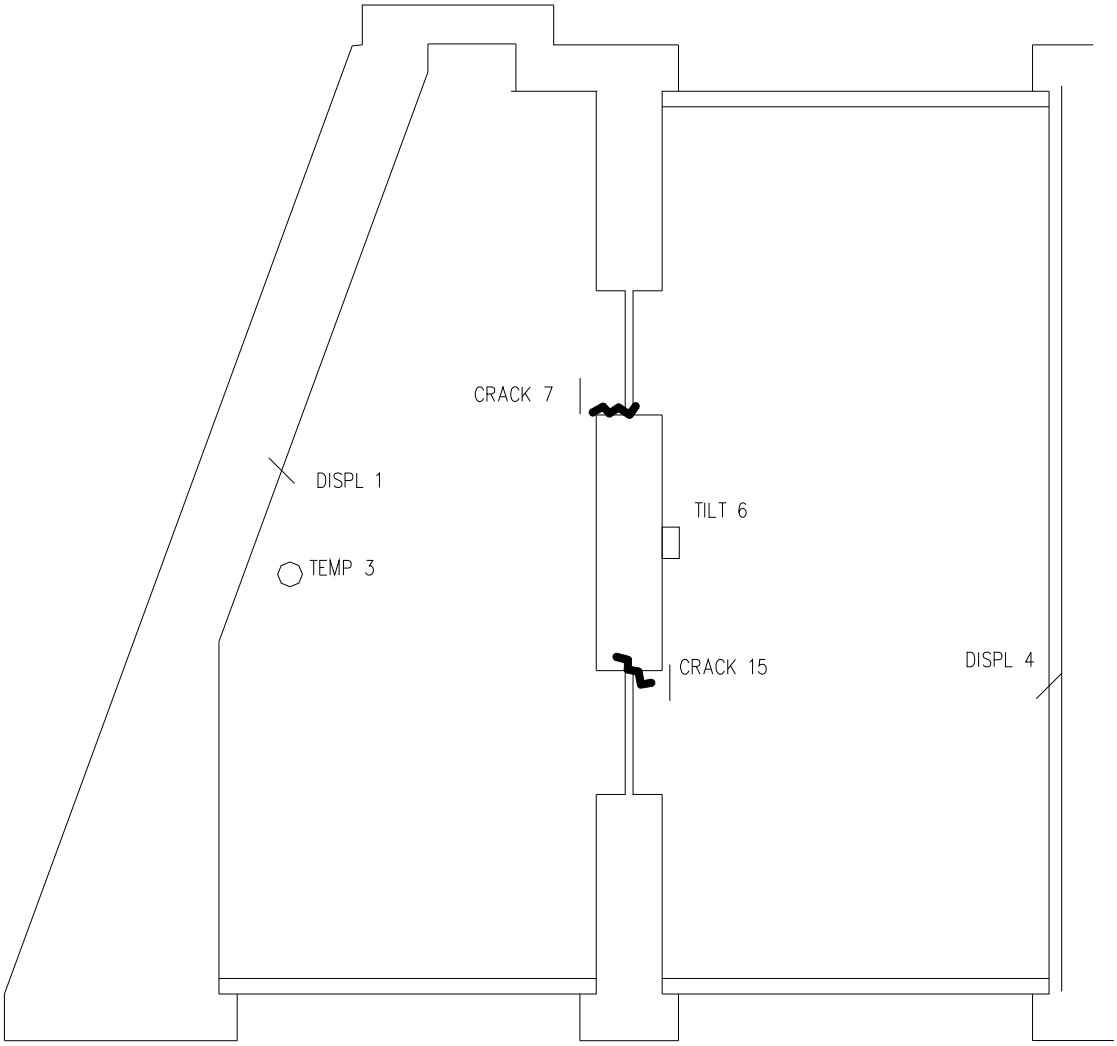

Figure 33. Sensor layout at second floor.

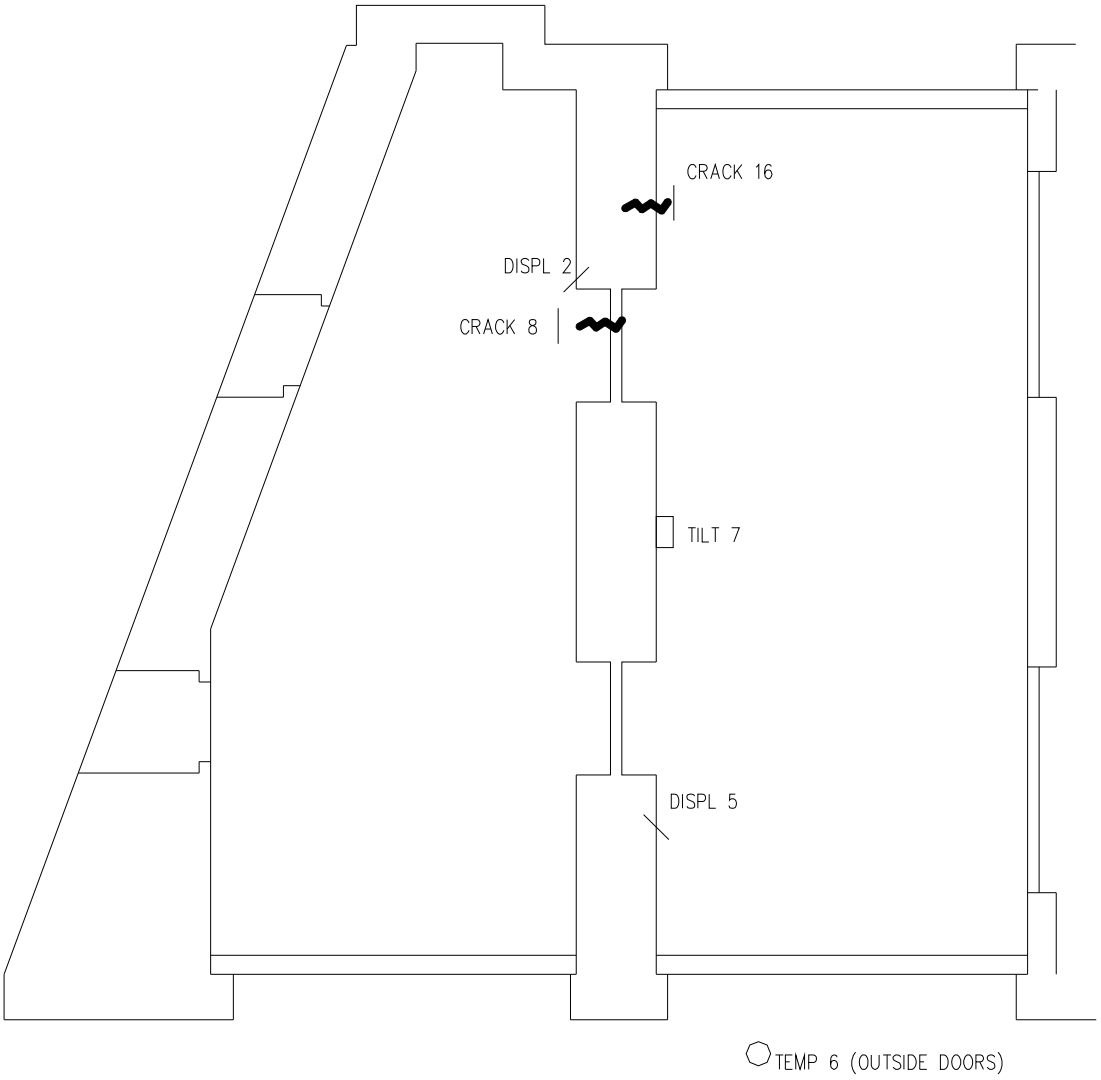

Figure 34. Sensor layout at first floor.

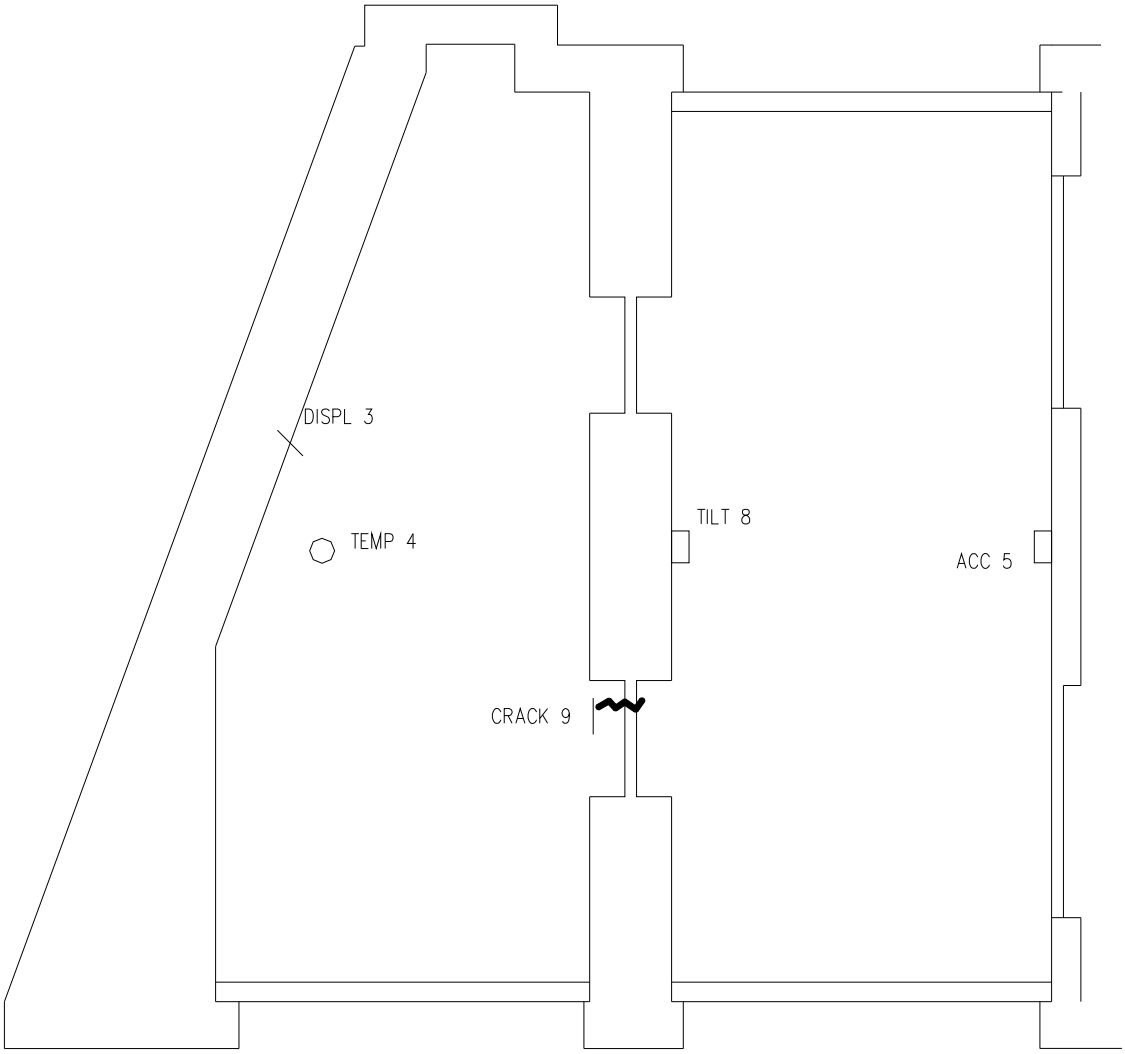

Figure 35. Sensor layout at basement.

3.3. Long Term Monitoring Over Remote Data Network

At any point during the day, a user could remotely log in to view the real-time readings. Figure 36 shows a typical screenshot of the remote bridge monitoring software. Threshold limits were set for each sensor. Should any sensor exceed its threshold limit, a message is sent via email to the user. For example this did occur in one instance where

one of the tiltmeters gave unusually high readings. On-site investigation revealed that water had been dripping onto the tiltmeter and had caused the false readings.

Due to hard drive size limits, the real time data was not continuously saved to the on-site computer. Instead, the sensor data was recorded at various selected time intervals and saved to the on-site computer. At any point thereafter, the data sets were downloaded via an FTP server for further detailed analysis. Data sets were recorded and downloaded to analyze daily, weekly and monthly changes.

Data recorded at regular intervals throughout the day showed little change. Figure 37 shows typical data for the crack sensor #3. Data were recorded on April 28, 2009 for a period of nearly 10 hours. Sensor readings showed insignificant change during the day. The maximum change in the sensor average readouts was about ± 25 micrometer. It should be noted that the average daily change for other crack sensors readings was similar.

For the weekly analysis of the sensor readings, data was recorded on four consecutive days starting from Monday, April 27, 2009 and ending on Thursday, April 30, 2009. Data were recorded at the same time each day, between 6pm and 8pm. The maximum difference between readings was about 27 micrometer. The average weekly readings change for other crack sensors was less than 50 micrometers.

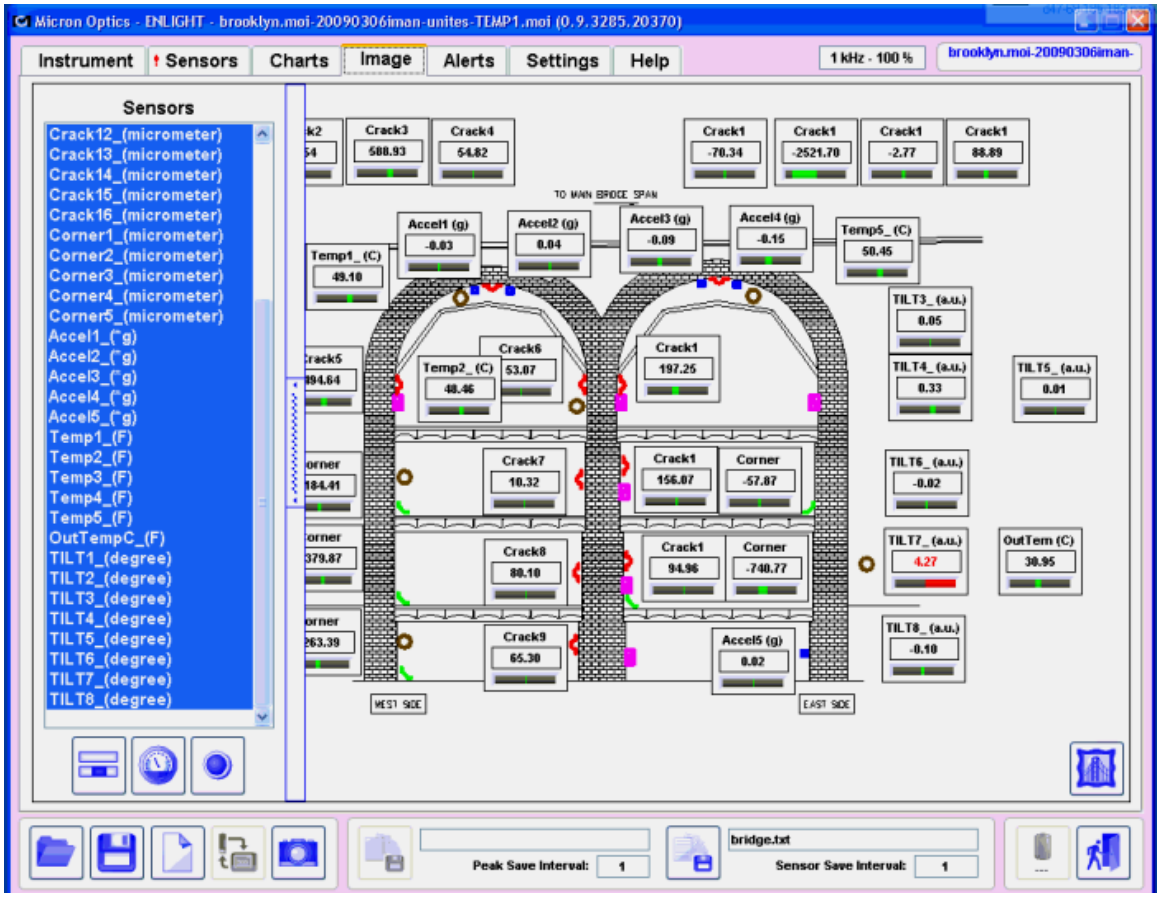

Figure 36. Screenshot of remote bridge monitoring software.

As there was little change in the short term, i.e. daily and weekly, monitoring of the cracks, the focus shifted to the long term performance of the crack openings. Monthly analysis of the sensor data was performed on the data to show the longer term history of the crack movements. The plotted data shows the sensor readings from March 2009 until May 2010. To plot these data, the sensors readings were taken from the average of a 15 minute data acquisition cycle. The data was then offset to zero for March 13, 2009 for the west arch and July 18, 2009 for the east arch as the reference points. The later reference point was used for the east arch due to an earlier sensor error. The crack

readings for the east and west arches are shown in Figure 38 and Figure 39, respectively.

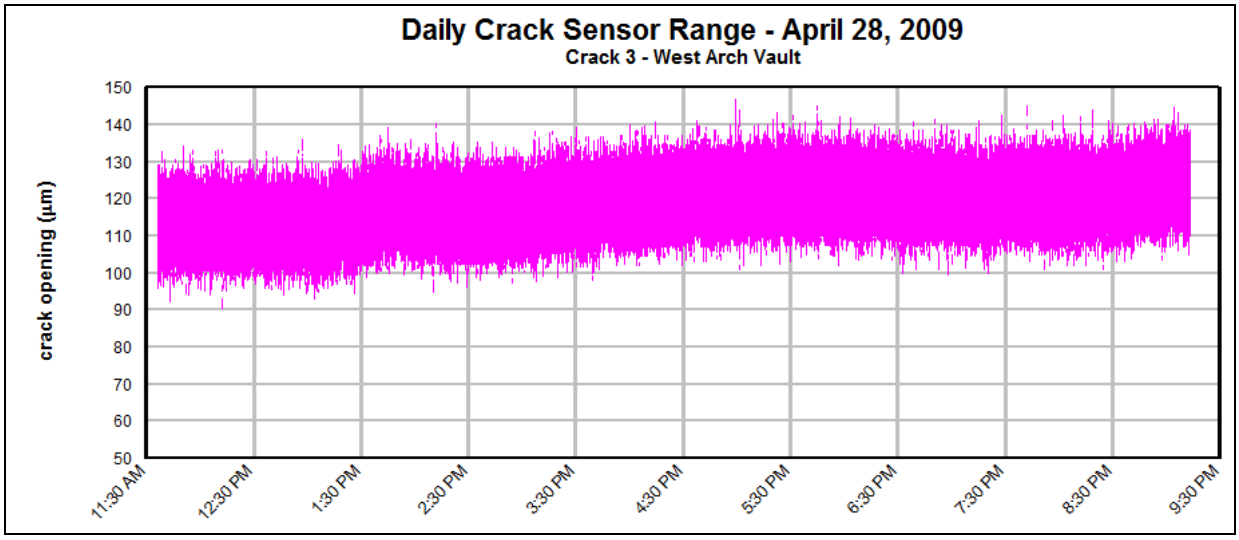

Figure 37. Typical example of daily FBG crack sensor reading.

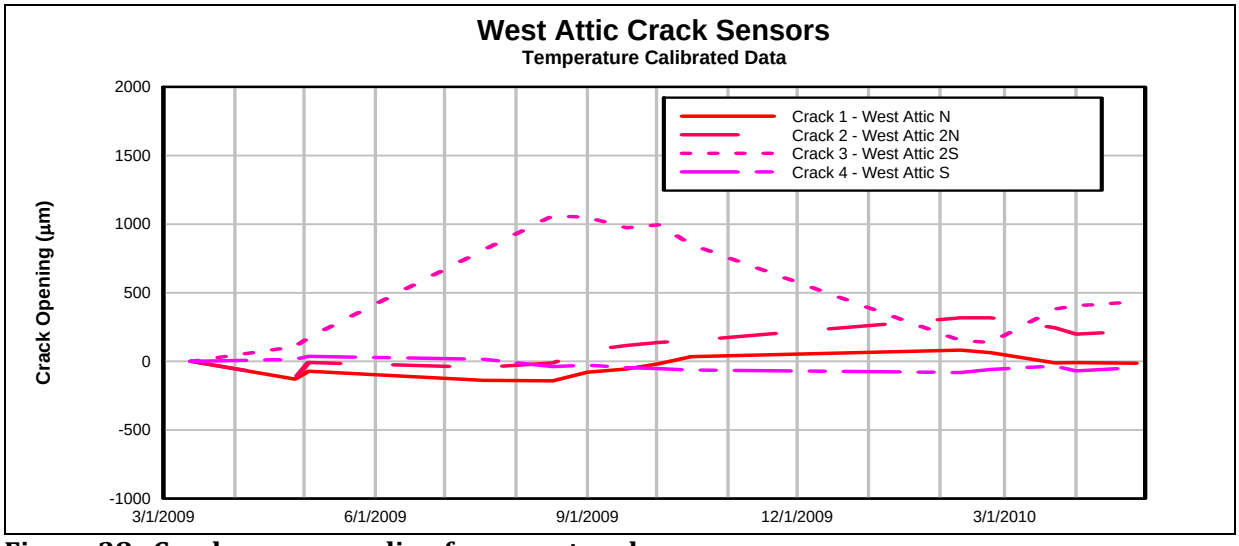

Figure 38. Crack sensor reading from west arch.

The long term crack readings have already been temperature-compensated. Figure 38 and Figure 39 show that the sensors in the middle of the vault (Crack Sensors 2, 3 and 10, 11) show more movement than those closer to the spandrel walls. The spandrel walls provide additional stiffness to the arch and restrict movement of the crack.

Figure 40 shows data recorded by temperature sensors mounted in different locations of the structure. Comparing Figure 40 with Figure 38 and Figure 39, Crack Sensor #3 follows the same trend as Temperature Sensor #1 while crack sensor #11 shows an inverse trend.

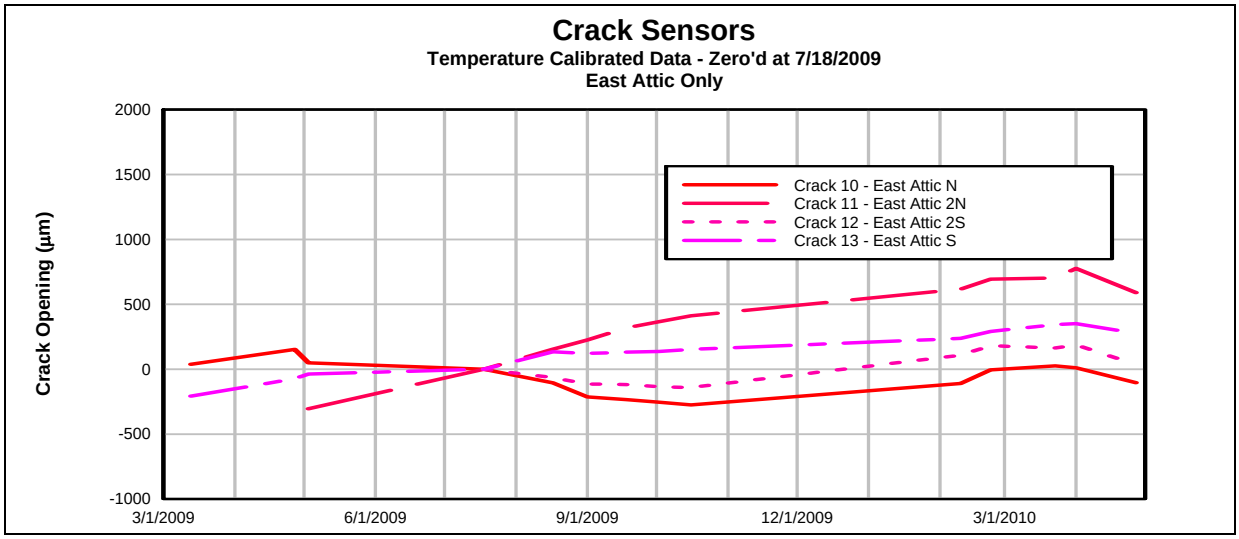

Figure 39. Crack sensor reading from east arch.

The fiber optic accelerometers used on the arch had a maximum resonant frequency of 50 Hz. These accelerometers showed negligible amounts of vibration in both the short term and long term. The masonry arches and supporting walls form a very rigid

structure. No significant or differential vibrations on opposing sides of the longitudinal arch cracks were occurring.

Figure 41 shows data recorded for tiltmeters 5 and 8 along the center wall. Tiltmeter 5 was located at the top floor, or directly under the arch. This tiltmeter shows the most movement. Tilt measurements show a pronounced decrease toward the lower floors. This would be expected as the floor framing provides greater restraint at the lower levels and the effect of the arch thrust is dissipated. The tiltmeters by design are automatically temperature compensated. Therefore, the recorded wall tilt is due to actual movement of the wall and not temperature related errors in the sensors. The wall tilt tends to follow the temperature fluctuations. The maximum and minimum peaks of Tiltmeter 5 correspond to the temperature peaks. Thus the tilt can be attributed to thermal expansion and contraction in the arch. The maximum tilt of Tiltmeter 5 was just over 0.3 degrees.

For comparison, Figure 41 also shows the 2 tiltmeters on the west wall. This wall is restrained on the outside edge by masonry counterforts supporting the steel trusses spanning over the adjacent roadway. In other words, the data confirm that this wall is more rigidly constrained.

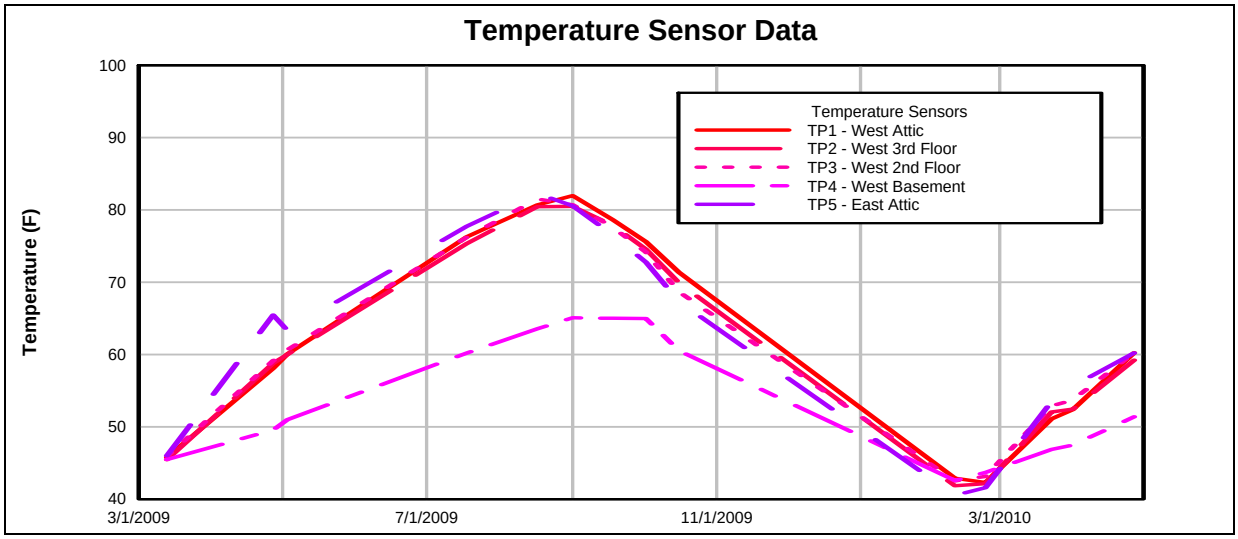

Figure 40. Temperature sensor readings.

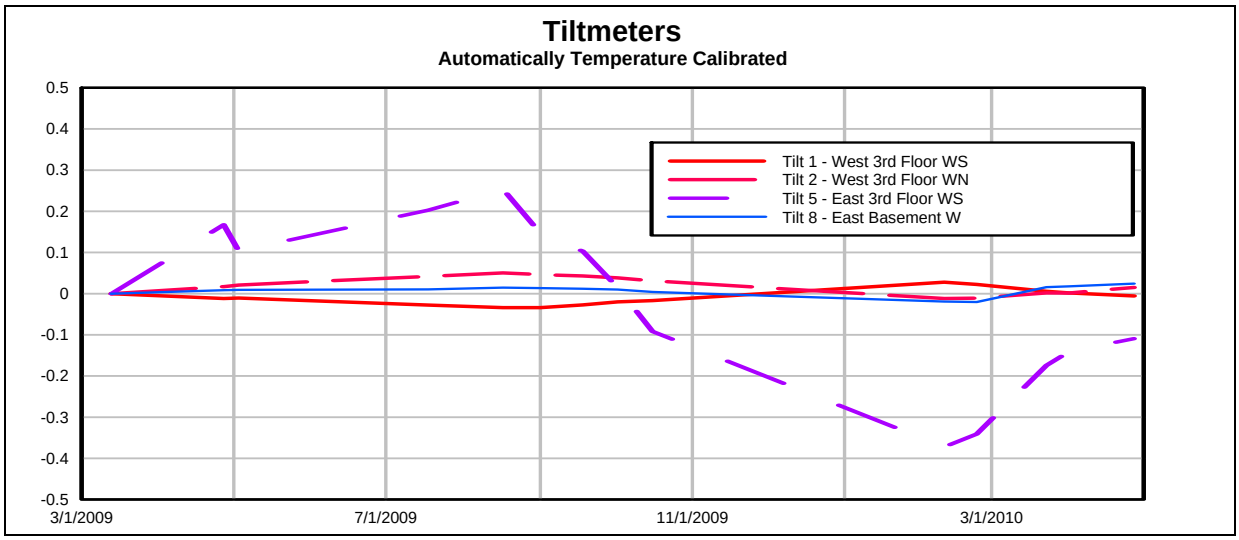

Figure 41. Tiltmeter sensor readings.

4. LABORATORY TESTING: SUPPORT MOVEMENT TESTS OF SCALED LABORATORY MODELS OF BROOKLYN BRIDGE ARCH

4.1. Arch Design and Test Setup

In order to better understand the effects of support movement on semi-circular masonry arches, a series of scaled brick arch models were created and tested in the laboratory. The brick arches were built at 1/12 scale when compared to the Brooklyn Approach Span 3.

Five arches were tested. Figure 42 shows a diagram of the test setup and Figure 43 shows the dimensions of the test arch. Table 2 lists a summary of the tests performed on the arches. Three of the arches were tested by spreading, or pulling, the foundation supports. The other two arches were tested by compressing, or squeezing the supports. Arch Test E was also tested by cyclic movement of the arch supports. The cyclic test assisted with the visualization of the hinge formations and their behavior.

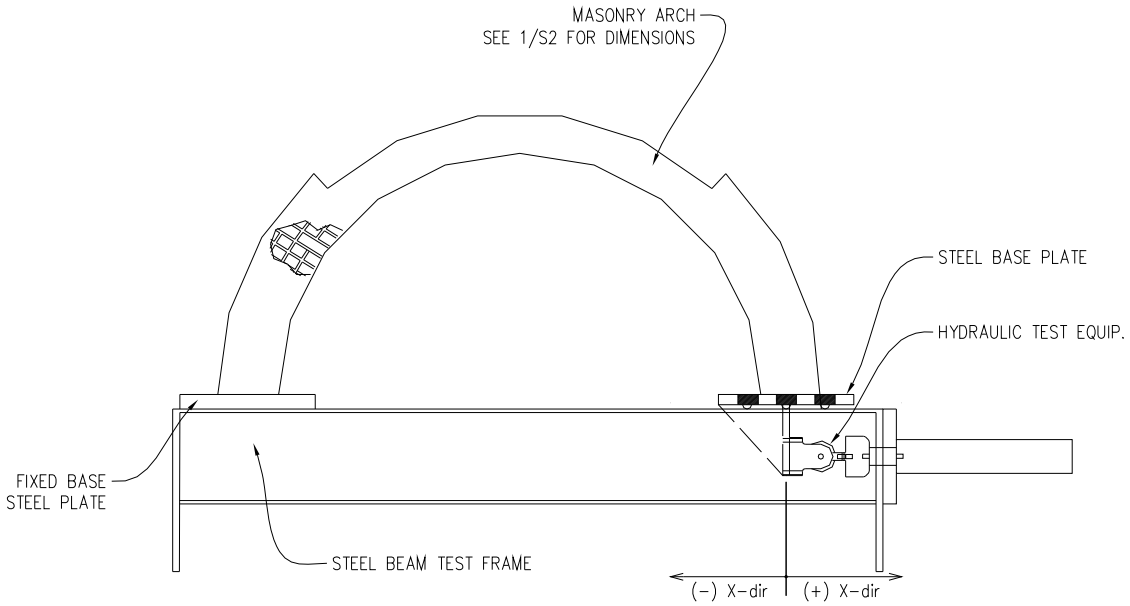

Figure 42. Test setup configuration of laboratory arch tests.

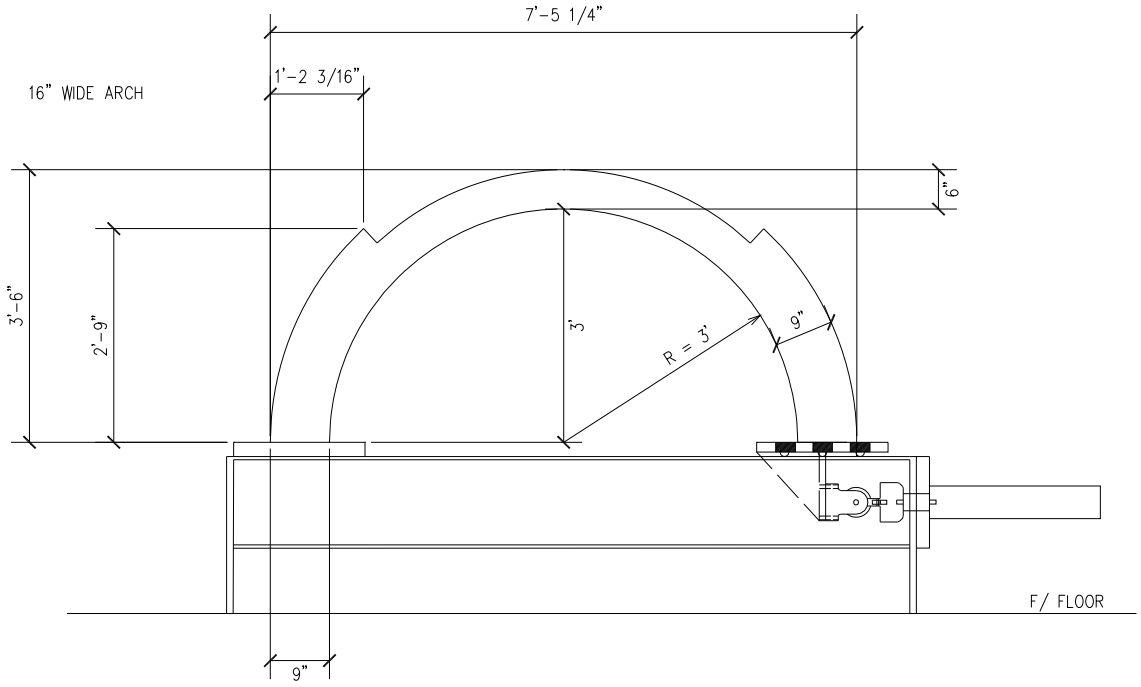

Figure 43. Dimensions of laboratory test arches.

Arch Test	Test Stage	Tested Support Movement
Test A		
	A.1	0 to 0.60"
	A.2	0 to 2.20"
Test B		
	B.1	0 to 0.16"
	B.2	0.16" to 0"
	B.3	0 to 1.00"
Test C		
	C.1	0 to -0.10"
	C.2	0 to -0.15"
	C.3	0 to -0.15"
	C.4	0 to -0.15"
	C.5	0 to -0.15"
Test D		
	D.1	0 to -0.05"
	D.2	0 to -0.10"
	D.3	0 to - 0.30"
	D.4	0 to -0.80"
	D.5	0 to -0.80"
Test E		
	E.1	0 to 0.10"
	E.2	0 to 0.10"
	E.3	0 to 0.60"
	E.4	0.60" to 0
	E.5	0 to 1.00"
	E.6	1.00" to 0
	E.7	cyclic +/- 1.00"
	E.8	0 to 3.00"

Table 2. Test summary, refer to Figure 42 for defined support movement direction.

4.2. Material Properties

The arches were constructed of solid clay bricks. The bricks were new brick supplied by a local brick manufacturer.

In order to construct the scaled model, the full size bricks were cut down. A full size brick with the dimensions of 2-1/4" (t) x 3-1/2" (W) x 7-1/2" (L) was cut into four pieces. The bricks used in the test arches had the dimensions of 1-1/8" (t) x 1-1/4" (W) x 7-1/2 (L). The bricks were cut to a smaller size to maintain a mortar to brick ratio comparable to that of the original structure. The brick lengths were not critical to the mortar to brick ratio in the laboratory tests and hence the lengths had their original dimension.

A type N mortar was used for the construction of the arches. The mortar was intentionally mixed to a weaker ratio to be a better comparison of the mortar in historic arch bridge structures. From a practicality of construction point of view, the mortar joint thickness was scaled slightly less than the 4:1 ratio used for the bricks. The mortar joints thickness was approximately 1/4".

In order to determine the strength and modulus of elasticity of the masonry used for the arch construction, a number of tests were made on brick prisms. The compression tests were conducted per ASTM 1314 (Figure 44). Various types and sizes of prisms were constructed in order to gain an understanding of the effects of the slenderness and mortar joint thickness effects. However, it was discovered that the range of test results was relatively similar despite the varying conditions used for the prism construction. Four compression prisms were tested for each of the five test arches. A summary of the

test results from one set of prisms is plotted in Figure 45 and the average compressive strength and Young's modulus for all of the tested prisms is shown in Table 3.

Figure 44. Masonry compression tests.

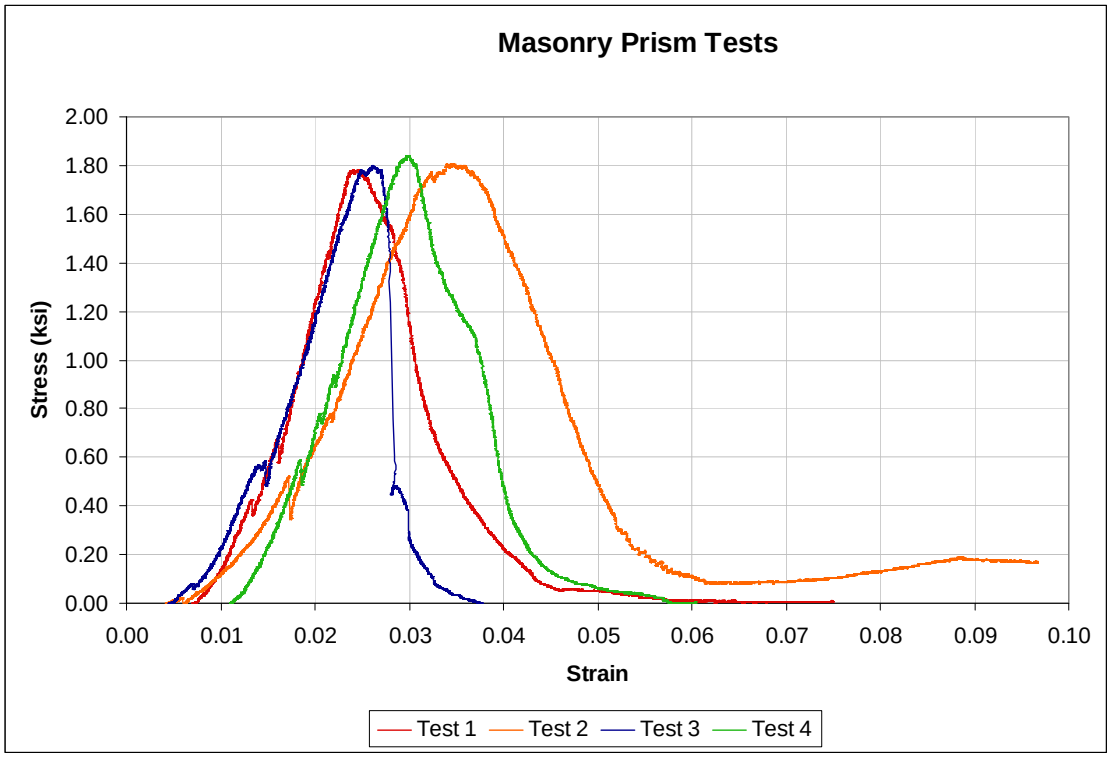

Figure 45. Summary of sample masonry prism tests.

Masonry Properties	
$f`_m$	1780 psi
E	132000 psi
f_t	40 psi

where,

$f`_m$ = ultimate compressive strength (psi)

E = Young's Modulus (psi)

f_t = modulus of rupture (psi)

Table 3. Average material properties for test arch.

Figure 46. Modulus of rupture test setup.

In addition to the standard compression tests, three modulus of rupture tests per ASTM C293 were performed (Figure 46). These tests were completed in order to confirm the performance of the mortar joints in tension. The underlying assumption in many masonry arch analyses is that the mortar joints have no strength in tension. The results of the modulus of rupture tests confirmed that such an assumption would be valid for our laboratory model. The tests concluded that the tensile strength of the mortar joints was 2% of the compressive strength.

4.3. Test Summary and Results

The following is a summary of the test results.

4.3.1. Arch Test A

This arch was tested by pulling the right abutment, or simulating support spread. Figure 47 and Figure 48 shows the arch test setup. Figure 47(a) shows the measurement setup for vertical deflection at the crown. The support at the right side of this photograph will be moved to simulate the support spread. Figure 47(b) shows the opposite side of the arch. The laser measuring device and computer setup can be seen in the background.

Fiber optic crack sensors were employed on the crown of the arch (Figure 48). As the exact location of the crack formation was not known prior to the test, three sensors were staggered across the intrados and extrados of the arch to insure that the crack displacement would be captured as it formed (Figure 49). Figure 50 shows the hinge near the crown. The crack, shown in its early stages before it fully extended across the entire cross section, was located one course off of the crown. This type of variation can be expected in masonry structures where the quality control of materials and mortar joints can vary greatly. At larger displacements, a second and third hinge formed at each of the supports. Figure 51 shows an example of this hinge creation. The crack openings at the support hinges were smaller than at the crown.

(a) (b)

Figure 47. Arch test setup.

(a) (b)

Figure 48. Fiber optic sensor layout.

Figure 49. Crack at crown being measured by fiber optic crack sensors.

Figure 50. Hinge formation just off center of crown.

Figure 51. Typical hinge formation at support.

Two primary tests were completed. The first test involved a support movement ranging from 0 to +0.60 inches. The second test involved a support movement ranging from 0 to +2.20 inches. Prior to the two primary tests, a low amplitude test was conducted up to 0.10 inches in order to measure the initial stiffness of the newly constructed, undamaged arch. Figure 52 shows the horizontal thrust vs. displacement plots for the three tests. As can be seen in the plots, the horizontal thrust of the arch decreases as the support movement increases.

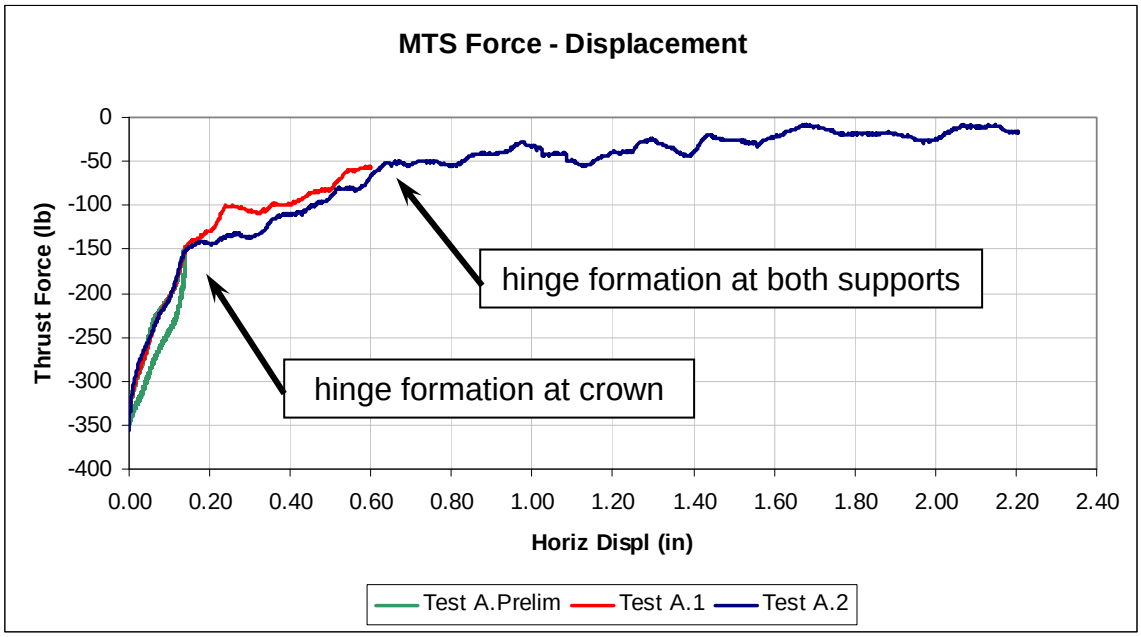

Figure 52. Horizontal thrust vs. horizontal displacement plots for Test A.

The tests show a very linear elastic response up to 0.15" of support movement, or less than 0.2% of the span length. Beyond that point, the stiffness of the arch greatly decreases. This point at 0.15" marks the initiation of the crack at the crown. At 0.60" of displacement, the cracks at the crown and supports have extended across the cross section thickness of the arch; hence marking the occurrence of a three hinged arch. At this point, there is essentially no change in the thrust force with increasing support movement which is by definition of analysis the expected behavior of a three-hinged arch.

Figure 53 shows the linear approximation of the data in Figure 52 in order to assess the arch stiffness. The stiffness of the arch prior to 0.15" of support movement for Tests A.1

and A.2 was 1139 lb/in. This is in the linear elastic range before any crack formation. Beyond that point, the stiffness tapers of to a value almost a full order of magnitude less than the initial stiffness value. The stiffness from Test A.1 was 146 lb/in and for Test A.2 was 105 lb/in. As can be seen from the stiffness values, there was some degradation between the two tests. This can be attributed to some wear of the mortar joints and additional microcracking.

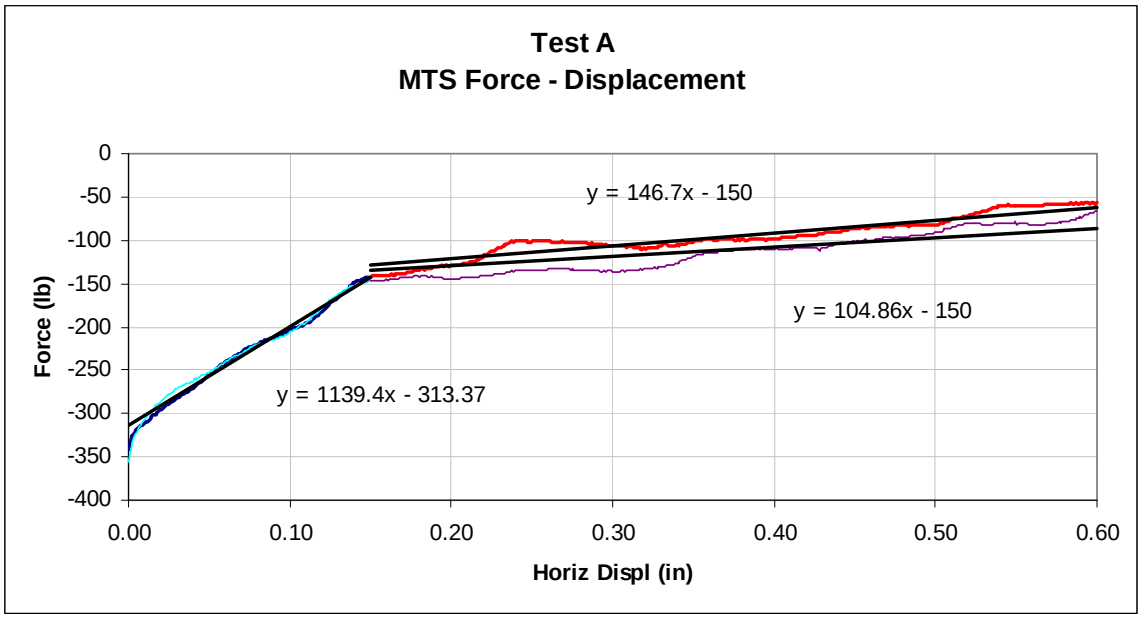

Figure 53. Arch stiffness from Test A.1 and Test A.2 (plot zoomed into range of 0.0 inches to 0.60 inches).

During the tests, the relationship between the deflections at the crown and horizontal support movement was compared. The vertical displacement at the crown was measured with both a dial gauge and a laser Doppler vibrometer. As can be seen in Figure 54 from Test A.2, the relationship is approximately equal to:

$$0.4 \times \Delta H_{\text{sup}\,port} = \Delta V_{crown} \qquad (33)$$

where,

$\Delta H_{\text{sup port}}$ = horizontal support movement

ΔV_{crown} = vertical displacement at crown

This relationship was found to be fairly consisted between all of the laboratory arch tests in which the support spread was simulated.

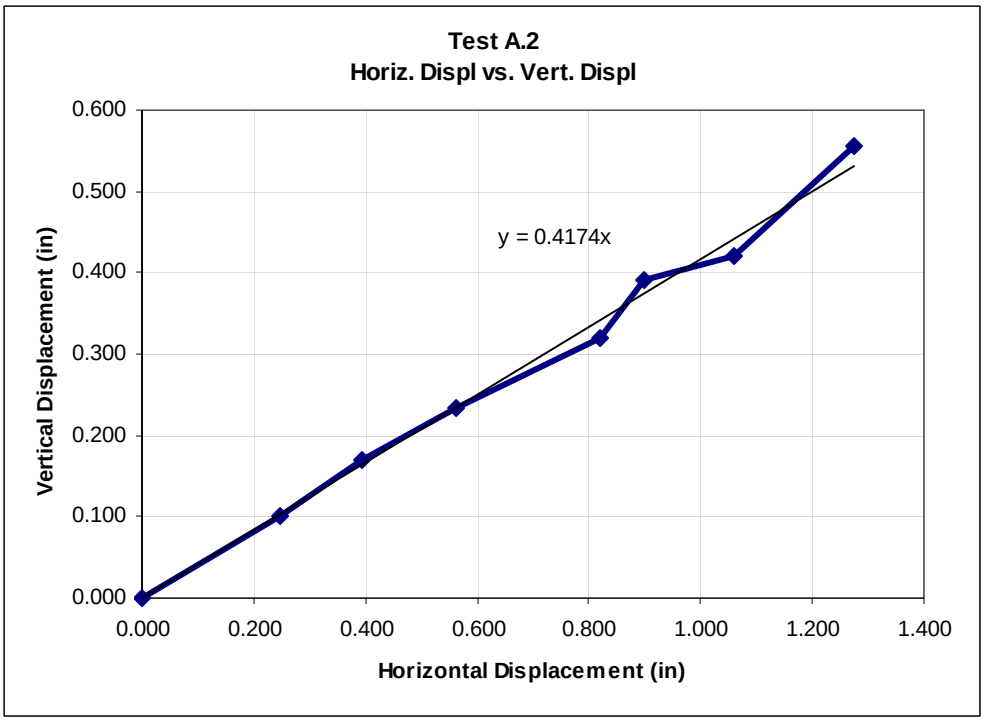

Figure 54. Relationship between support movement and vertical displacement at crown.

4.3.2. Arch Test B

Three support movement tests were conducted for Arch Test B. In general, these tests were comparable to the results from Test Arch A. A hinge crack again occurred near the crown (Figure 55). As the support movement increased, the crack grew until it had fully

traversed the width of the arch section (Figure 56). Also, as in Arch Test A, the support points of the arch rotated and hinge cracks opened at these locations (Figure 57).

Figure 55. Initial hinge formation at crown.

Figure 56. Fully cracked hinge at crown (located 2 courses from center).

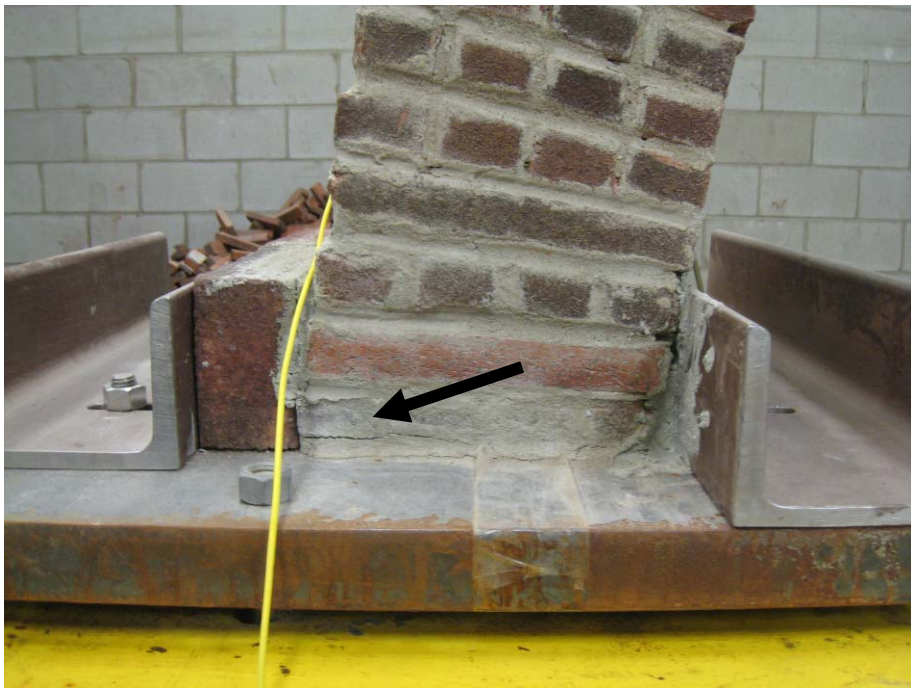

Figure 57. Hinge formation at supports.

The horizontal displacement vs. thrust plots for the three tests on Arch B are shown in Figure 58. As with Test A, there are three distinct phases of the load displacement plot. The first section is from 0 to 0.04" of displacement, the second section is from 0.04" to 0.16" of displacement and the final section in which the arch is acting fully as a three-hinged arch is beyond 0.16" of displacement.

Figure 59 shows the stiffness values for the various stages of the load displacement test. When compared to the stiffness values of Figure 53, it can be seen that this arch behavior was stiffer than Arch A and the hinge cracks occurred at slightly lower displacement values. This is to be expected in tests on masonry construction. Masonry is an orthotropic material made up of bricks and mortar joints. Also, there is much variability in the ratio of ingredients for mortar and how the mortar itself is placed by the mason. All of these factors contribute to the variation in the displacement at which the hinge cracks occur. However, the most important conclusion to take away from the data comparison of Test A and Test B is that the hinge cracks form at very low displacements; less than 0.2% of the span length. Therefore, it can be concluded that almost all existing in-use arch bridges already have cracks at three hinge points. The crack openings may be very small and difficult to visually identify, but it is likely that they exist. Also, it should be noted that the hinge cracks may not always occur only at the crown and supports. In the case of the laboratory test arches, these hinge locations are expected based on the arch geometry and the fact that there are no fill loads on the

arch. In-situ bridges may have hinge cracks occurring at different locations. This will be discussed further in the ensuing section of this dissertation.

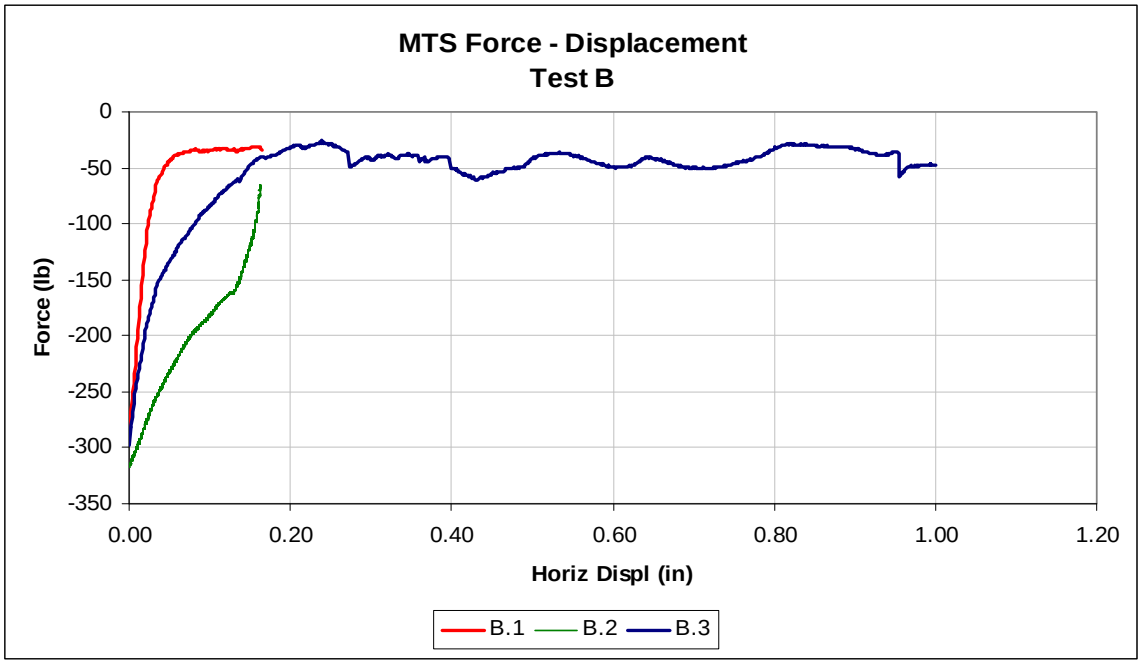

Figure 58. Thrust vs. displacement plot, Arch Test B.

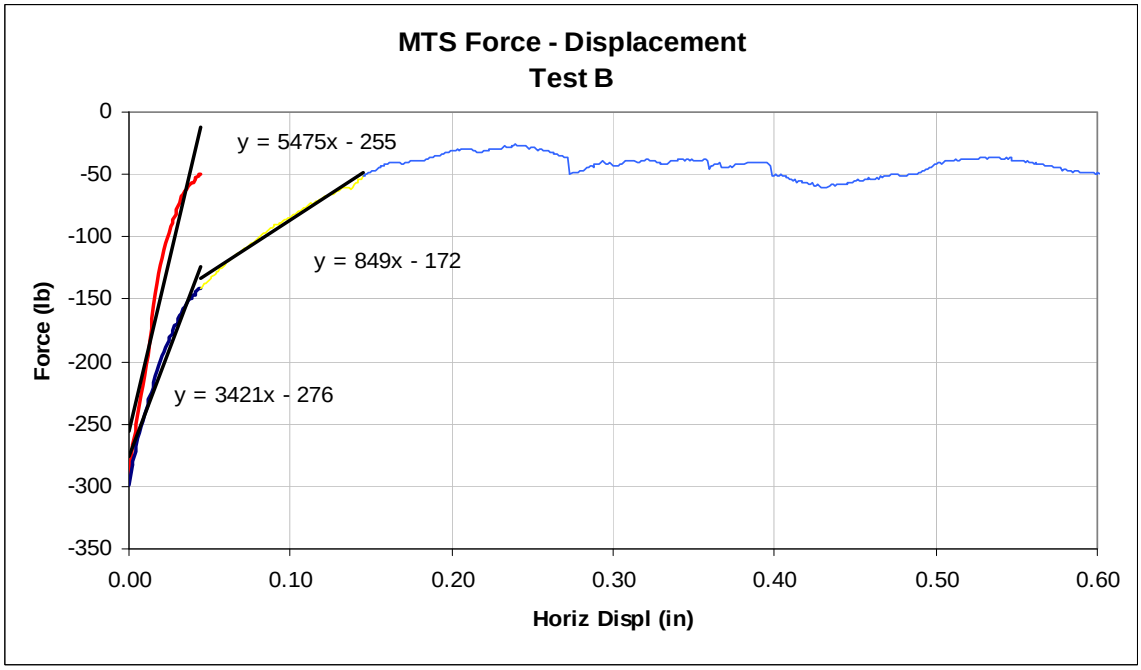

Figure 59. Stiffness values for Test B load displacement plot.

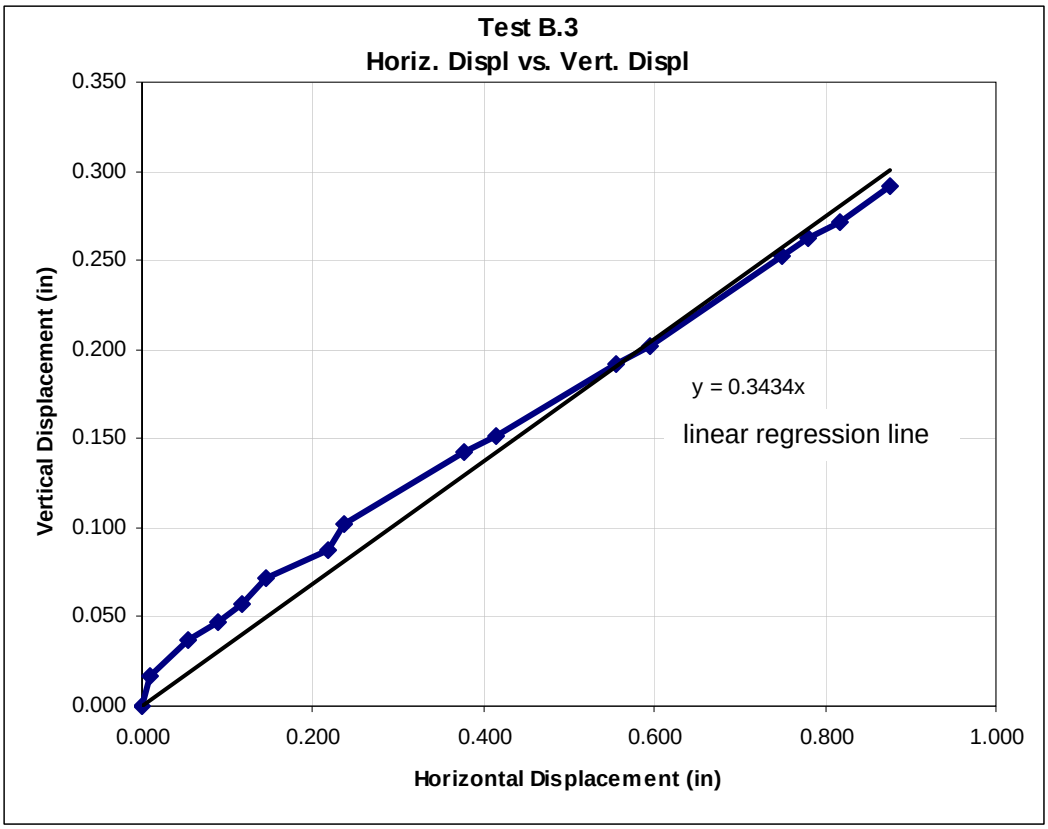

Figure 60. Horizontal displacement vs. vertical deflection for Test B.

For comparison to Test A data, Figure 60 shows the ratios of horizontal displacement vs. vertical deflection. For Test B, the ratio is was 0.34 which is slightly less, but still with the range of the results found for Test A.

As noted in Test A, fiber optic crack gauges were used to measure strain across the mortar joints and then crack opening displacement if a crack were to occur at the location of one of the sensors.

Figure 61 is a plot of the recorded data for Test B.3. As can be seen in the plot, the hinge crack at the crown went through the left side crack sensors. The crack opening displacement was recorded by both the sensors on top and bottom of the arch. The circled locations in Figure 61 show the locations where the hinges occur at 0.03" and 0.16". At these points, the slope of the recorded crack opening data changes reflecting the lower global stiffness of the masonry arch.

In addition to the recorded lateral movement and crack opening data, a few measurements were made in regards to a vertical point load at the crown for later calibration with the numerical modeling. A point load of 200 pounds was applied at the crown of the arch. In the uncracked, or point of no lateral support movement, no vertical deflection was measured when the point load was applied. However, when the 200 pound point load was applied following 1" of lateral support movement, an average deflection of 0.014" was measured. This shows the serviceability effects that can be encountered when an arch experiences lateral movement at the supports. This will be further elaborated upon later in the thesis as it is shown that while the ultimate load strength of arch will remain the same with or without support movement, there is a much more noticeable difference in vertical deflection in the case with support movement. This can cause serviceability problems with masonry arch bridges.

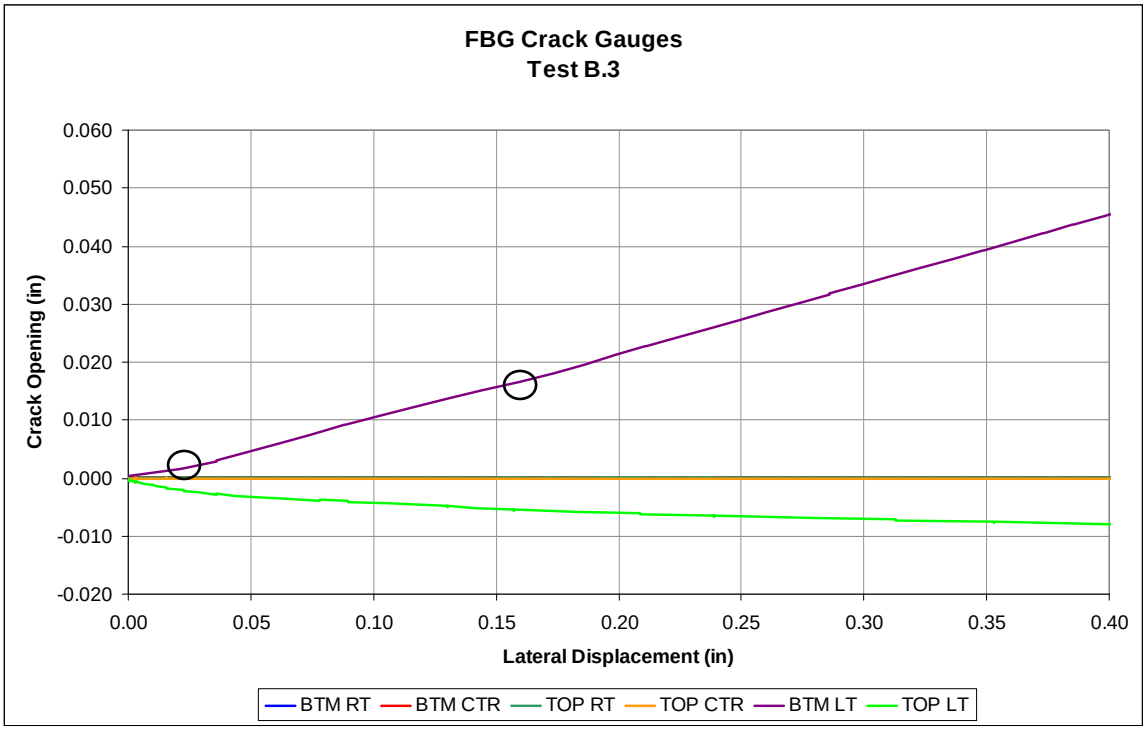

Figure 61. FBG crack gauge data for test B.3. (BTMLT is the top most data line, TOPLT is the lower plotted data line, the other sensor data lines track along y=0).

4.3.3. Test C

Arch C was the first arch tested by pushing the arch support inward as opposed to outward for lateral spread. Five tests from 0 to -0.15" were carried out for this arch.

The primary difference with this inward support movement test as compared to the previous two lateral support spread tests was the location of the hinges. Hinge points still occurred at each of the abutments, but instead of at the crown, a hinge occurred at approximately near the quarter point of the span on the extrados side of the arch (Figure 62). As the test cycles progressed, the condition of the mortar at this hinge crack

worsened. During Test C.4, a piece of brick adjacent to the hinge crack at the intrados side fell out. This was a good example of the type of deterioration and degradation that can occur in masonry arches that may not cause an immediate structural collapse, but would pose maintenance problems for the bridge owner and safety concerns of falling debris.

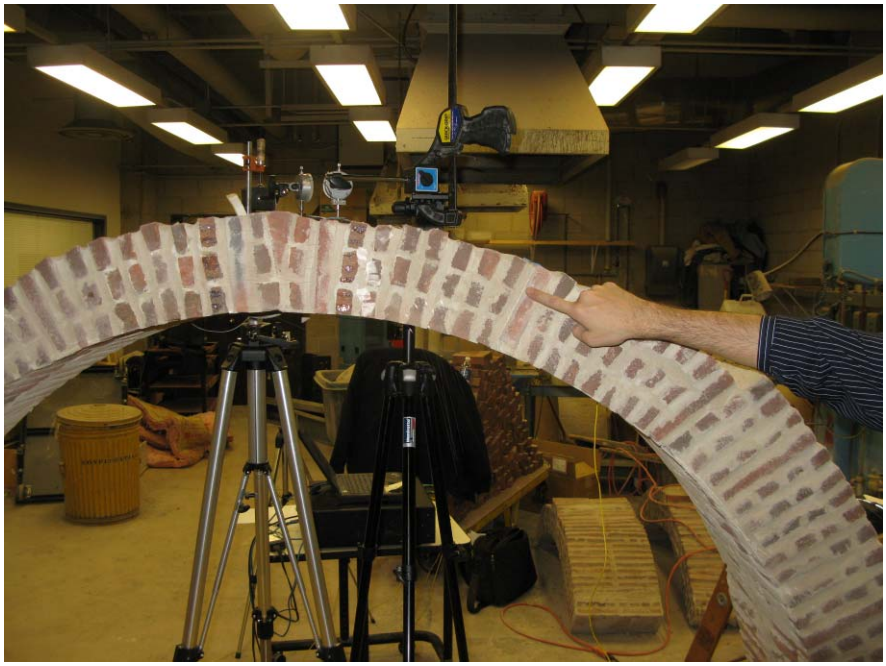

Figure 62. Crack at quarter point, Arch Test C.

Figure 63. Crack condition after repetitive test cycles.

Figure 64 shows the horizontal thrust vs. support displacement data for the five tests. The most significant occurrence was the first formation of the quarter point hinge during Test C.2 at approximately 0.13" of support movement. After that point, the stiffness of the arch began to decrease in subsequent tests until tests C.4 and C.5 when there was little residual stiffness. The lateral thrust force of approximately 250 pounds in these two tests was the reaction of the arch weight providing resistance against the inward support movement. While there was little remaining arch stiffness in Tests C.4 and C.5, it should be noted that the arch was not in a state of collapse. Other factors such as weight from the fill material and the vertical load configuration on an arch will influence the ultimate collapse load. In the case of this test arch, it was only supporting

its self weight. Despite the fact that the arch was still stable, uncontrolled crack growth is a concern for an arch such as this if it were to undergo additional support movement.

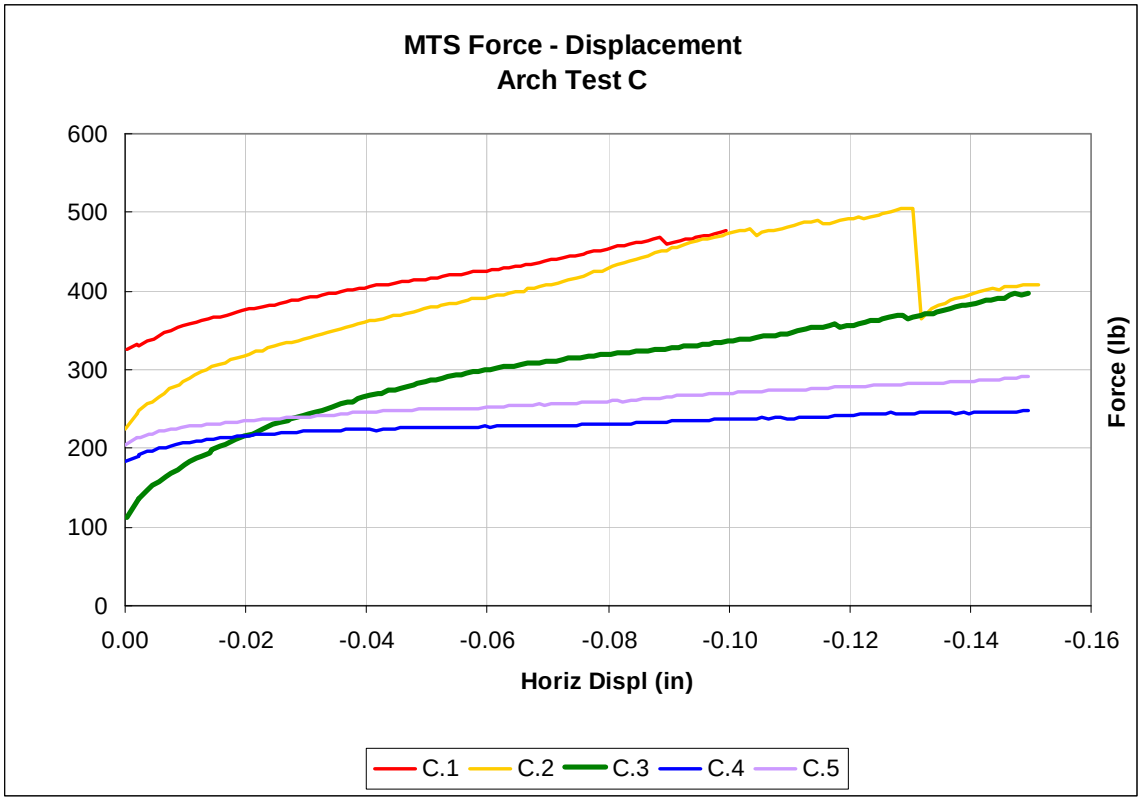

Figure 64. Thrust vs. displacement plot for Test Arch C.

Figure 65 shows low level stain recordings from the crack sensors near the crown of the arch in the first arch test of this series. A visible hinge crack was never observed at this arch but there was measureable strain across several mortar joints. In Test C.4 more significant crack opening displacements were recorded at the quarter point crack (Figure 66).

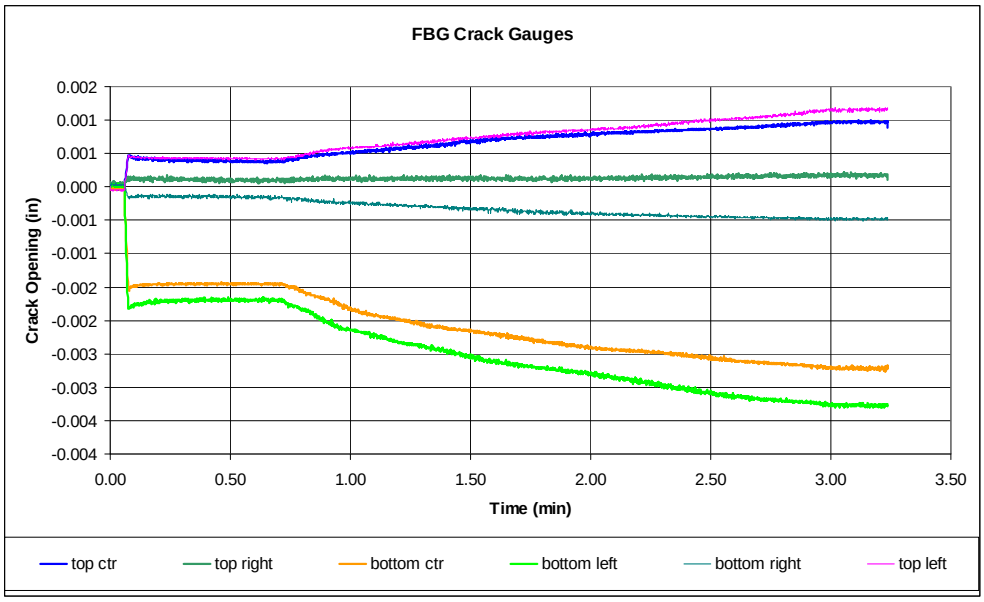

Figure 65. Low level strain readings near crown of test C.1.

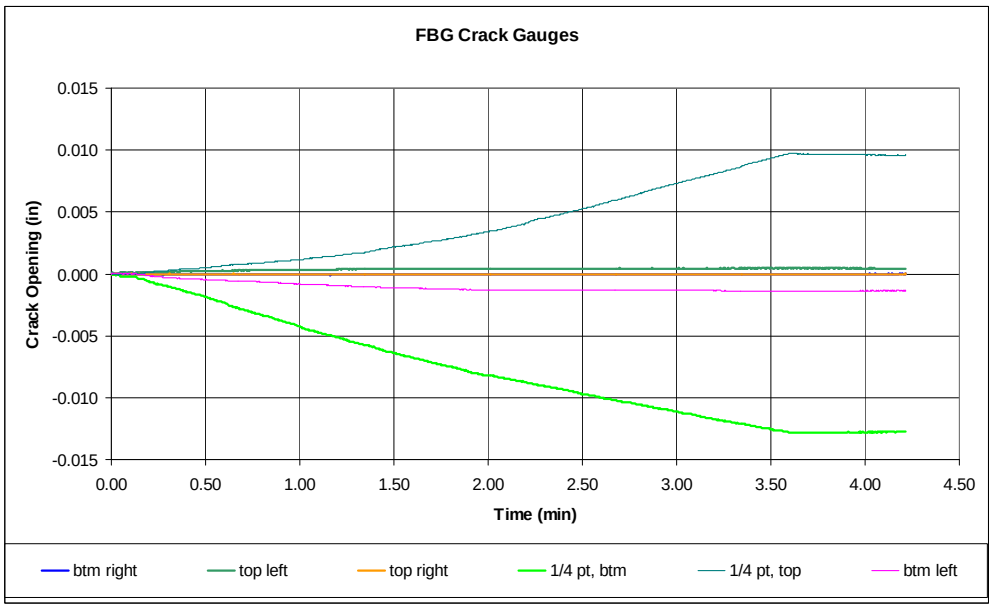

Figure 66. Larger crack opening displacement at 1/4 point span crack.

4.3.4. Test D

Test D also consisted of inward support movements. While not wholly unexpected, the hinge locations of Test D occurred at locations slightly different than those in prior tests. A hinge still occurred at the right support, although about 8" above the bottom surface of the arch base (Figure 67). Another hinge occurred near the quarter point on the opposing side from the moving support (Figure 68). This was similar to the quarter point hinge of Test C, just slightly closer to the abutment. The third hinge instead of occurring at the other support occurred at the crown (Figure 69).

The location of hinge cracks in masonry arches is primarily dictated by the internal forces of the arch and the location of the thrust line. However, as discussed earlier, masonry is an orthotropic material of mortar and bricks. Expected variability of workmanship also contributed to the orthotropic nature of masonry. As a result, the exact hinge locations can not always be precisely predicted by numerical analysis. A less compacted mortar joint or a differently proportioned batch of mortar may cause a slight drift in the location of a hinge crack.

Figure 67. Hinge formation at right support.

Figure 68. Hinge formation at arch quarter point.

Figure 69. Hinge formation at crown.

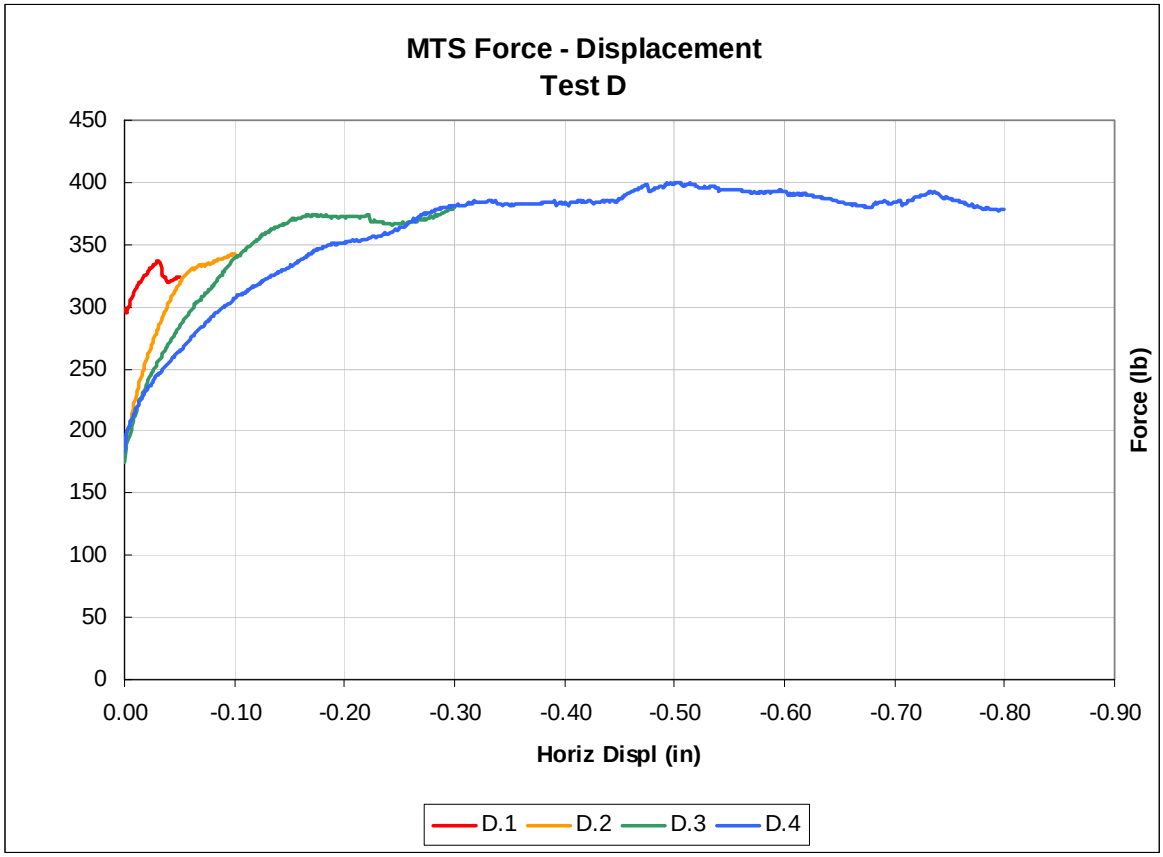

Figure 70. Thrust vs. displacement plot for Test Arch D.

The horizontal load deflection data for Arch D (Figure 70) was very similar to that of Arch C. As subsequent testing progressed, the stiffness of the arch lessened. In Test D.1, it can be observed that the quarter point hinge crack formed at a horizontal displacement of 0.05", or less than 0.1% of the span length. Again, this small amount of support displacement would be expected to have occurred of an arch bridge of any significant age due to normal soil settlement. Therefore, it would be expected that most in-service masonry arch bridges are in a three-hinge configuration due to existing cracks.

5. CURRENT STUDY AND PROPOSED FORMULATION

As discussed in preceding chapters, there is a need for a masonry arch bridge analysis method that can be used to verify field data obtained from a structural health monitoring program. Current analysis methods estimate the ultimate load capacity of the bridge but do not provide any guidance for estimates of crack opening displacement and deflection under service loads. Also, current analysis methods do not fully model the response of a bridge that has experienced support movement.

For bridges constructed of steel or reinforced concrete, a finite element analysis is typically used to assist with the understanding of strains, crack openings, and deflections measured during a structural health monitoring program. However, as discussed previously, there are many difficulties when modeling a masonry arch structure in a finite element program in particular due to the nonlinear behavior and lack of tensile strength across mortar joints. In recent years, various analysis techniques for masonry arch analysis using limit state and rigid block algorithms have been developed. These techniques have shown promising results for calculating the ultimate load capacity of a masonry arch, but again do not provide any assistance for understanding the in-situ performance of the arch in terms of crack openings and support movement.

The mechanism based model developed for this dissertation implements the modeling strategies and assumptions of a limit state analysis into a methodology that can be analyzed within the framework of a finite element software program. The mechanism based model has similar hinge formation and material assumptions as a limit state, or rigid block analysis method. However, creating the arch model using the proposed methodology allows for deflection and crack opening data to be calculated for easy interpretation and comparison with structural health monitoring data. Also, the methodology can be modeled with support movement to determine its effect on load capacity and crack opening displacement. Modeling the proposed methodology in a finite element program requires no specialized software and allows for any geometric shape, any load combination, and any fill loads to be analyzed.

The following is an overview of the proposed methodology. The details, derivations, and explanations of the steps are presented in the subsequent sections.

1. Model the two dimensional geometry of the masonry arch bridge to be analyzed as shell elements in a finite element program (Figure 71).
    a. It is not necessary to model each individual stone voussoir or course of brick, but it is recommended that the arch model be discretized into a minimum of 12 to 15 elements.
    b. Modulus and density of shell elements should be an accurate estimate of the actual material properties.

c. Model the shell elements as having a unit width.

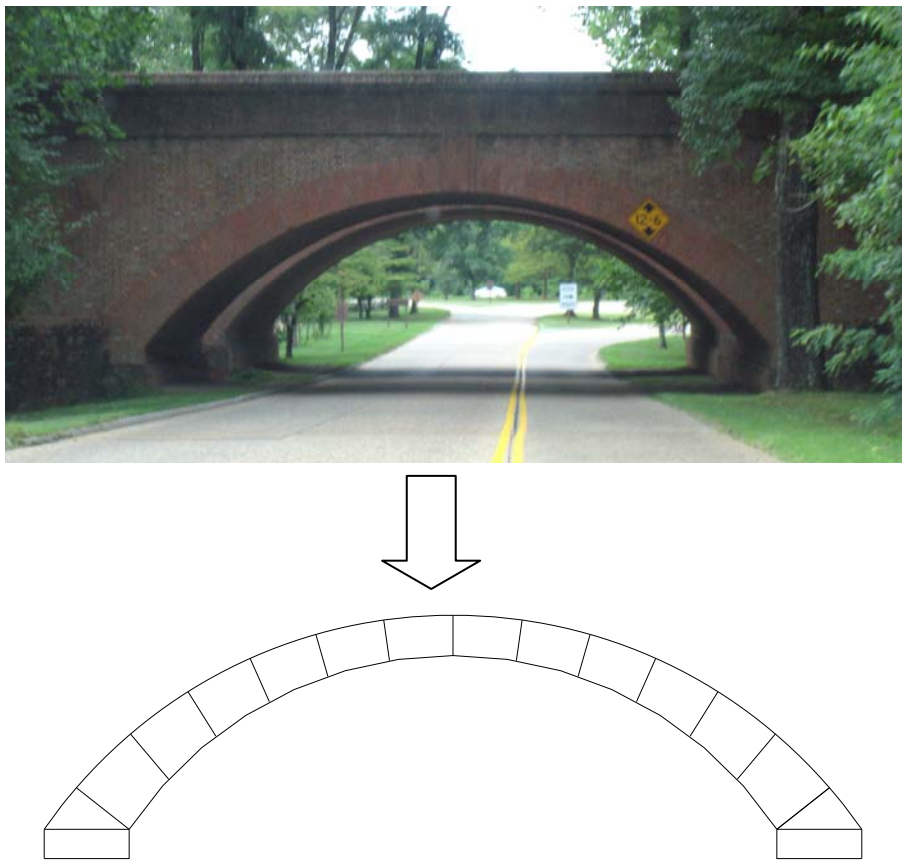

Figure 71. Modeling arch bridge as shell elements.

2. A small gap should be modeled between each of the shell elements (Figure 72). This will later be connected with the compression only links. The compression only links across the gap allow for the formation of hinges in the arch.

    a. The width of the gap can be arbitrarily chosen since the links across it are modeled with the same stiffness as the masonry shell elements. However, in order to eliminate the possibility of any geometric based errors, it is

recommended that the gap be modeled as less than 2% of the total length of the individual shell elements.

3. Each of the shell elements is divided into multiple layers of the same (Figure 73). The discretized mesh can be as small as desired, but it has been found that five elements across the cross section yield accurate results while minimizing the amount of modeling and computation time. Dividing the arch into smaller elements across the cross section allows for a more accurate representation of the thrust line in the analysis.

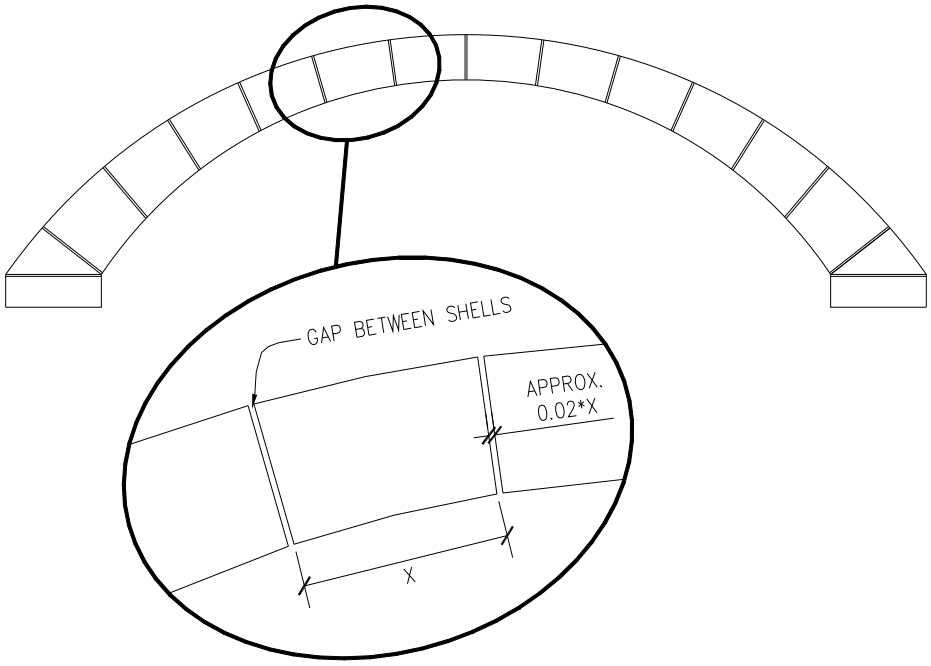

Figure 72. Small gap modeled between shell elements.

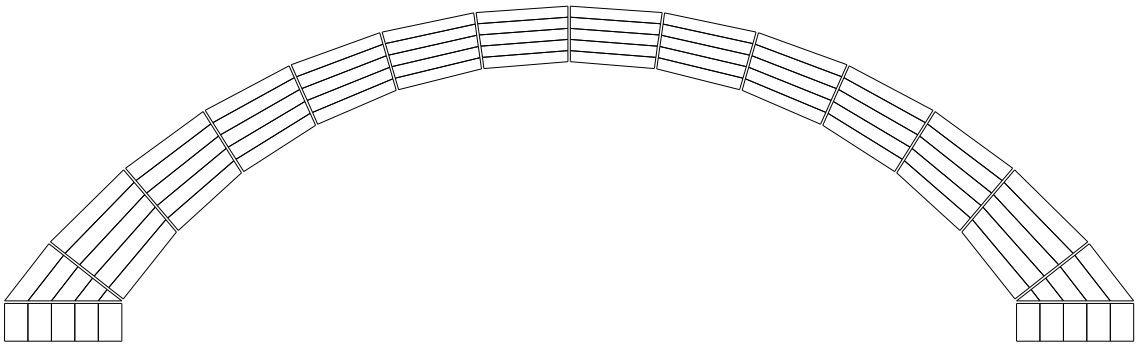

Figure 73. Shell elements discretized into five elements across the cross section of arch.

4. The gaps between adjacent shell elements nodes are connected with compression only links (Figure 74).
    a. The links transfer only compression forces in the axial direction with a stiffness, $k = EA_{tributary} / L_{link}$, where $E = E_{masonry}$.
    b. The links can allow the joints to open up, and do not have any tensile strength or stiffness.
    c. The links are fixed in the shear direction.
    d. The links are pinned at the ends allowing for rotation between adjacent shell elements.

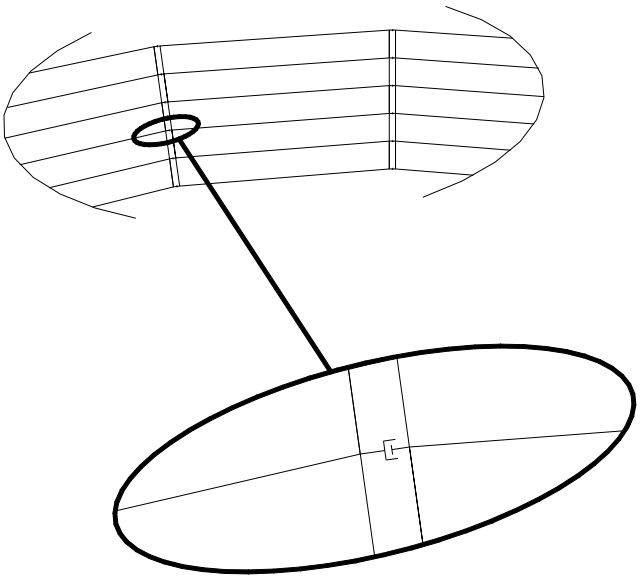

Figure 74. Compression only link between nodes of shell elements.

5. The weight of the masonry arch and fill is added to the bridge.
    a. The self-weight of the masonry is defined by applying the density of the masonry to the shell elements.
    b. The fill weight is modeled based on a tributary area basis and applied as point loads to the top of the arch bridge (Figure 75a and 75b).

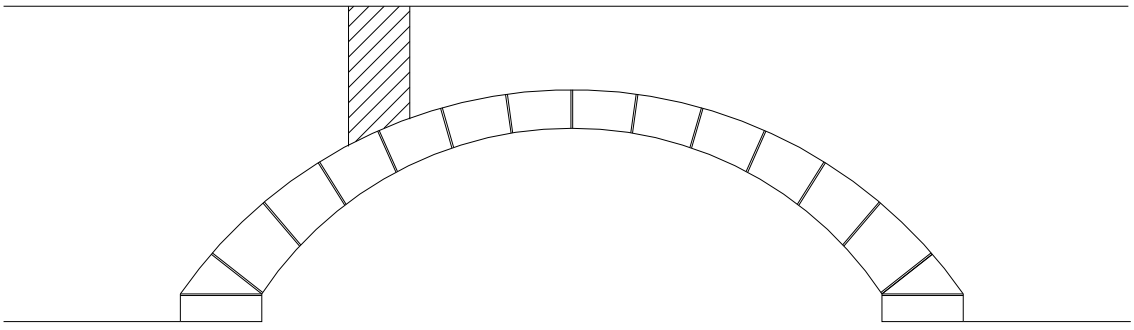

Figure 75a. Area of fill to be modeled as a point load.

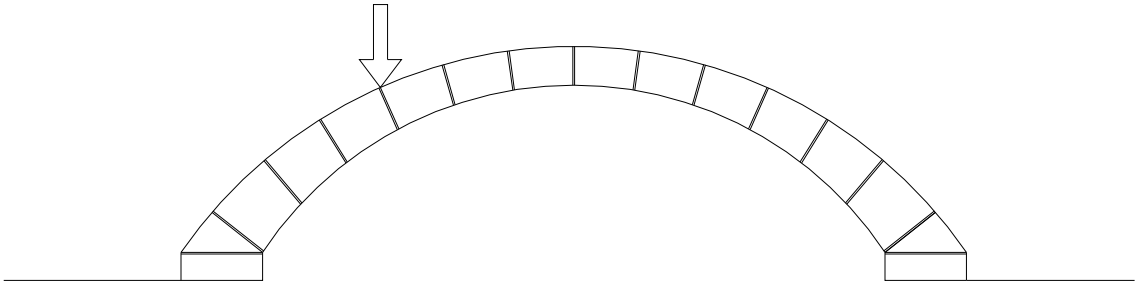

Figure 75b. Weight of fill represented by a point load. (Shown for one section only, repeat along the length of the bridge.)

6. An abutment element is modeled as a masonry block shell. The abutment element is connected to the masonry arch with the same compression only links as the ones in between the shell elements of the arch. The bottom of the element is modeled as a pinned connection.

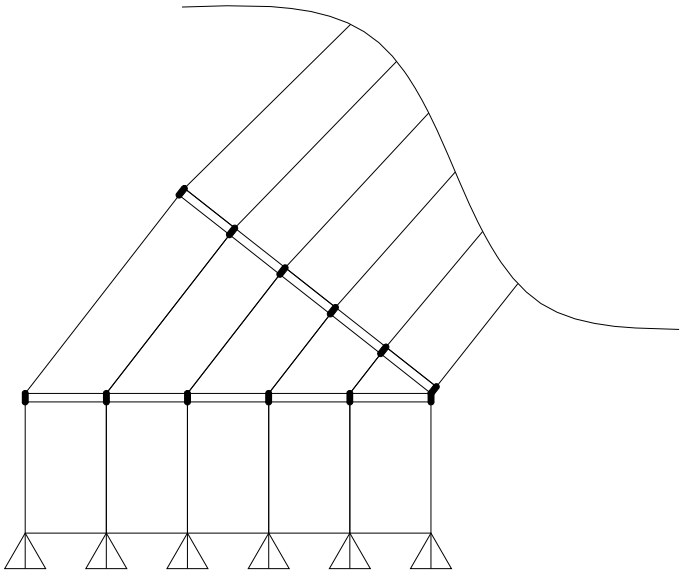

Figure 76. Abutment pin connection.

7. Apply point loads for vehicle live load (Figure 77).
    a. Various axle and vehicle load cases can be modeled as individual load cases
    b. If desired, the axle load can be distributed on a 1 horizontal: 2 vertical ratio through the fill (Figure 78). However, for simplicity modeling the axle loads as point loads will be sufficient (Figure 79).
    c. The vehicle axle load should be converted to a load per unit width per the following equation (Department of Transport 2001b):

$$w = h + 1.5 \tag{34}$$

where,
$w =$ effective width of arch, in meters
$h =$ height of fill at point of load, in meters

8. Apply any support movement to load cases (Figure 80).

9. Run a non-linear analysis. Nonlinear analysis required to account for the compression only link elements and the geometric nonlinearities. No material nonlinearities are considered in this method.

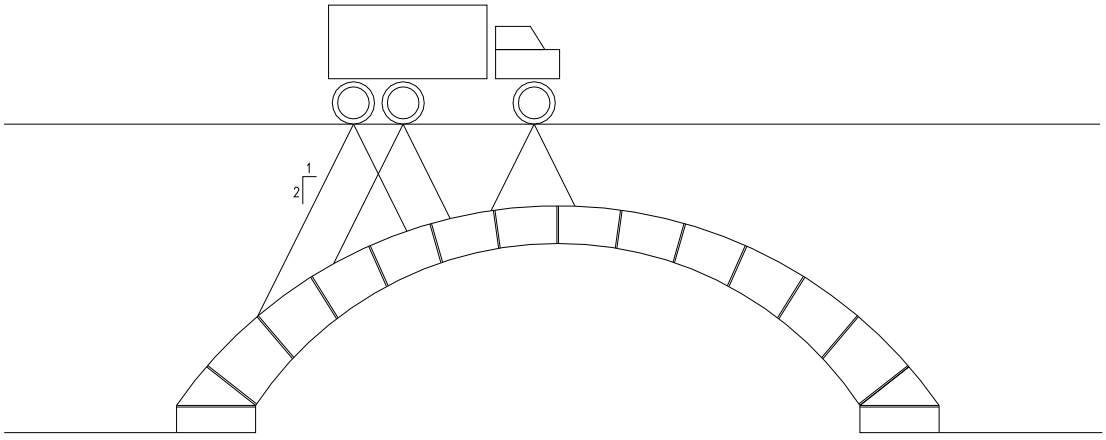

Figure 77. Truck load on arch bridge.

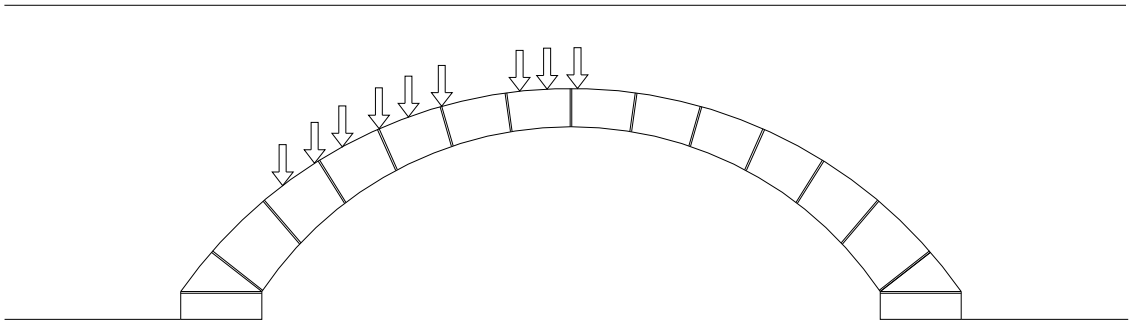

Figure 78. Modeled loading condition if represented as distributed load through fill.

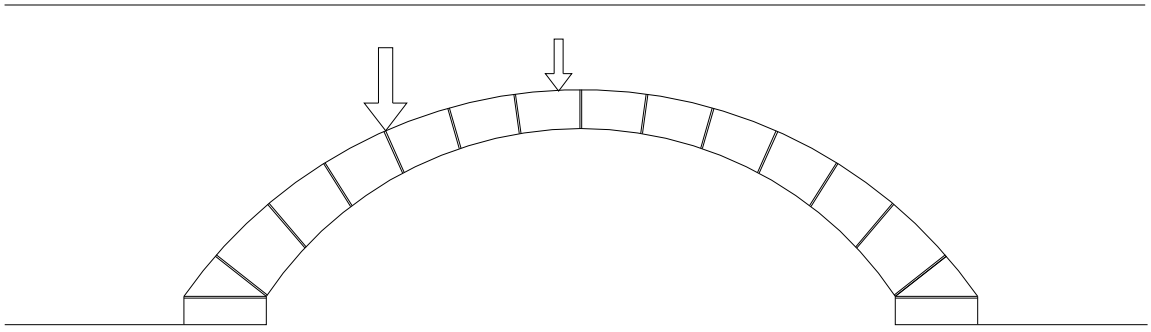

Figure 79. Modeled loading condition as point loads for each axle load.

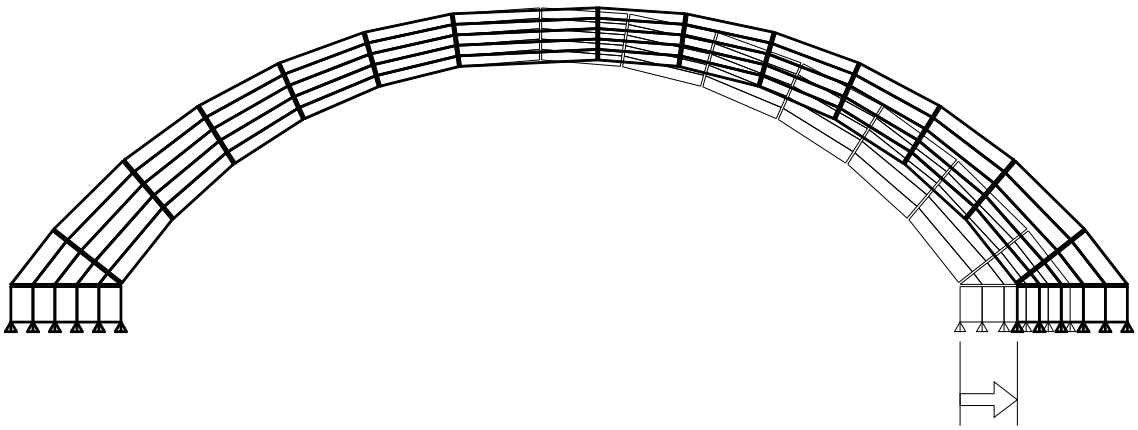

Figure 80. Support movement modeled.

After completion of the analysis, the following observations can be made from the resultant data.

1. Observe the deformation in the link elements for estimates of crack opening displacements at hinge locations.

2. The centroid of the compression forces at each gap corresponds to the location of the thrust line.

3. The ultimate capacity of the arch for a specified load case and support movement can be determined by completing a buckling analysis of the arch. Either the vertical deflection of a point on the arch or the deformation of a link at a hinge point can be used for the controlling parameter of the buckling analysis.

4. Compare the buckling load analysis of an arch with and without support movement to visualize the effects of the support movement on the load-displacement performance of the arch.

5.1. Methodology Background and Development

For the study of this analysis method, the following arch will be used. This semicircular arch is similar in shape to that of the Brooklyn Bridge arches and those used in the laboratory testing. Figure 81 shows a schematic of this arch. Table 4 lists the dimensions used for both of the arches. Both the Brooklyn Bridge and laboratory models were constructed of clay bricks. However, this analysis is equally applicable to arches of stone voussoirs or common brick construction.

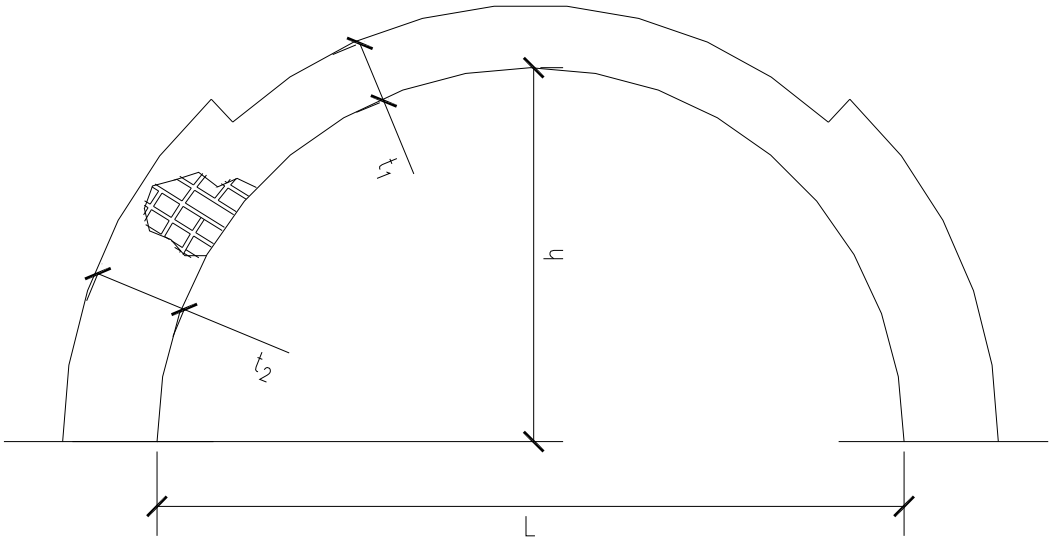

Figure 81. Example arch for explanation of analysis model.

	L (ft)	h (ft)	t_1 (in)	t_2 (in)
Laboratory Arch	6	3	6	9
Brooklyn Bridge Arch	34	17	24	36

Table 4. Arch dimensions used in analysis models.

For the analysis model, the arch was discretized into shell elements as shown in Figure 82. The arch examples used in this thesis were all discretized into 12 elements. The arch could be discretized into any number of elements along its length. However, twelve elements were suggested in the ICE Manual of Bridge Engineering (ICE 2008) for traditional finite element modeling of arches. Through the research and modeling as part of this study, twelve elements were found to be a reasonable modeling parameter for this methodology as well. It provided accurate results while limiting excessive computation and modeling time. An argument could be made that in the case of a brick arch, that each individual brick should be discretized in the model. This is not necessary since once a crack, or 'hinge', forms in the arch, a second crack is not likely to occur at the adjacent mortar joint or even in the next several adjacent mortar joints. Also, in actual masonry arches, the hinge will occur at an approximate location in a section of the masonry arch. The approximate hinge location can be determined, but it is not possible to pinpoint the exact mortar joint in which the hinge will occur. Variations in workmanship and the condition of the mortar joints will dictate at exactly which joint the crack will occur. For instance, if there is a poor mortar to brick bond or

deterioration in a mortar joint, it can offset the location of the hinge formation by one or more courses of brick.

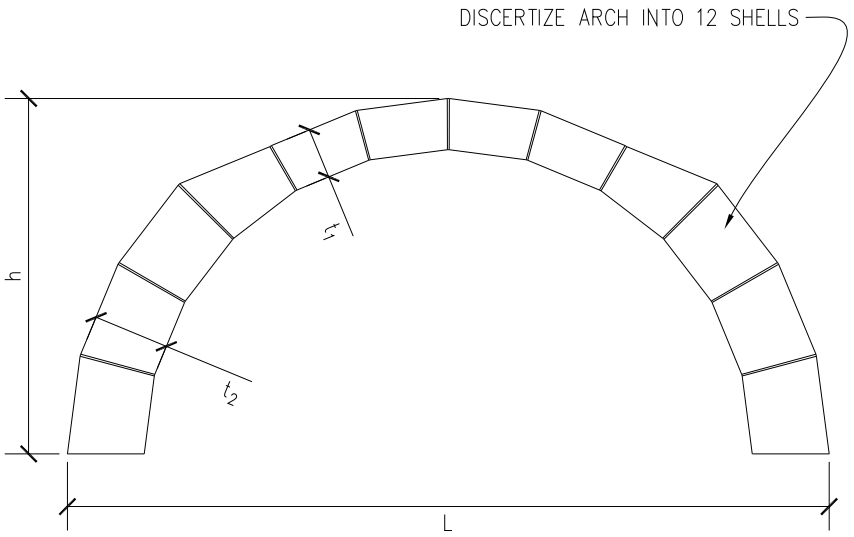

Figure 82. Arch model discretized into shell elements.

For this analysis model, the joints between each shell element were connected using a modified rigid link. A similar rigid link was used at the supports to attach the bottom element to the ground. As a starting point for the discussion of this method, the links will be modeled as rigid links connecting both the intrados and extrados corners of the discretized masonry elements (Figure 83).

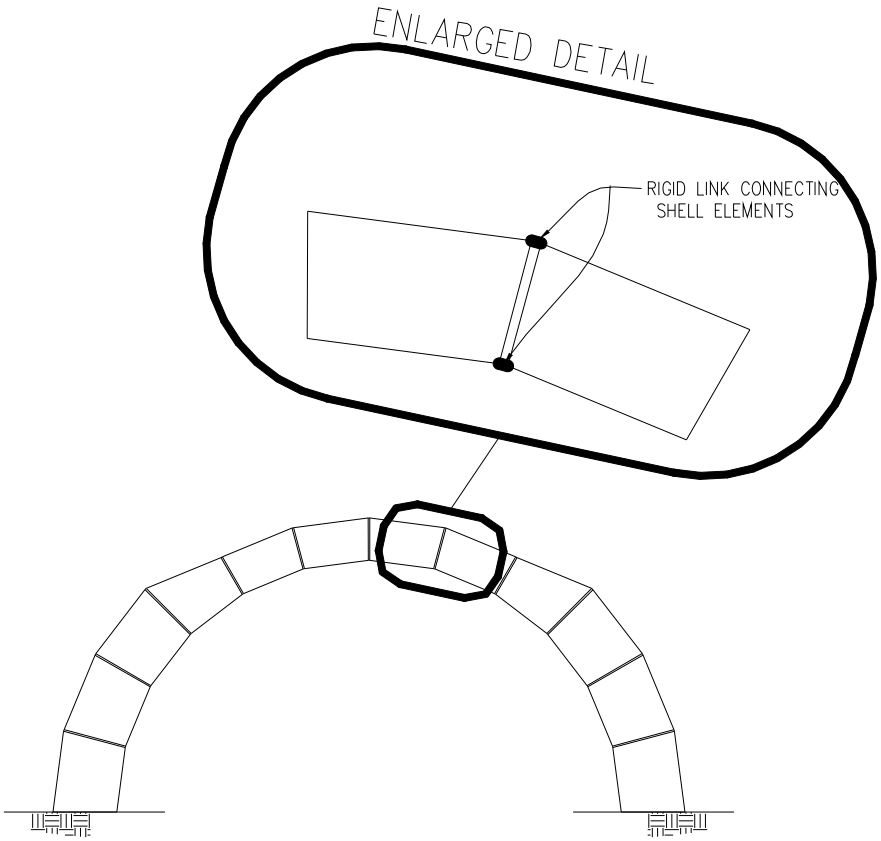

Figure 83. Rigid links connecting the joints of the shell elements.

A standard rigid link transfers axial force, shear, and moment at the connection. Figure 84 shows a free body diagram of the rigid link forces at the two highlighted elements shown in Figure 83 above.

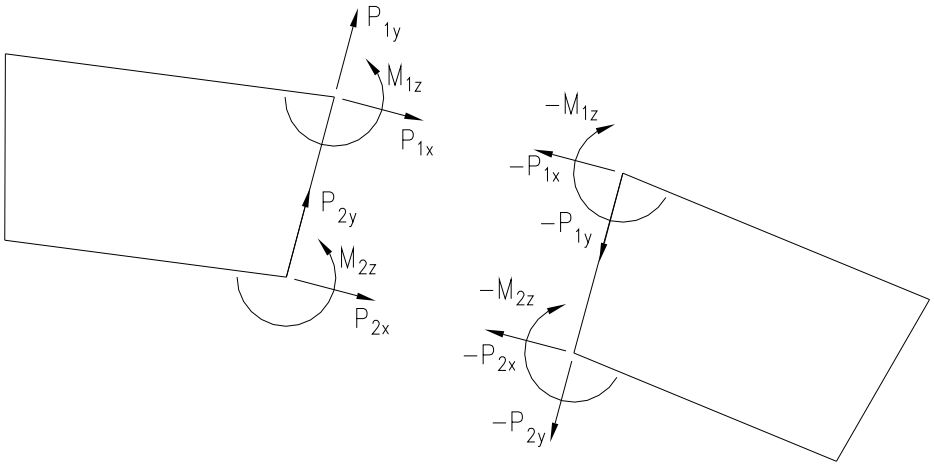

Figure 84. Free body diagram of rigid links connecting shell elements.

However, a standard rigid link with three degrees of freedom does not accurately represent the behavior of a masonry arch. The connection of the two rigid links between adjacent shell elements can best be described as two flat mating surfaces. Only compression and shear can be transferred across the surface. As discussed previously, mortar in tension has negligible strength and is neglected in the analysis of masonry arches. Similarly, there is no true moment connection or fixity of the mating surfaces. Instead, rotational moment is only provided by the reactive compressive forces over the surface of the section.

The inter-element connection can best be compared to that of a spread footing on rigid soil. A spread footing can similarly transfer compressive forces from vertical loads and shear forces from lateral forces to the supporting soil. For the following discussion, shear forces will temporarily be omitted.

When the resultant force, P, on a foundation is located at the center line of the footing, the resultant soil pressure will be uniform across the base of the footing (Figure 85). As the resultant force moves away from the center line, the resultant soil pressure starts to become unbalanced (Figure 86 and Figure 87).

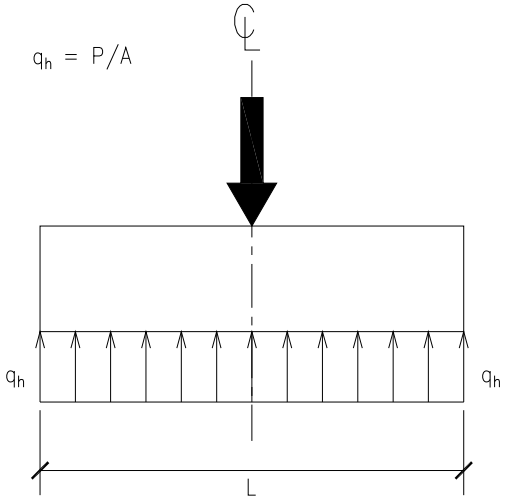

Figure 85. Resultant vertical force at center of footing (i.e. no eccentricity).

As long as the resultant force is less than or equal to L/6 away from the center line of the footing, the entire base of the footing will remain in compression. This condition is typically referred to as the resultant force being within the kern. As the resultant force moves outside of the kern, a portion of the footing would essentially have a resulting tensile pressure. Since tensile pressures are not possible in the contact surfaces of a footing on soil, a portion of the foundation no longer reacts with the soil and the pressure on the compressive side of the footing increases (Figure 88).

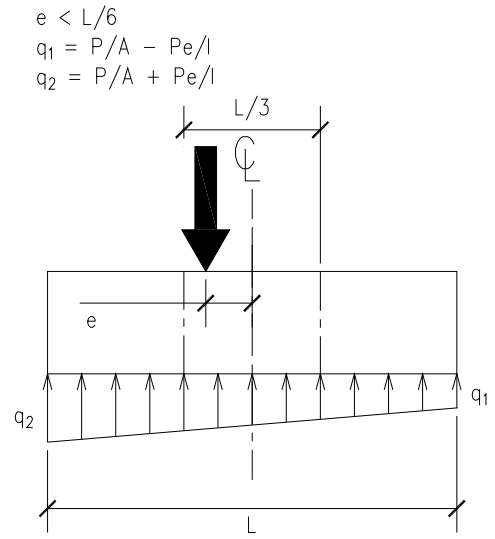

Figure 86. Eccentricity less than L/6.

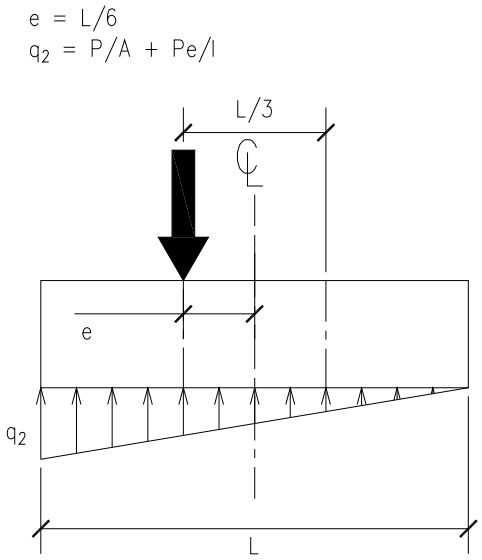

Figure 87. Eccentricity equal to L/6.

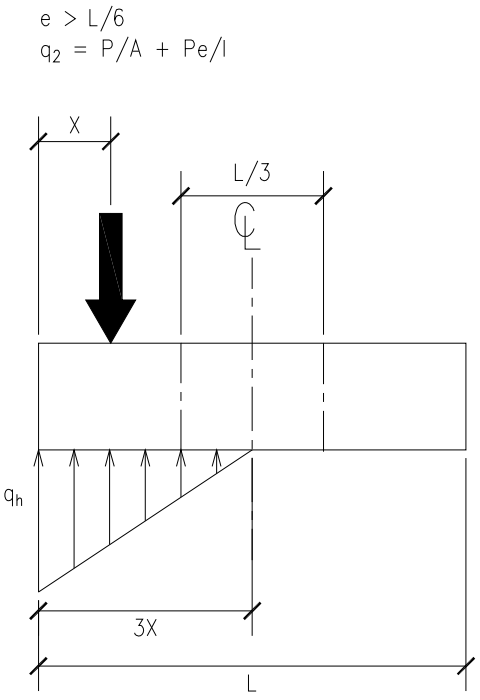

Figure 88. Eccentricity outside of kern.

If the resultant force on the footing continues to approach the outer edge of the footing the soil pressure becomes very high. In the case of a footing, there will reach a point

where there is a bearing failure of the soil because the stresses exceed the strength of the soil. In the case of the masonry arches, the strength of the masonry in compression typically far exceeds the resultant compressive stresses. If for a specific masonry arch case the compression stresses approach the compressive strength limits of the arch, the mortar would locally crush and the compressive force would be redistributed over a slightly larger area. The local crushing and redistribution area would be small and would have no significant effect on the results of the analysis as proposed by the hinged arch model in this study.

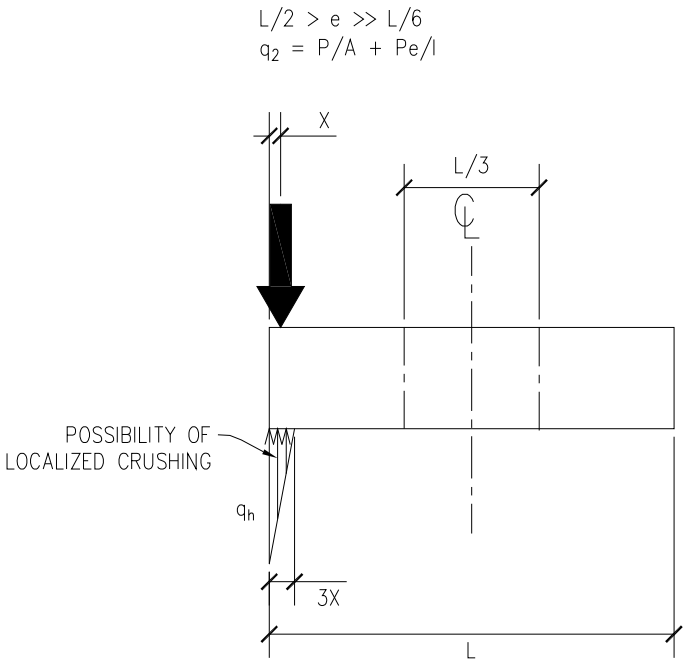

Figure 89. Resultant force approaches the outer limits of the footing.

Finally, as the eccentricity of resultant force extends beyond the outer limits of the footing, a rotation of rigid body motion will occur (

Figure 90). In the case of a masonry arch, this condition occurs when the thrust line falls outside of the arch section. This creates a hinge in the arch.

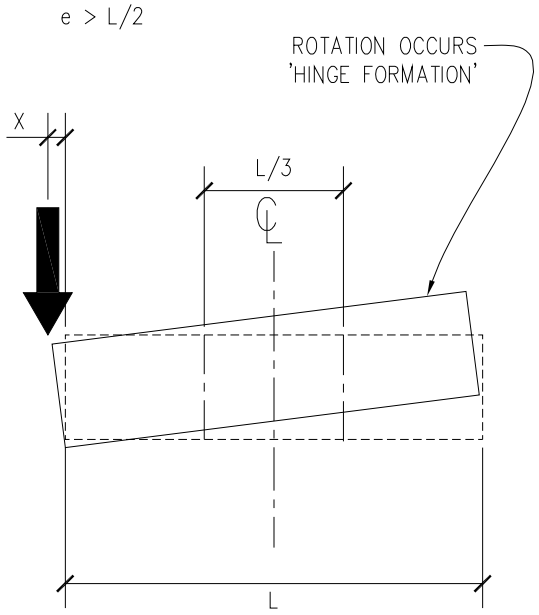

Figure 90. Eccentricity of resultant point load outside the limits footing section.

In order to represent the behavior described above, the modeling shown in Figure 91 was developed to replace the free body diagram constraints of Figure 84. The link elements represented by the axial forces P_{ix} are compression only elements, or otherwise referred to as gap elements. The stiffness for the link element was calculated to be equal to the stiffness estimated for the masonry material. Figure 92 shows a schematic diagram of the compression only link element being proposed to connect the discretized elements. The only deformation degree of freedom is the axial direction. The two perpendicular translational degrees of freedom are fixed. The opening and

closing of the gap does not affect the behavior of the other directions. The nonlinear force-deformation relationship for the gap element is:

$$f = \begin{Bmatrix} k(d + open) & \text{if } d + open < 0 \\ 0 & \text{otherwise} \end{Bmatrix} \tag{35}$$

where,

f = force in link element

k = spring constant, $k = EA_{tributary} / L_{link}$, where $E = E_{masonry}$,

$A_{tributary}$ = tributary area of link element, L_{link} = lenght of link element

open = initial gap opening, must be ≥ 0.

Use = 0 for almost all cases of arch analysis unless

modeling a mortar joint defect or eroded mortar.

d = deformation across link

Based on the analysis completed as part of this research, it was found that it was most practical to divide the voussoir elements into 5 smaller elements (see later discussion). Of course, the divisions could be made into more elements, but this increased computation time with no significant increase in the accuracy of the results. Less than 5 elements did not do a good job of modeling the distributed reaction force across the contact surfaces and made calculating an accurate thrust line location difficult. Each of the five divisions within the voussoir was connected to each other, but the connections between the voussoirs consisted of a stiff axial link.

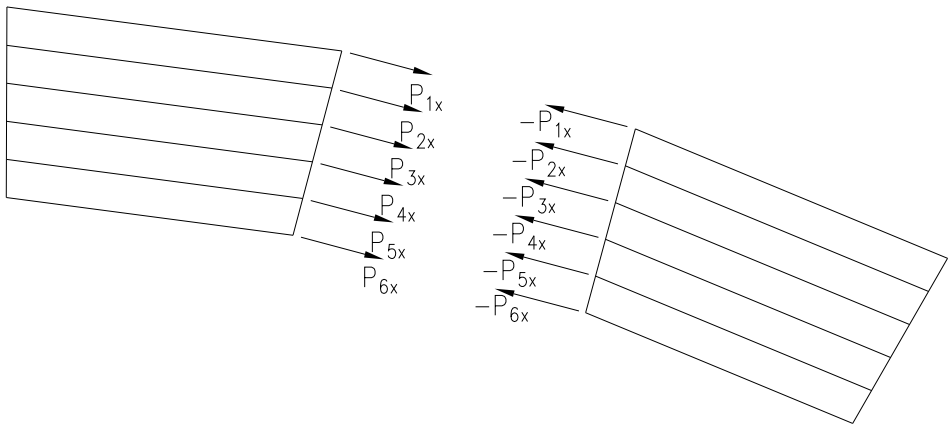

Figure 91. Proposed modeling formulation for link connection between voussoirs or bricks of arch.

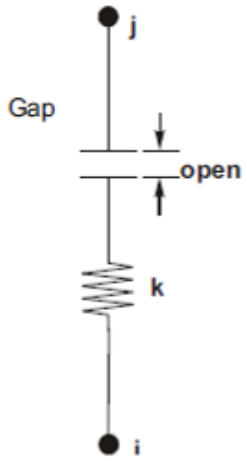

Figure 92. Gap element used for rigid link connection between elements.

Up to this point, discussion of shear transfer between discretized elements, or individual, voussoirs had been ignored. As long as the resultant thrust force remains within the boundaries of the arch, there is a normal force across at least some portion of the contact surface between the elements. Coulomb modeled friction per the following relationship:

$$F_f = \mu F_N \tag{36}$$

where,

F_f = friction force

μ = coefficient of static friction, ≈ 0.65 for masonry

F_N = normal force

As long as there is some contact between elements, the friction force will be sufficient to resist shear across the joint. In only very few instances has sliding across mortar joints ever been a failure mechanism in masonry arches. If this is a possible concern, the user is referred to alternate analysis methods such as the rigid block method to model this behavior (Gilbert 2001). In order to keep the model simplistic, shear deformations were held constant at each end of the rigid compression only links. In other words, there can be no slippage across the mortar joints. This is a reasonable assumption since as long as one point is fixed in the shear direction. Then, all points will remain in the same relationship to each other per the following equation:

$$if \;\; v_{1L} = v_{1R} \;\; , \text{ then } v_{2L} = v_{2R} = ...v_{iL} = v_{iR} \tag{37}$$

where,

v_i = vertical deformation at link i

$_{R,L}$ = subscript noting the right and left sides of link i

5.1.1. Applying the Methodology

The above methodology can be used to model an arch of any shape in any readily available finite element program. For the purposes of this research, SAP2000 by CSI

Berkeley was used. The dimensions of the arch were the same as those of the laboratory test arch (Table 4).

Figure 93 is an example of the arch model shown in Figure 81. The arch was modeled using the methodology as described in the introduction of this chapter. For the initial analysis, the arch supports were held in place, i.e. without support movement, and only subject to loading from its self weight. As would be expected, there is minimal deflection at the crown when the arch is supporting only its self weight and the supports are rigidly held in place. There are compressive forces across the joints and no hinges formed under this analysis case.

Figure 94 shows the same arch subjected to a horizontal support displacement of 0.12 inches at the right support (less than 0.2% of the span length). Note the beginning of the creation of three hinge points. These were highlighted with bold dots in the figure in order to emphasize their location. When a hinge fully forms, only the outermost link element transfers any force across the masonry joint. The other link elements at the joint open up respective amounts but do not transfer any axial forces between adjacent elements.

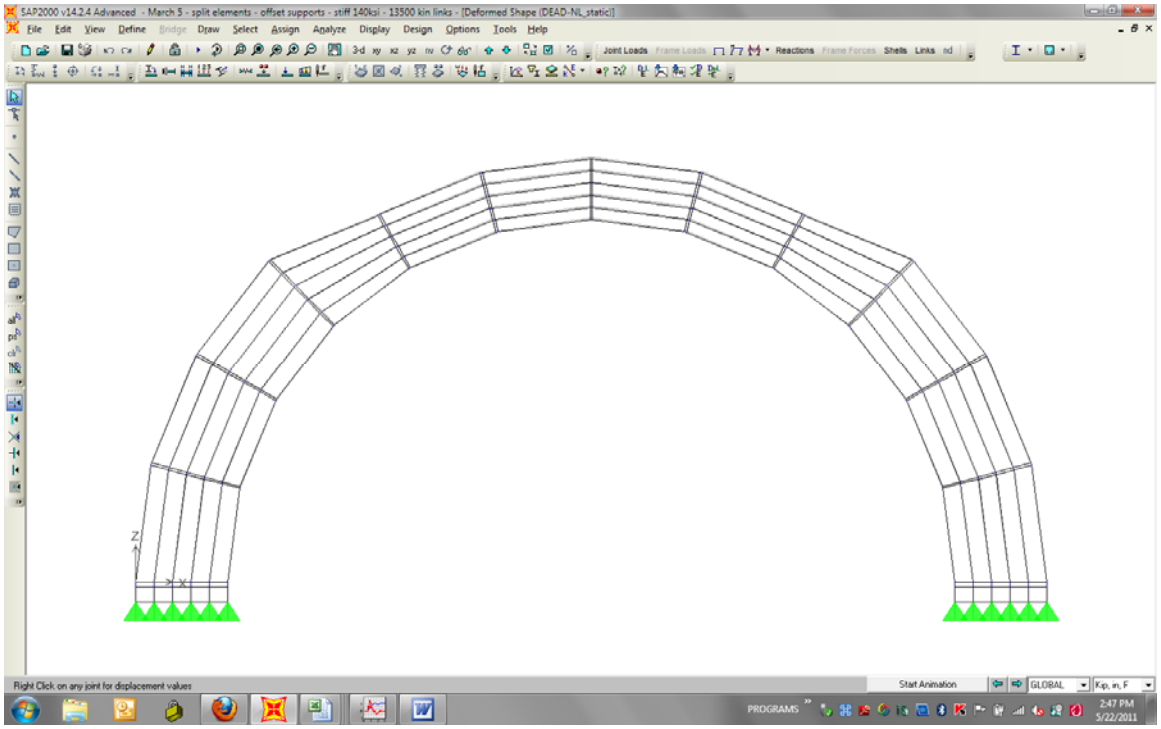

Figure 93. Arch model under dead load (deflection is scaled at 50x for illustration).

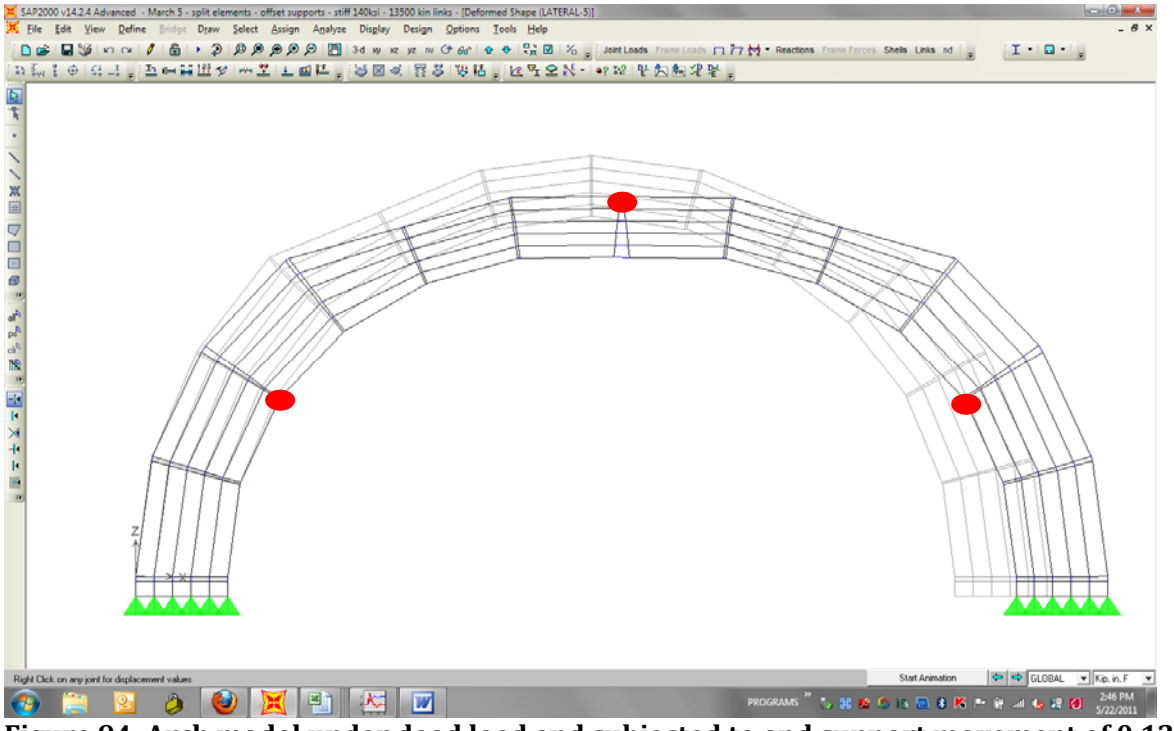

Figure 94. Arch model under dead load and subjected to and support movement of 0.12 inches (deflection is scaled at 50x for illustration). Hinge points are highlight with bold dots.

5.1.2. Estimating Crack Opening Displacement

The deformations of the links at the open end of the hinges can be monitored under various load combinations and cases. When using this proposed modeling methodology, these deformations have been found to be an accurate indicator of actual crack openings. Further explanation and examples of estimating the width of the crack openings from the laboratory testing and the Brooklyn Bridge structural health monitoring data using the proposed methodology will be provided in later sections

5.1.3. Thrust Line Visualization

An additional benefit of analyzing the arch with the proposed mathematical model with link elements is that the user can quickly calculate the location of the thrust line. Using the analytical model, the resultant thrust is determined by calculating the centroid of the axial forces of the link elements. The centroid of the resultant force corresponds to the location of the thrust line at that point on the arch (Figure 95). This can then be plotted across the arch to locate the entire thrust line (Figure 96). As the thrust line approaches the edge of the masonry arch, a hinge is formed.

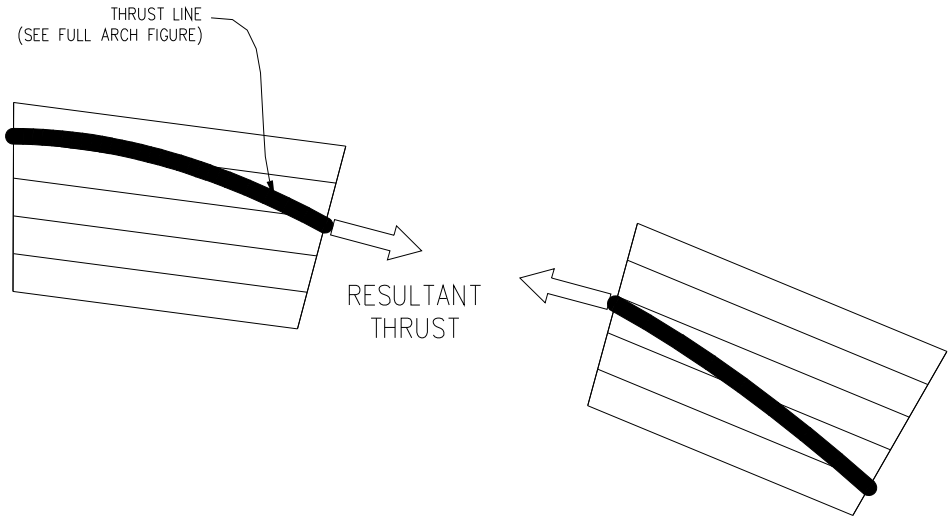

Figure 95. Development of thrust line model using the analysis model.

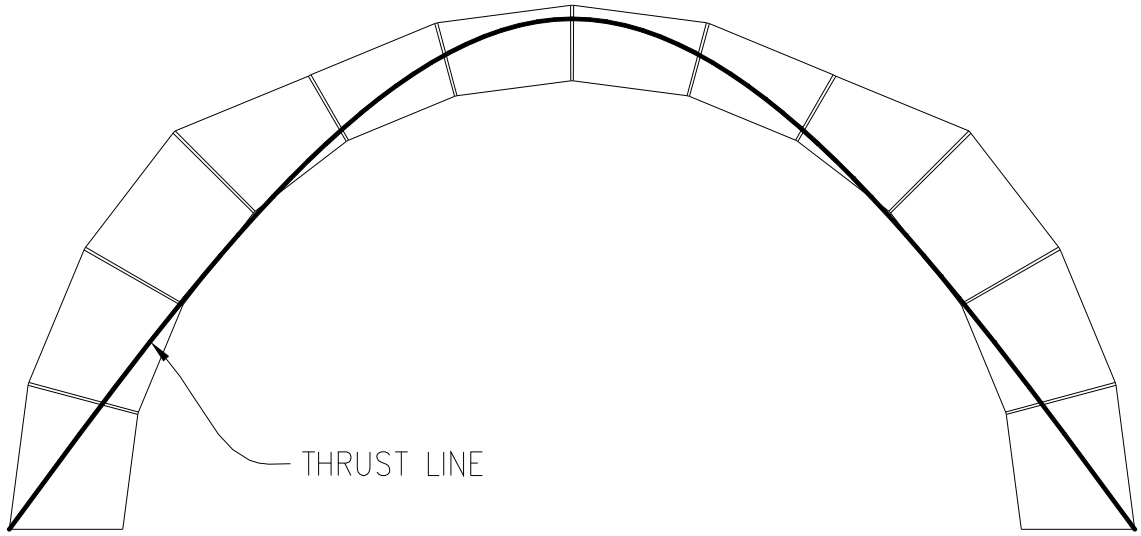

Figure 96. Thrust line model for entire arch as developed from link model.

5.1.4. Nonlinear Buckling Analysis for Failure Load

A linear buckling analysis is conducted by applying perturbations to the undeformed shape of a structure and identifying deflections that become unstable due to the P-delta

effects under a specified set of loads. The output of the linear buckling analysis is a set of buckling factors and corresponding mode shapes (CSI 2010). For each buckling factor, the corresponding mode shape shows the buckled shape of the structure at failure. The buckling factor is the multiplied factor of the perturbation load that causes failure in the corresponding buckling mode shape.

Linear buckling analysis solves the instability mode of a structure due to the P-delta effect under an applied set of loads. Buckling analysis entails the solution of the following generalized eigenvalue equation:

$$\left[K - \lambda G(r)\right]\Psi = 0 \qquad (38)$$

where,

K = stiffness matrix

$G(r)$ = geometric (P-delta) stiffness due to the load vector, r

λ = diagonal matrix of eigenvalues

Ψ = matrix of corrsonponding eigenvectors

The first eigenvalue, λ_1, and corresponding eigenvector are referred to as the buckled mode of the structure. Multiple buckling modes can be solved for; however, in most cases only the lowest buckled factor is of interest.

A nonlinear static analysis can be implemented to complete a similar buckling analysis while at the same time incorporating the effects of material or structural nonlinearities. In the case of the arch model, the nonlinearity of the compression only link elements is

of particular interest when calculating the failure load of the arch. A unit load, or series of loads, representing the moving traffic load, is applied sequentially at various locations along the length of the arch. The stiffness and response of the arch is then evaluated at each incremental step increase of the load. The stiffness may change from load step to load step as a result of one of the following effects:

1. P-delta Effect
2. Large Displacement Effects
3. Nonlinear Material Properties.

In the case of the arch model, significant changes in the large displacement effects are the key in identifying the buckling load.

Unlike the linear buckling analysis, the nonlinear static analysis provides an "actual response" of the structure (displacements, internal forces, etc.) for each load increment. You can review the deformation path of the structure to determine when the structure starts softening, which may be viewed as initiation of buckling.

An example of the buckling load model is shown in Figure 97 using the dimensions of the laboratory test arch (Table 4). In this case, a unit point load is applied at the quarter point of the span. This point load could similarly be moved to different locations across the span of the arch to simulate the axle load of a moving truck. A separate buckling analysis would need to be completed for each location of the axle load. The minimum

buckling load of all the point load locations would be the governing buckling load for the overall structure.

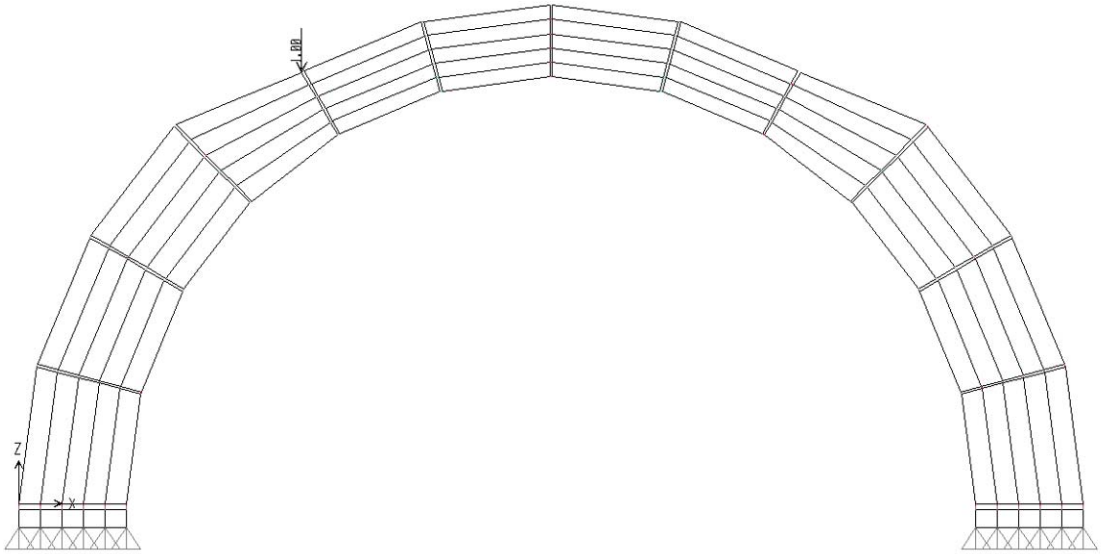

Figure 97. Example of buckling load model with unit load applied at quarter point of span.

Figure 98 shows the results of the buckling analysis. Figure 99 is a close-up of Figure 98 over the range of 0 to 0.5 inches along the x-axis. The unit load was incrementally increased while observing the behavior of Joint 15. Joint 15 is located on the intrados below the unit point load. As can be seen from the plot, the buckling load for this configuration without any support movement is approximately 0.4 kips. Figure 100 shows the deflected shape of the arch at the load step for 0.15 kips. At this point, three hinge points have occurred, but the applied load is well below the buckling load and the arch is still stable. Figure 101 shows the deflected shape at the point of the buckling

load. Note the location of the four hinges indicating the failure of the arch. Figure 102 overlays a 4 - rigid bar graphic on the buckled shape of the arch demonstrating its instability as a load carrying frame at this point.

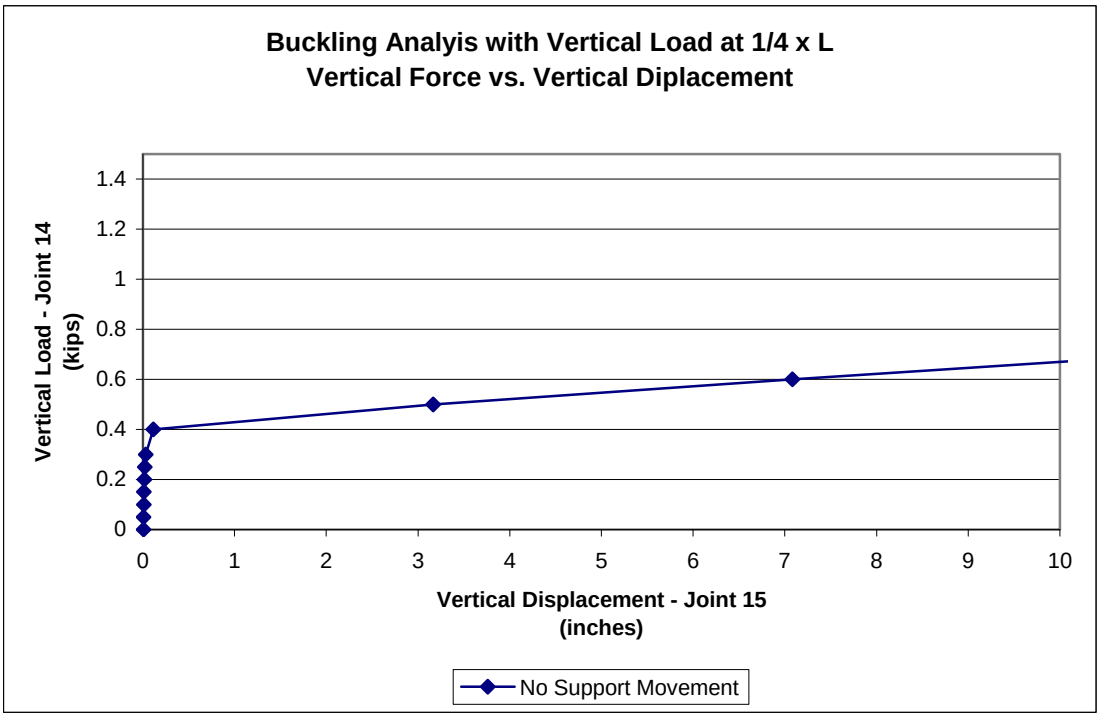

Figure 98. Buckling analysis of example arch with vertical load at 1/4 point.

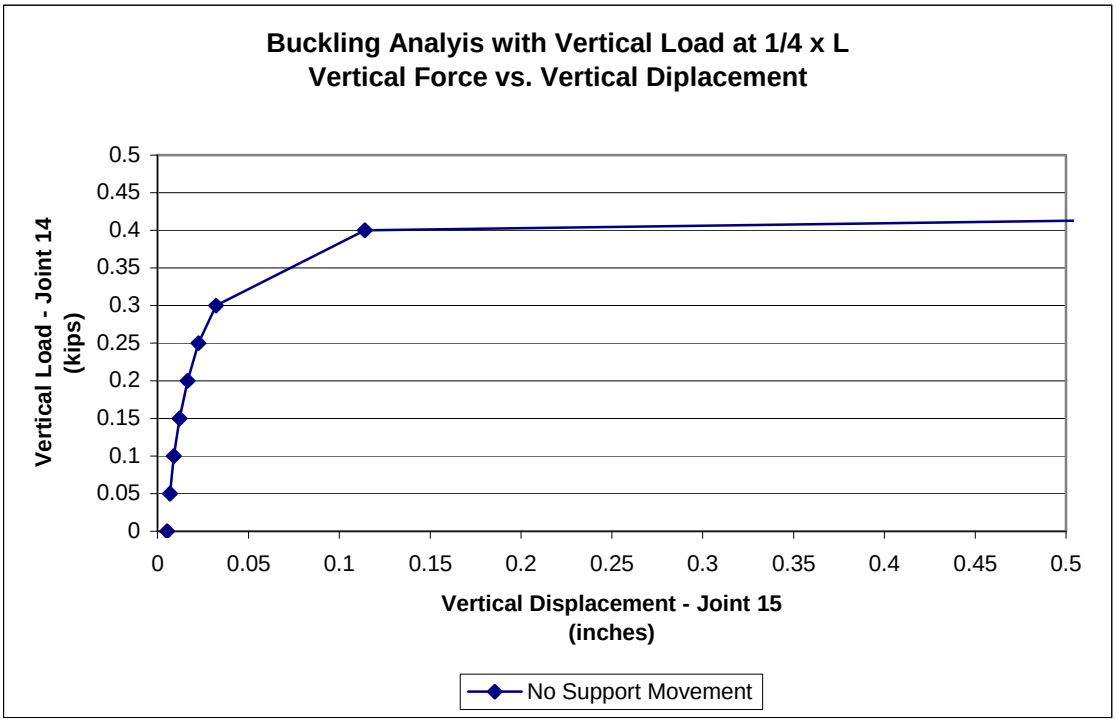

Figure 99. Close-up plot of Figure 98.

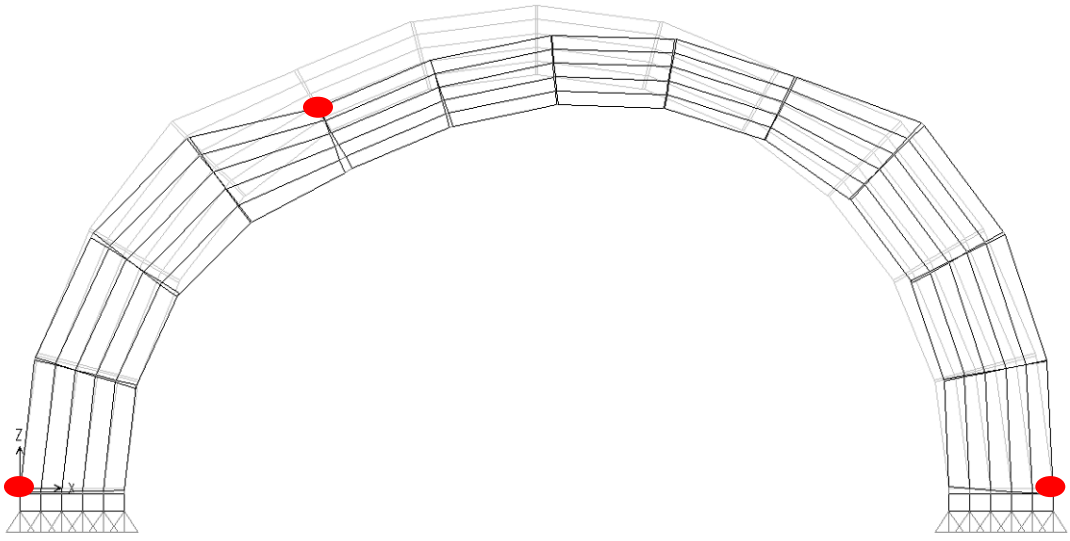

Figure 100. Step in buckling analysis without support movement (scaled 300x) at 0.15 kips.

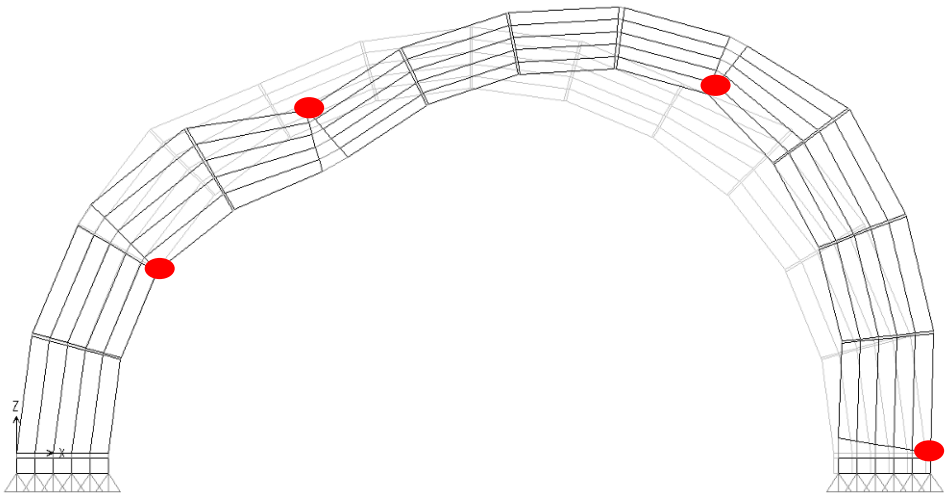

Figure 101. Deflected shape at buckled load. Note four hinge locations. (without support movement, scaled 1x)

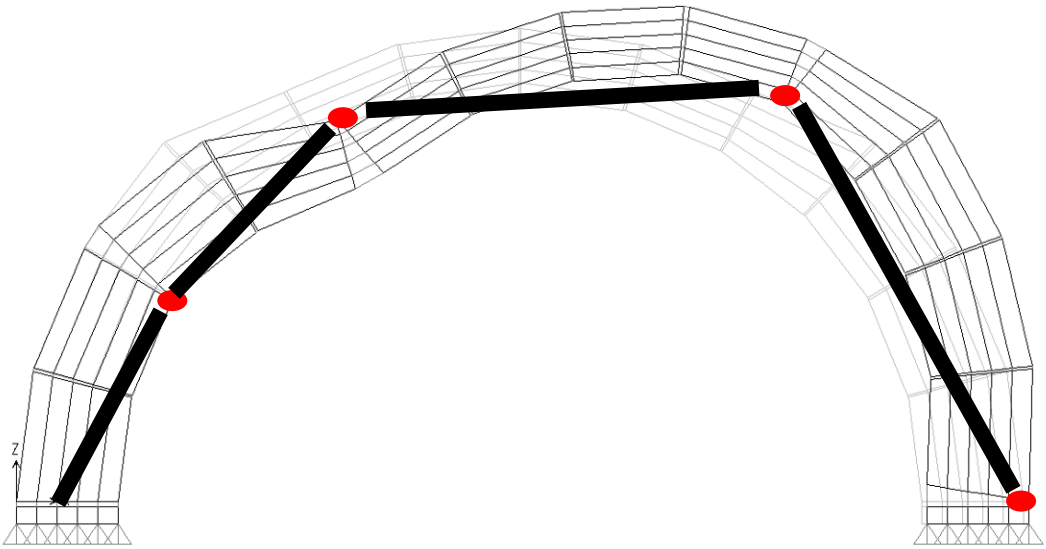

Figure 102. Buckled shape of arch at failure load represented as a 4 bar mechanism.

An advantage to the proposed arch modeling methodology is that support movement can be modeled and the effects on the arch load re-analyzed for the effects of support settlement. As discussed earlier, there are a number of possible reasons for support

settlement in historic masonry arches. No prior analysis methods have truly addressed the effect of support settlement on the load carrying capacity of a masonry arch.

Using the same example arch shown in Figure 97, a horizontal support movement of 1 inch (approximately 1% of the span length) was introduced to the right support. Figure 103 shows the deflected shape and hinge locations of the arch after it has been subjected to both the support movement at the right support and the vertical load as applied at the quarter point of the span. Figure 104 plots the difference in the buckling analysis for the cases with support movement (Figure 103) and without support movement (Figure 100). While the ultimate buckling load of the arch remains the same, the performance of the arch is much less stiff beginning at loads less than 25% of the ultimate buckling load. At approximately 0.1 kips, the vertical deflection is nearly an order of magnitude greater in the arch with lateral support movement as opposed to the arch without support movement.

It could be argued that the change in vertical defection from 0.01 inches to 0.1 inches, or similarly from 0.03 inches to 0.3 inches is not significant, but it should be remembered that this analysis is for a short span arch (L = 6 feet) and a support movement of just slightly more than 1% of span length. Comparatively, if the support movement is increased to 3 inches, or 3.5% of the span length, the vertical deflection above 25% of the total buckling load nearly doubles from the values observed in the model with 1" support movement (Figure 105).

While the ultimate load capacity of an arch bridge with some support movement will remain the same as an arch bridge without support settlement, the stiffness of the bridge is much lower. This causes greater vertical deflection of the bridge and wider crack openings. The greater vertical deflections and wider crack openings begin to become a problem for a bridge owner trying to maintain such a bridge. Large deflections such as this not only cause problems with premature mortar erosion and deterioration, but also can create a public perception problem as such deflections leads to noticeable crack openings.

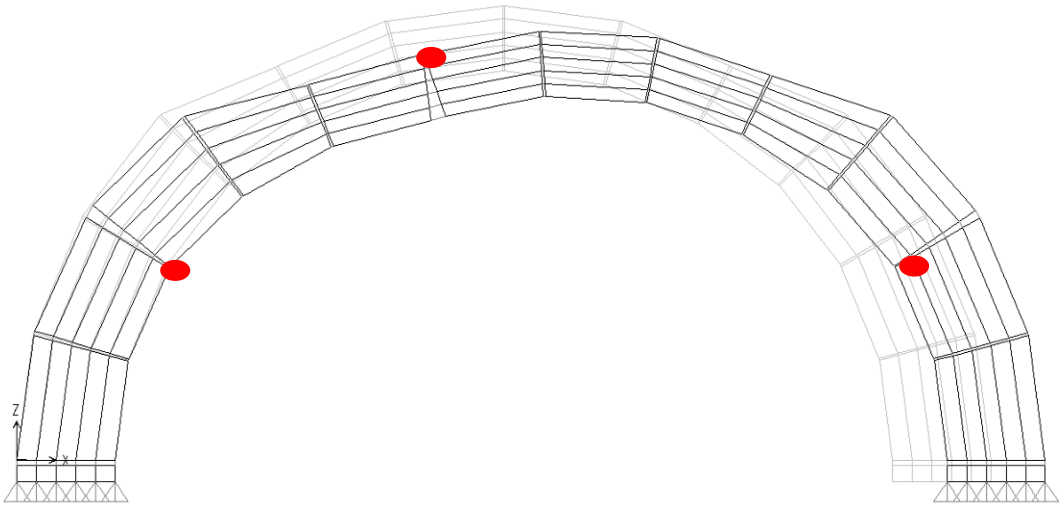

Figure 103. Deflected shape of buckling analysis with 1" support movement (scaled 10x).

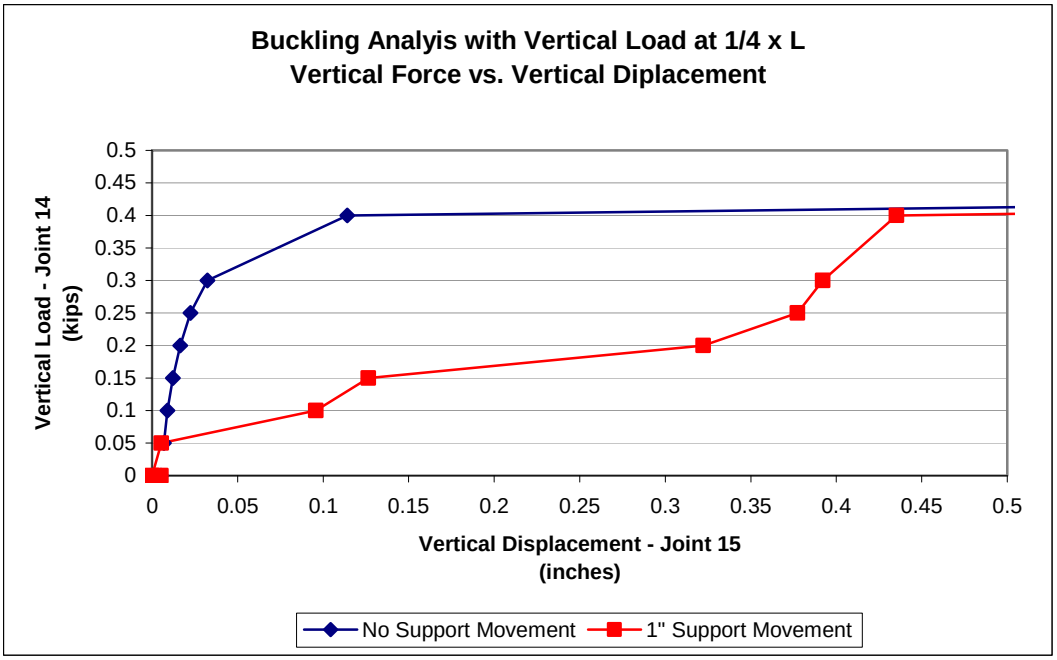

Figure 104. Comparison of buckling analysis with and without support movement.

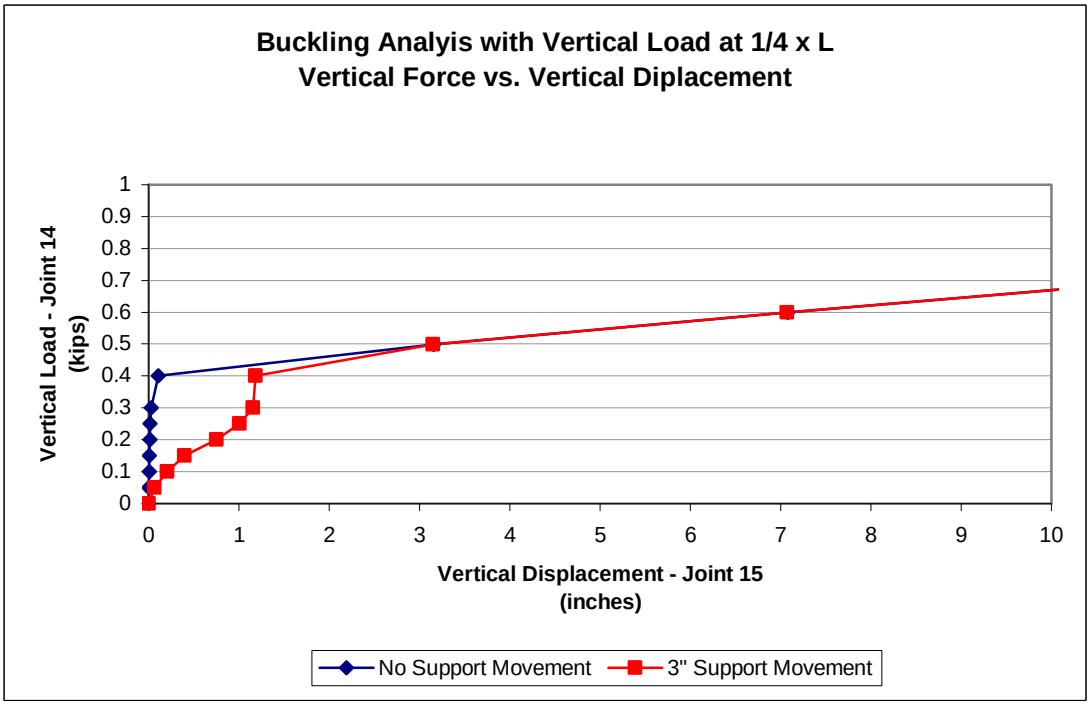

Figure 105. Buckling analysis with 3" support movement.

5.1.5. Study on the Number of Gap Elements

Earlier in the explanation of the methodology, it was suggested that each of the elements be divided in to 5 elements across the width of the arch. In order to further explain this assumption and demonstrate the most effective number of gap elements to be modeled, a study was undertaken using the original example arch of Figure 97.

As with traditional finite element modeling, the greater the number of elements the model is discretized into, the more accurate the results. However, there becomes a tradeoff between computation time and accuracy. Computation time is composed of both model creation time and computer solving time. Various models were created using 1, 2, 5, 10, and 20 elements across the cross section of the arch. Nonlinear gap elements connected the respective nodal points. A vertical point load was positioned at the quarter point and the buckling analysis completed. Figure 106 shows an example of the arch modeled with only 1 element across its width and with 10 elements modeled across its width.

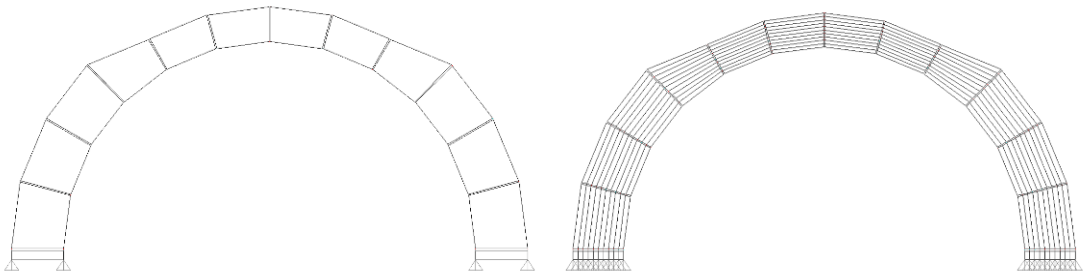

Figure 106. Example of mesh study: left = 1 element, right = 10 elements.

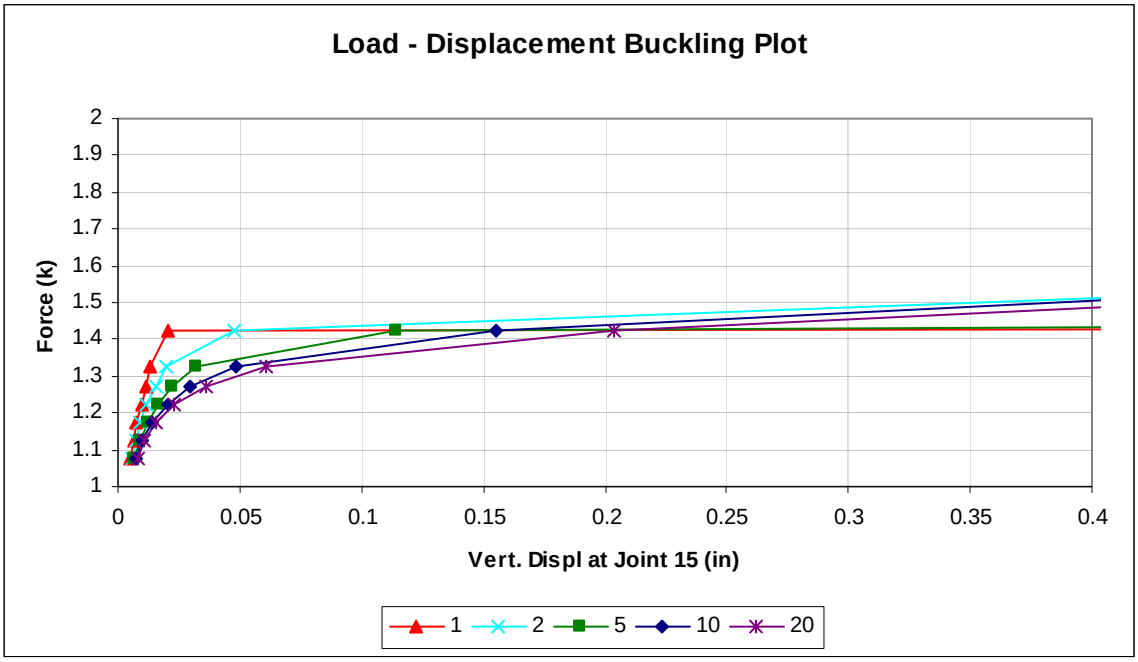

Figure 107. Comparison of the effects of the number of elements modeled in cross section.

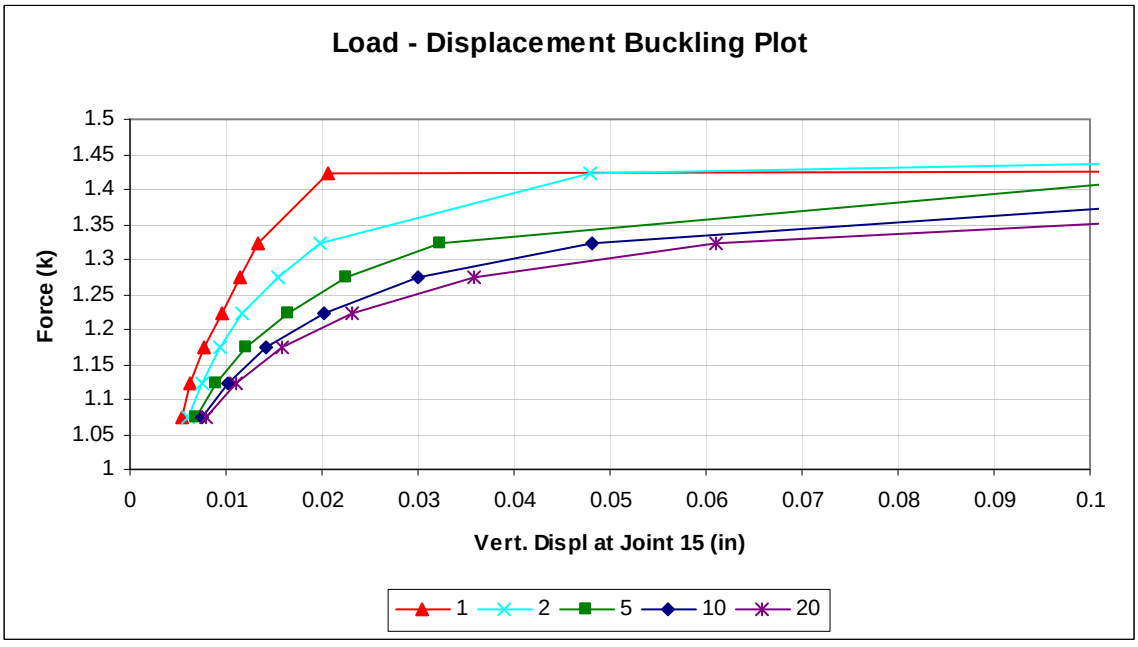

Figure 108. Close-up of Figure 107.

Figure 107 and Figure 108 show the results of the study. While all of the models very nearly calculated the same buckling load, the models with only 1 and 2 elements across the cross section were very stiff. This is due to the fact that these models do not allow for a hinge mechanism to slowly develop with the load as it would in a full scale model. For the instance of a single element model, the resultant forces (and line of thrust) are forced to either the intrados or extrados.

The load deflection plot does continue to soften as more elements are introduced, it was decided that the tradeoff begins to become insignificant compared to the increased modeling and computation time. A cross section with 5 elements was chosen to be a reasonable tradeoff between accuracy of result and modeling time, with the understanding that if very detailed results are desired, they could be obtained with more accurate modeling.

A study was also undertaken to investigate the effects of the number of elements across the span of the arch. The arch bridge used for this study was a parabolic arch with a span to rise ratio of 6.42. One arch model was typically divided into the 12 elements across the span. The other arch model was discretized into 62 elements across the span to represent all of the actual voussoirs of the bridge (Figure 109). The results of the two load deflection plots for a point load at the 1/4 point of the span are shown in Figure 110. There is minimal difference between the two analysis cases.

While arch models typically make the assumption of no tension in the mortar joints, the reality is that there is in fact some nominal tension capacity. When a hinge forms in a masonry arch, it cracks the joints and the hinge then rotates around the intrados or extrados point. Once this occurs, the tensile stresses in the local area are relieved and a second hinge point is not likely to occur at the next adjacent joint. Therefore, modeling with 12 elements does not necessarily provide any better representation the behavior of the masonry arch than discretizing the arch span into many elements.

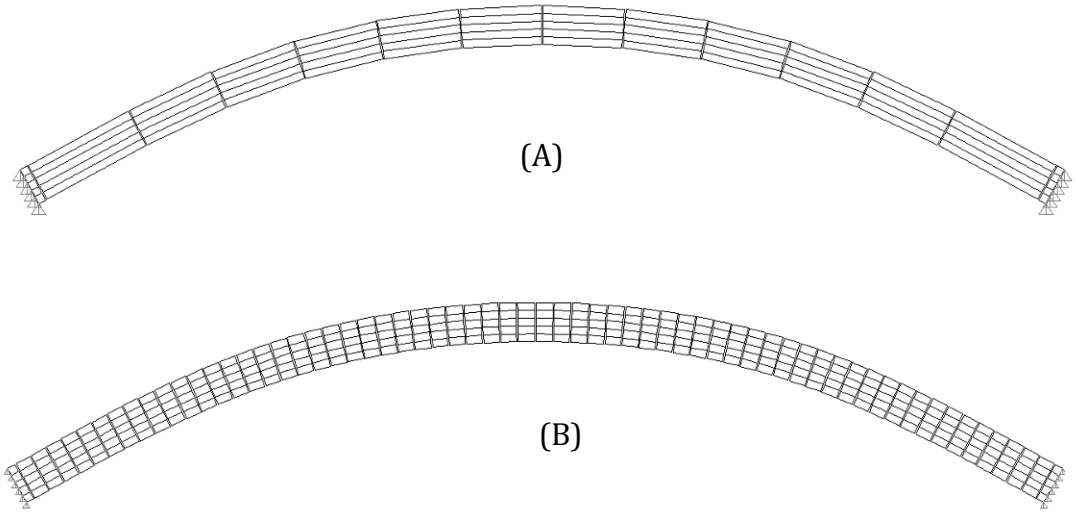

Figure 109. (A) 12 element and (B) 62 element models used for comparison.

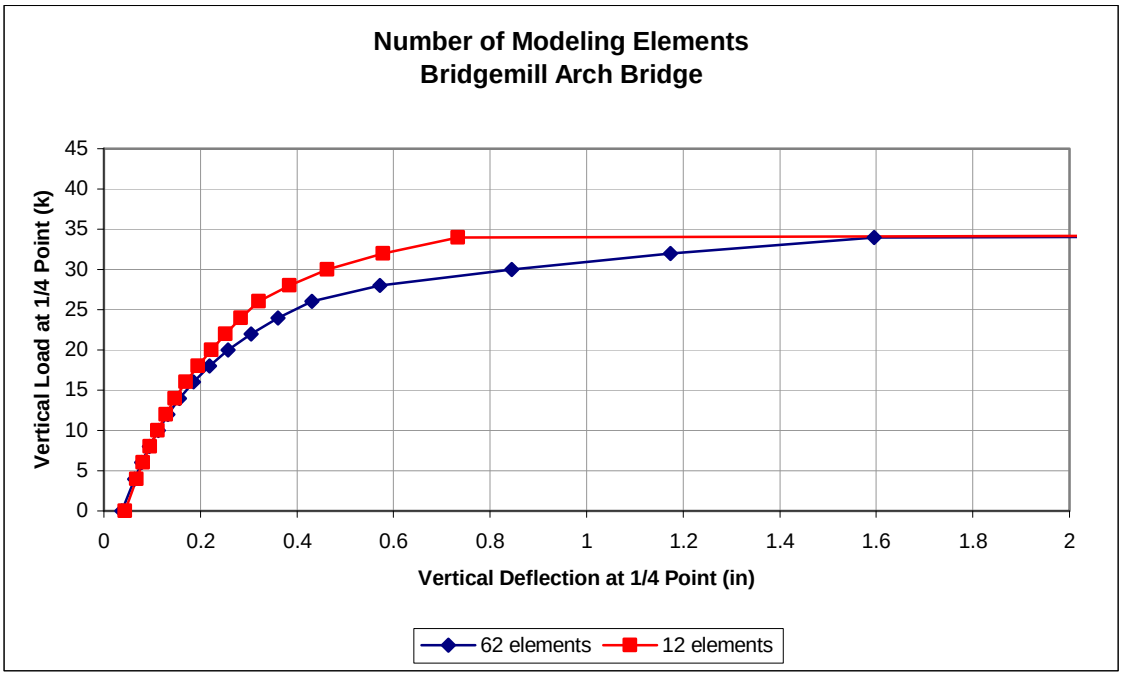

Figure 110. Comparison of load deflection data on the number of elements modeled.

5.2. Methodology Verification

The proposed methodology was validated by comparisons with existing analysis methods, laboratory testing at the University of Illinois at Chicago of a scale model brick arch, prior full scale load tests from literature and published results form laboratory tests using steel block voussoirs by Pippard.

5.2.1. Comparison with Laboratory Tests

Several parameters were measured during the laboratory tests of horizontal support movement. The crack opening displacements were measured with fiber optic crack gauges. The vertical deflection at the crown was measured with a laser Doppler

vibrometer and also dial gauges (Talebinejad et al 2001). The lateral thrust reactions were documented by the internal load cell of the MTS piston as was the lateral deflection loading rate. The following are comparisons of the deflection and crack opening predications as made by the proposed methodology with the recorded data from the laboratory data.

Vertical Deflection at Crown vs. Horizontal Support Movement

As the supports move outward, hinge points form in the masonry arch and the crown deflects downward. For the laboratory tests, the vertical load on the arch consisted of the self-weight of the masonry, or dead load of the structure.

Laboratory Tests A, B, and E were conducted with outward movement of one of the supports. In each of the tests, the hinges occurred at the same location: at the crown and at each of the abutments (Figure 111). As each of the tests progressed, the vertical deflection at the crown was recorded with a laser Doppler vibrometer and dial gauges. Figure 112 is an example of the vertical deflection vs. support movement plot. The ratio for this test was 0.42 and ratios for other tests can be seen in Table 5, with the average of all tests being 0.39.

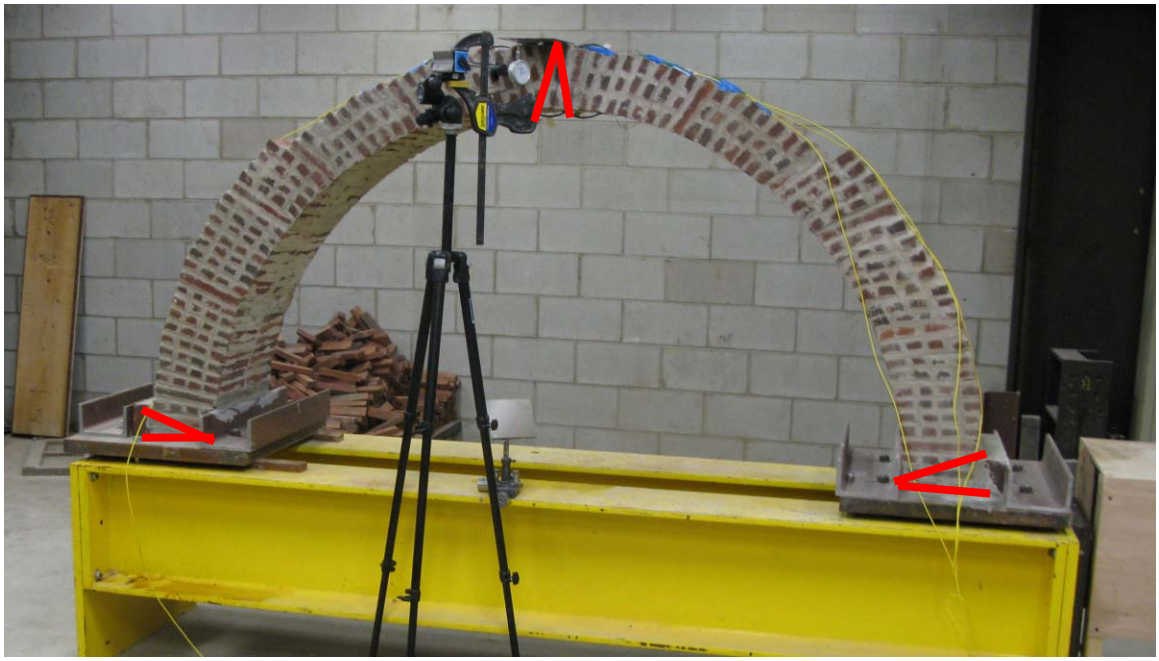

Figure 111. Hinge locations highlight in support movement lab test.

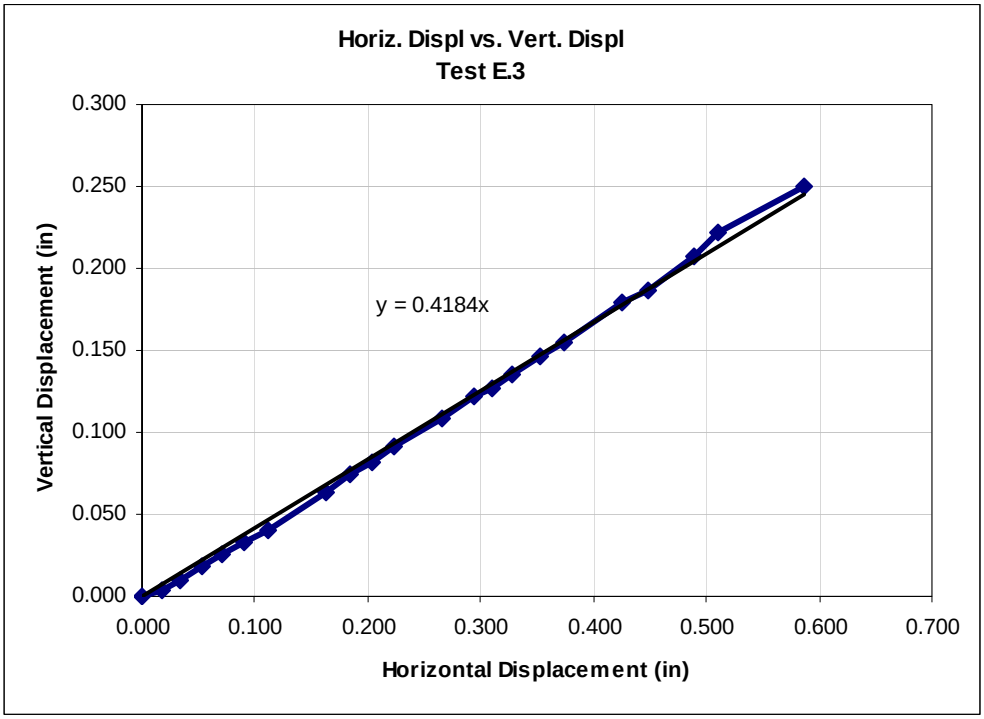

Figure 112. Typical horizontal displacement vs. vertical displacement plot.

Test A		
	A.1	0.40
	A.2	0.42
Test B		
	B.1	0.33
	B.2	reverse movement
	B.3	0.34
Test E		
	E.1	data error
	E.2	0.34
	E.3	0.42
	E.4	reverse movement
	E.5	0.45

Table 5. Horizontal vs. vertical displacement ratios for all outward support movement tests.

For comparison, a model of the laboratory test arch was created using the proposed methodology (Figure 113). The vertical displacement vs. support movement plot, shown in Figure 114, displays a displacement ratio of 0.64. In comparison to the laboratory tests, this is a somewhat higher value. Inspection of the numerical model deflected shape (Figure 113) shows the intrados hinge points to occur two blocks above the abutments, where as the hinges in the lab tests occurred exactly at the abutments. The higher hinge location in the numerical model is due to the assumption of no tensile strength of the mortar joints. In fact a study of two other numerical methodologies, the kinematic study by Block and Ochsendorf (Block 2006 and Ochsendorf 2006) (Figure 115) and rigid block analysis by Ring 2.0 (Figure 116), find the hinges to occur at the exact same location as that in the proposed methodology.

The laboratory arch model was newly constructed with a Portland cement based mortar. While the mortar was proportioned to be as weak as possible, it was still new and had some tensile strength. Also, the abutments of the lab arch were constructed on the steel plate of the test fixture. The combination of the mortar joints having some tensile strength and no tensile strength at the abutment joints on the steel plates caused the hinges in the lab test to occur at the abutment joint on the steel plates. For the sake of comparison, the numerical model was recalculated with a link element with tensile capacity to represent the laboratory conditions. This forced the hinge location to occur at the abutment points (Figure 117). The ratio of support movement with vertical deflection displays a ratio of 0.42 (Figure 118), which is very good correlation with the laboratory testing. In an older bridge structure that has some deterioration of the mortar joints and is bearing on a concrete or masonry foundation, it would be expected that the intrados hinges would occur higher above the abutments as predicted using the proposed methodology.

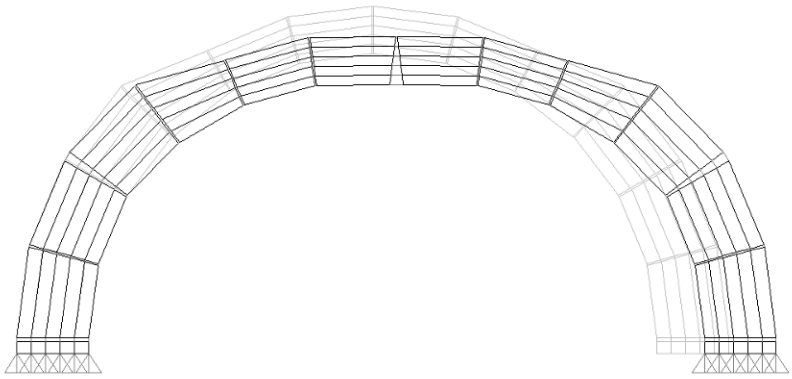

Figure 113. Numerical model of laboratory arch.

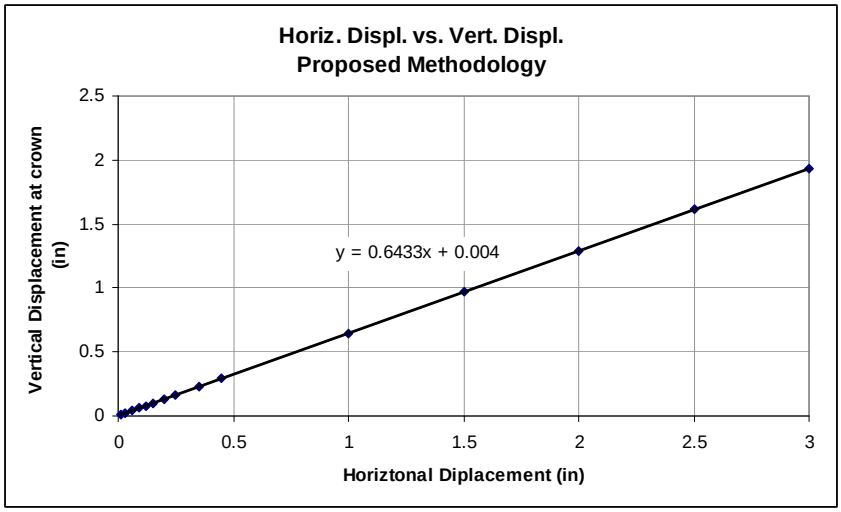

Figure 114. Horizontal displacement vs. vertical displacement plot for numerical model.

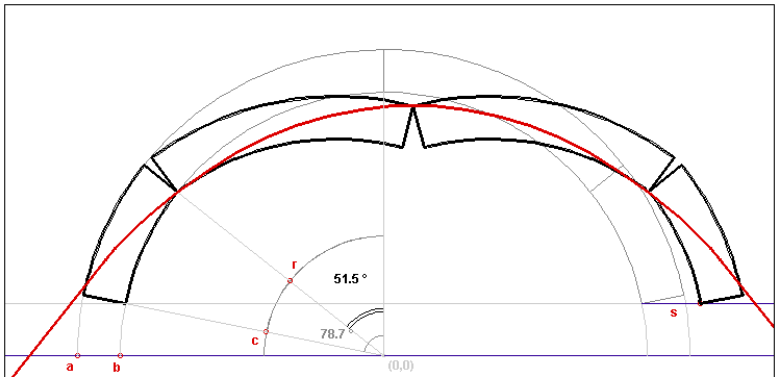

Figure 115. Hinge locations in kinematic study by MIT.

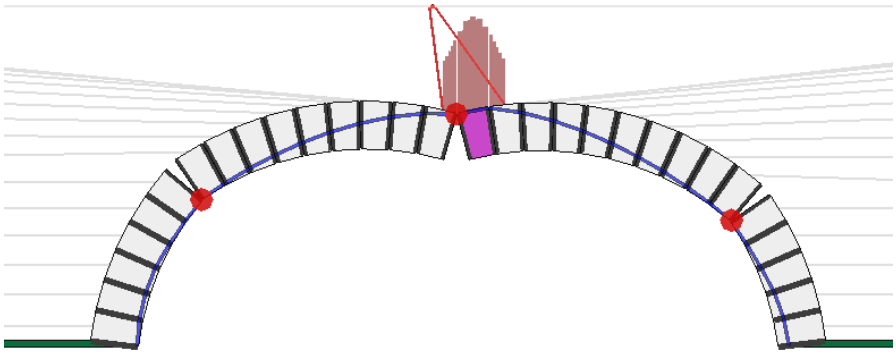

Figure 116. Hinge locations in rigid block limit state analysis (Ring 2.0).

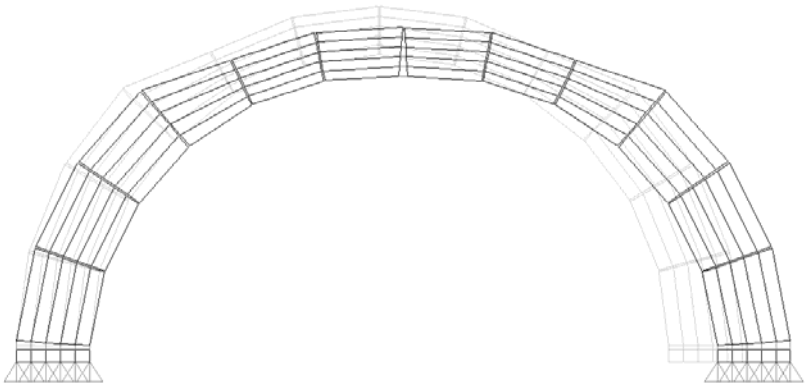

Figure 117. Numerical model of laboratory arch with hinges at abutments.

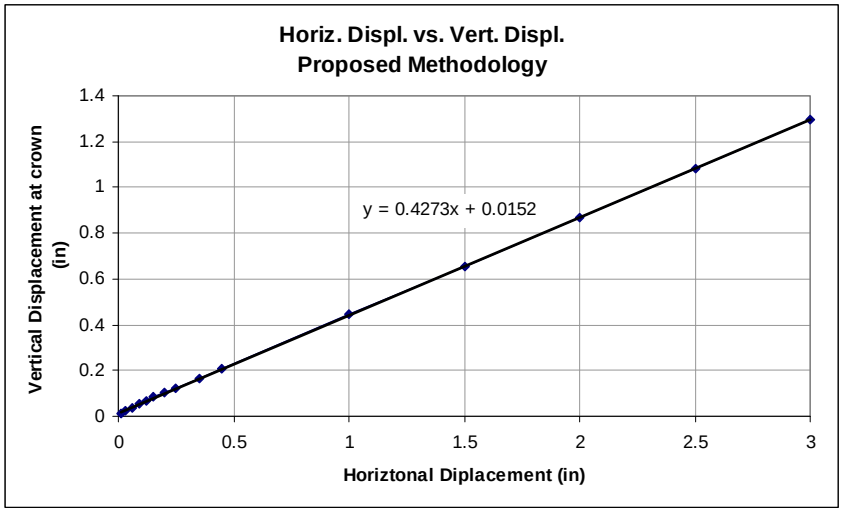

Figure 118. Horizontal displacement vs. vertical displacement plot for numerical model shown in previous figure.

Crack Opening Prediction as a Result of Support Movement

The initial uncracked arch has an inherent stiffness value. However, as discussed in the introductory chapters, as soon as the arch experiences any minor amount of movement at the abutments or from a loading condition, crack locations will begin to occur. This type of hinge development has been observed to occur as soon as the centering supports are moved immediately after arch construction. At this point forward, the mortar joints

act as contact points as described in the presentation of the proposed methodology. The laboratory tests used for comparison in the crack opening predictions will be those with arches that have experienced some initial cracking. These correspond to the second series of tests for Arches A, B, and E, and also the third series test of Arch E.

As the arch experienced support movement, cracks opened up at either the intrados or extrados forming hinge points. In a masonry arch bridge, it is much more practical to measure the crack opening displacements instead of mounting strain gauges on the surface of the arch. During the laboratory tests, the crack openings were measured and plotted against the lateral movement of the supports. For comparison to that data, predictions of the crack openings were made using the proposed methodology.

Figure 119 shows the FBG crack opening data from Test B.3. The data for Test A.2, E.2, and E.3 were very similar. In this case, the initial hinge formation occurred at a lateral displacement of 0.03 inches and was captured by the bottom left crack sensor (labeled as crown hinge in Figure 119). The hinges at the abutments occurred at approximately 0.16 inches of lateral displacement (labeled as abutment hinges in Figure 119).

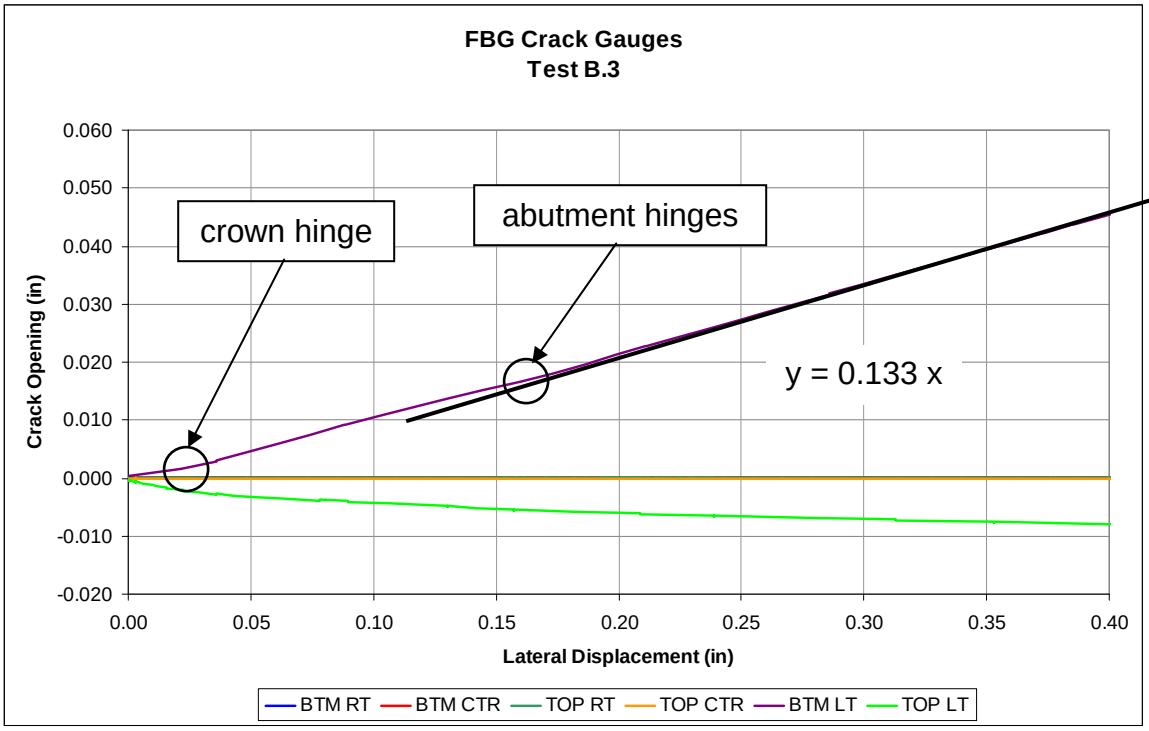

Figure 119. Reprint of Figure 61. FBG crack data from Test B.3

The same support movement was modeled using the proposed methodology. Figure 120 shows the model at 0.02 inches of support movement. This point was the onset of the full hinge formation at the crown. The formation of the hinges at the abutments occurred at the support movement step of 0.14 inches as shown in Figure 121. The modeling points correlated very well with the measured values of 0.03 inches and 0.16 inches.

Figure 119 shows a best fit trend line for the crack opening data beyond the third hinge point creation. The crack opens at a ratio of 0.133 times the support displacement

movement. The numerical model predicted a reasonably close estimate of 0.144 for this ratio (8% difference). See Table 6 for a comparison of the data.

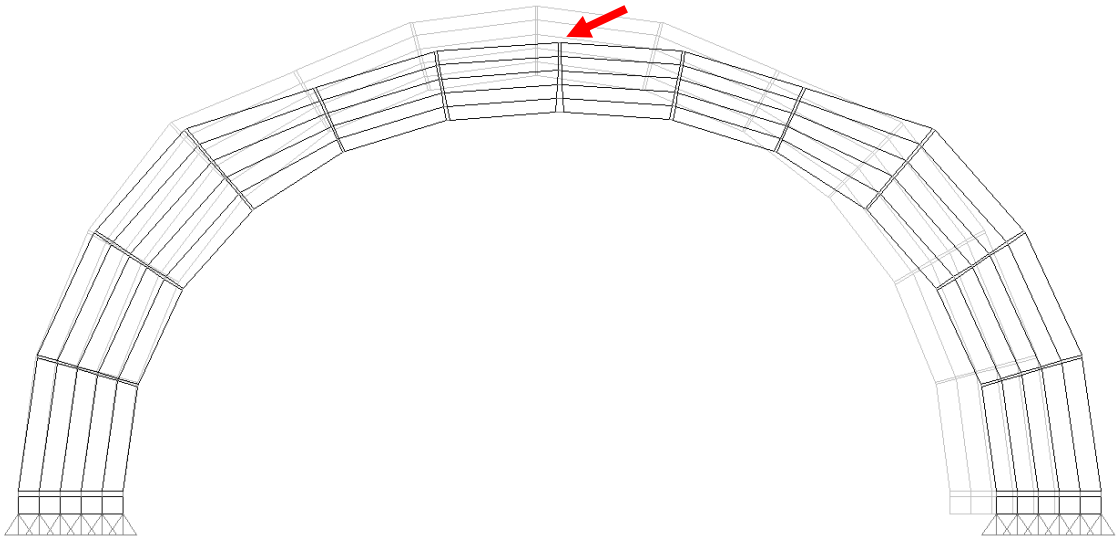

Figure 120. Numerical model at 0.02 inches of lateral support movement (scale 200x). Full hinge creation at this point.

	Laboratory Test	Proposed Methodology
Crown Hinge Formation (inches of horiztonal support movement)	0.03	0.02
Abutment Hinge Formation (inches of horiztonal support movement)	0.14	0.16
Crack Opening Displacement (COD) (as ratio of COD/Support Movement)	0.133	0.144

Table 6. Comparison of laboratory test data and proposed methodology analysis.

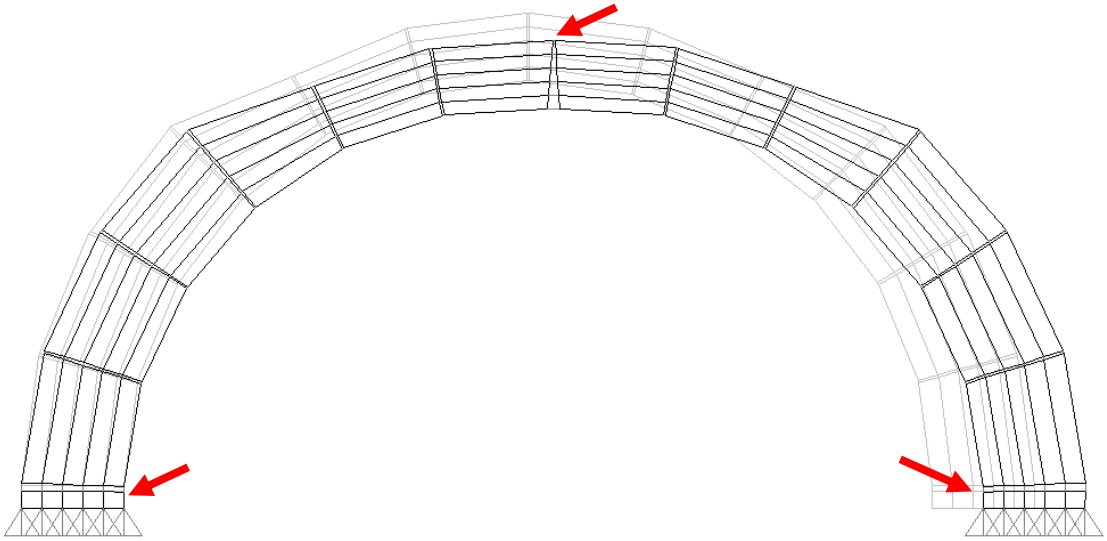

Figure 121. Numerical model at 0.14 inches of lateral support movement (scale 30x). Full hinge formation at abutments and at crown.

5.2.2. Comparison with Ultimate Load Analysis Methods

There are numerous existing techniques and formulations to calculate the ultimate, or failure load, of masonry arches. In order to validate this proposed modeling methodology, comparisons were made with some of the more prevalent methods. Two arch geometries were considered. The first was the geometry of a typical arch shape and the second was a geometry similar to that of the Brooklyn Bridge arch.

For the purposes of the first validation calculation, an example circular arch bridge model was chosen. Figure 122 shows this model. It had the following parameters:

- stone voussoir construction
- span (intrados) = 30 feet
- rise (intrados) = 8 feet

- thickness (consistent along length) = 2 feet
- depth of fill (above crown) = 1 feet

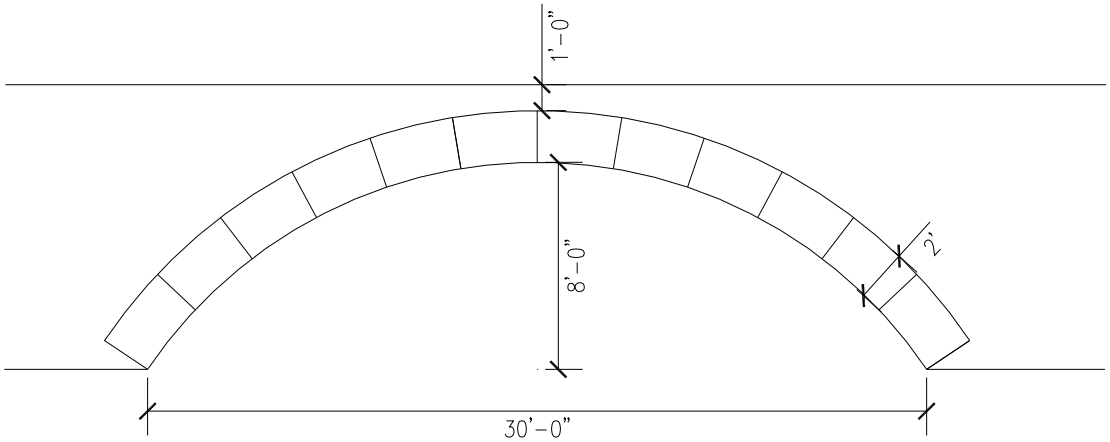

Figure 122. Sample arch bridge.

For the ultimate load comparison, four different analysis techniques were employed. These were the MEXE method, an iterative spreadsheet program developed by Hughes on the basis of the Castigliano theorem, a formula developed by Heyman for quickly checking the output of computer analysis, and rigid block method as programmed by the proprietary Ring 2.0 analysis software.

1. MEXE Method

The current standard methodology for arch brick assessments in the United Kingdom is the MEXE method. British National Standard BD 21/01 (Dept. of Transport 2001b) states the modified MEXE method as listed in companion document BA 16/97 (Dept. of Transport 2001a) is the preferred method for initial arch assessment. British Advice Note BA 16/97 document outlines how to use and apply the MEXE method which was

summarized earlier. A study as part of Advice Note shows a comparison with the results of an MEXE analysis to 10 actual full scale load tests. The MEXE consistently yielded conservative results. The popularity of the MEXE method likely hinges on the conservatism of its analysis and its ease of use as analysis method.

As noted earlier, the MEXE method is an easy to use analysis technique for masonry arches. However, it has some shortcomings. One particular shortcoming where an alternative analysis technique should be used is in the case where the depth of fill at the crown is greater than the thickness of the arch barrel (Dept. of Transport 2001b). Other shortcomings include the use of a number of arbitrary factors that are applied by the end user and the lack of capabilities for support movement. Nonetheless, the MEXE is considered to be the industry standard analysis method particularly for standard shape arches under typical loading conditions. Therefore, the MEXE will make for a suitable validation control for the proposed methodology.

The MEXE ultimate load is calculated using Equation (15). This equation has also been plotted in nomograph for ease of use prior to the popularity of personal computing. Using the nomograph show in Figure 123, the provisional axle load equals 34 tonnes (74.96 kips). It is then modified by the following adjustment factors,

F_{sr} = 1.00,	span to rise ratio < 4.0
F_p = 0.70,	semi-circular profile factor
F_m = 0.82,	based on brick material and fill
F_j = 0.90,	based on mortar joint type
F_{cm} = 1.00	assuming undamaged bridge.

This yields a modified axle load of 77.151 kips.

It is widely accepted that a single axle will load a width of an arch bridge in the transverse direction over an amount equal to (Department of Transport 2001b):

$$w = h + 1.5 \tag{39}$$

where,

w = effective width of arch, in meters

h = height of fill at point of load, in meters

When the modified axle load is divided by the effective width of 7.43 feet, the resultant load is 10.11 kips per foot width.

It should be noted that the MEXE method is know for being a very conservative analysis.

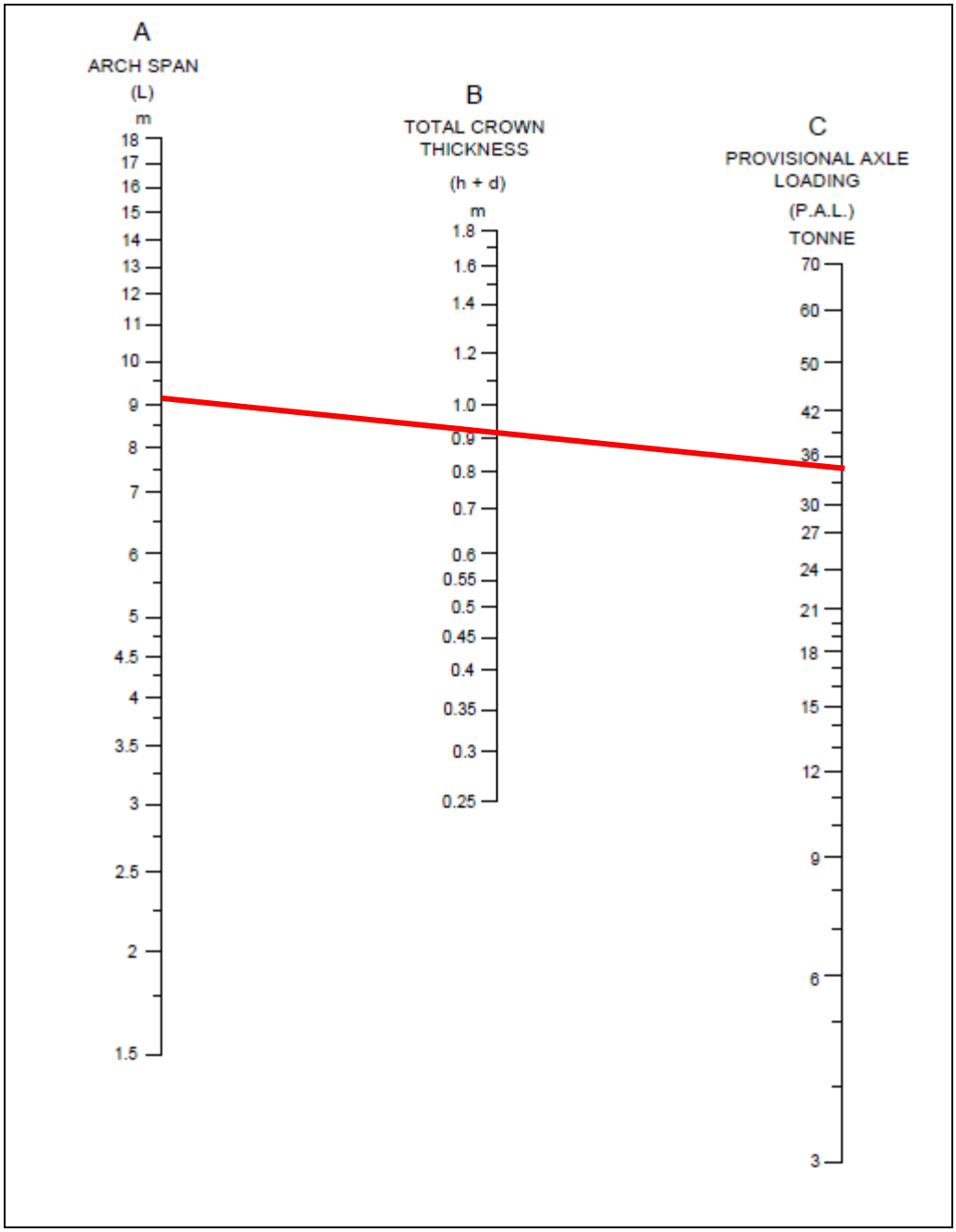

Figure 123. Nomograph for MEXE method.

2. Castigliano Method

Hughes developed a set of spreadsheets based on the Castigliano method. The main premise of the method is that it runs an elastic analysis of the arch. Then any sections of

the arch in tension are removed and the analysis is rerun. This is continued iteratively until all tension sections of the arch have been removed and the arch is still stable.

The elastic arch analysis yielded a result of 215 kN/m, or 14.73 k/ft as shown in Figure 124. Note that the thinned sections of the arch. These are locations where the tension sections of the arch were iteratively removed. The thinnest sections represent the locations of the hinges. This corresponds well with the hinge locations identified in the proposed analysis methodology.

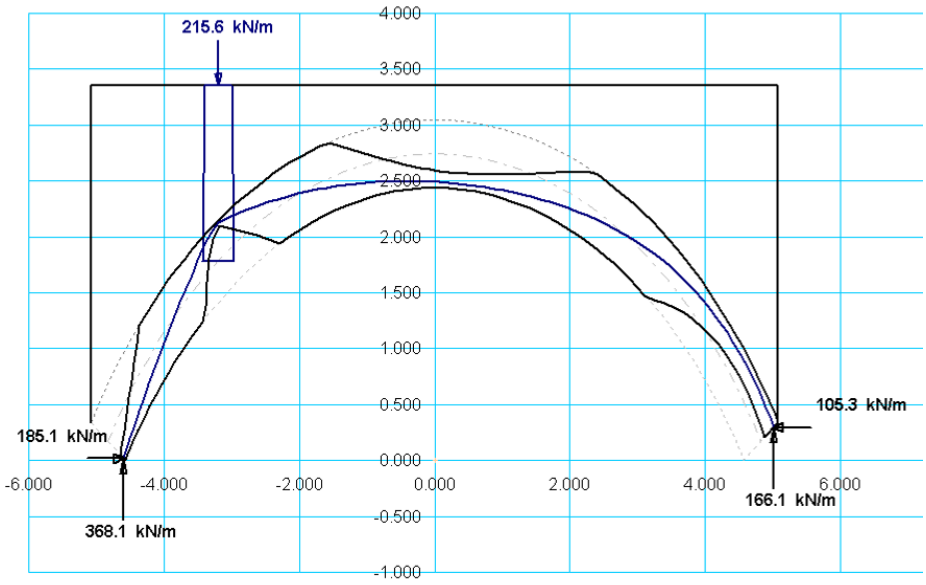

Figure 124. Castigliano analysis of sample arch.

3. Heyman Analysis

Heyman's methodology was based on hinge development in arches. He concluded in his book, The Masonry Arch, that a plastic method of analysis could be used for analyzing the capacity of masonry arches (Heyman 1982). The locations of a point load and hinges

had to be assumed and then the thrust line could be drawn. The thickness of the arch could be shrunk until all points of the thrust line were still contained within the arch. The ratio of the arch thickness to the arch thickness required to contain the thrust line provided the geometrical factor of safety for the structure.

This process is iterative and practically requires a specialized computer program to run this analysis, of which none are commercially or otherwise readily available. However, by making several assumptions, Heyman was able to simplify the iterative process into a single equation to calculate the ultimate load of a masonry arch (Equation (17)). This equation is based on the critical load being applied to the quarter point of the arch and that the thrust line is such that the hinges for failure form at each of the abutments, at the point of load and near the peak.

Heyman's equation (Equation (17)) yielded an ultimate load equal to 5.03 kips per foot width. The results of the Heyman quick analysis method are highly irregular in the studies undertaken for this thesis. This is because of the fixed hinge locations upon which his formulation is based. To accurately apply the Heyman method, an iterative computer program would need to be written. No such programs are currently available and the investment to write one is not worthwhile as there are other mechanism based software programs already available.

4. Ring 2.0

Ring 2.0 is a currently available commercial software program based on the rigid block and limit state model of arch analysis. The parameters of the example arch were input into the software with a single axle load at 1/4 point of the span.

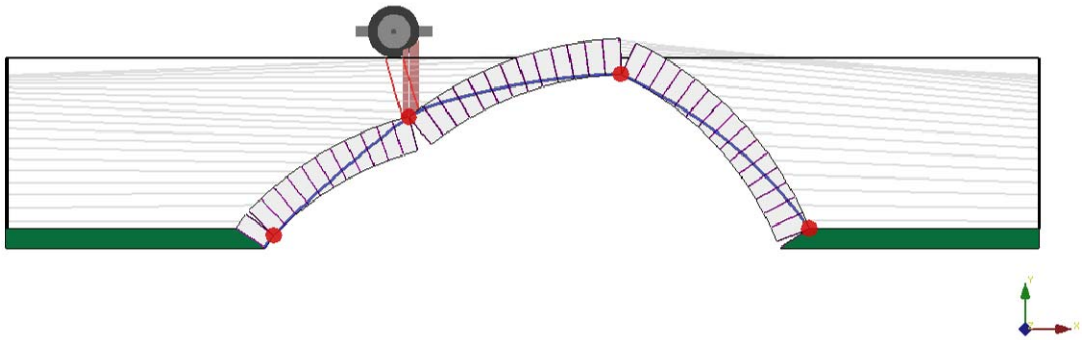

Figure 125. Ring 2.0 software output for example arch.

The software analysis presented a failure load of 424 kN per 7 foot wide bridge span. When calculated at a force per unit width, the result was equal to 13.61 k/feet.

For the second validation model, a typical semicircular arch bridge model was similar in shape and size to the Brooklyn Bridge was chosen. Figure 126 shows this model. It had the following parameters:

- tied brick arch construction
- span (intrados) = 34 feet
- rise (intrados) = 17 feet
- thickness (consistent along length) = 2 feet
- depth of fill (above crown) = 3 feet

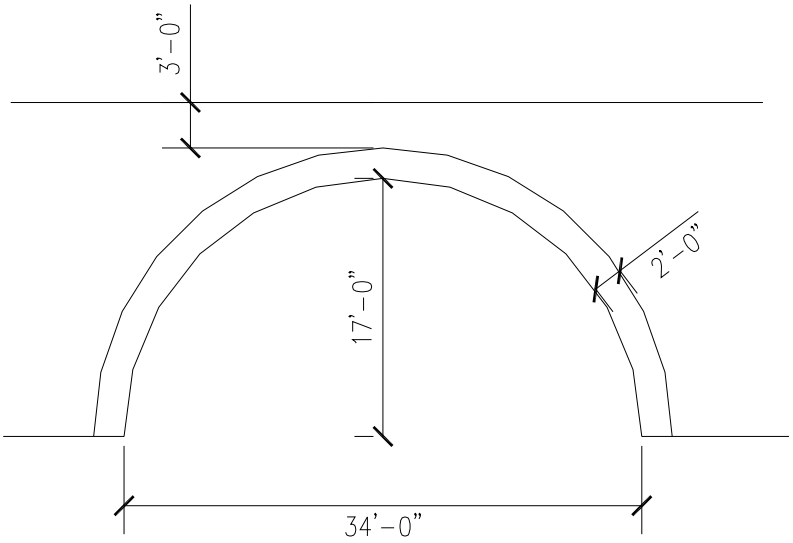

Figure 126. Dimensions of Brooklyn Bridge example arch for validation study.

1. MEXE Method

Using the following parameters and Equation (15) or the nomograph in Figure 123,

L = 10.36 m (34')
d = 0.61 m (2')
h = 0.91 m (3')

the provisional axle load equals 82.3 tonnes (181 kips).

It is then modified by the following adjustment factors,

F_{sr} = 1.00, span to rise ratio < 4.0
F_p = 0.70, semi-circular profile factor
F_m = 0.82, based on brick material and fill
F_j = 0.90, based on mortar joint type
F_{cm} = 1.00 assuming undamaged bridge. (However in the case of the actual Brooklyn Bridge arches, a condition factor of 0.6 should be taken for the longitudinal cracks.)

This yields a modified axle load of 93.5 kips.

When the modified axle load is divided by the effective width of 9.92 feet, the resultant load is 9.42 kips per foot width. This is slightly higher than the suggested new methodology for two reasons, the MEXE factor is known to be unconservative in instances were the depth of fill exceeds the thickness of the arch (McKibbons 2006) and the effective width equation is typically used in design situations with the MEXE method and is conservative in nature. The actual tests by Chettoe and Henderson (Chettoe 1957) on which these tests are based reveal the effective width was found to be 10 to 15% higher.

2. Castigliano Method

Using the Hughes spreadsheets based on the Castigliano method as described earlier, the elastic arch analysis yielded a result of 89.9 kN/m, or 6.10 k/ft as shown in Figure 127.

The actual geometry of the stepped change in thickness could not be accurately modeled in the Castigliano spreadsheets. However, the option for a tapered arch thickness was available. A second Brooklyn Bridge arch analysis was completed using a tapered arch thickness from 3 feet at the supports to 2 feet at the crown as shown in Figure 128. This yield a much higher ultimate load capacity with a result of 284.4 kN/m, or 13.80 k/ft.

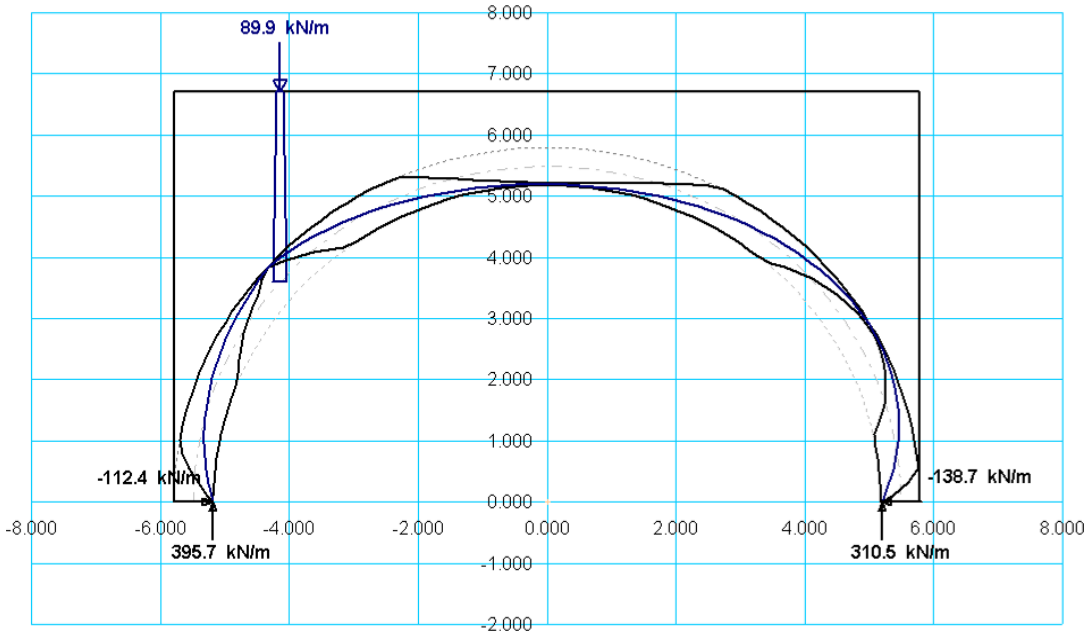

Figure 127. Castigliano analysis for 2' thick Brooklyn Bridge model.

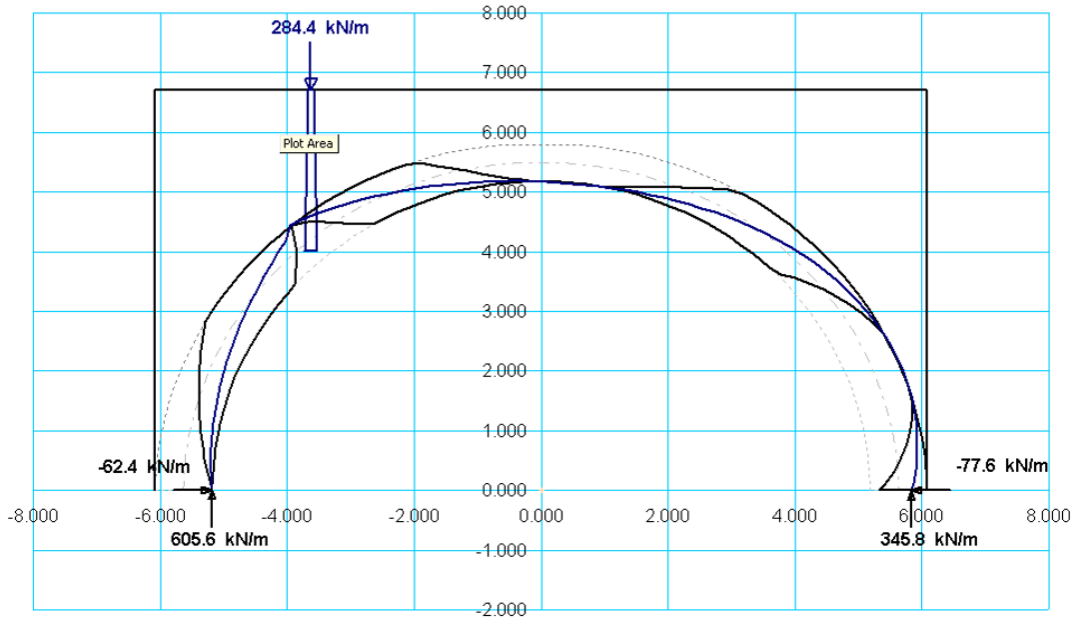

Figure 128. Castigliano analysis for tapered Brooklyn Bridge model (tapered thickness from 3' to 2').

3. Heyman

Using Equation (17) and Figure 13, an ultimate load of 9.82 kips per foot width was calculated

4. Ring 2.0

The software analysis presented a failure load of 133 kN. When calculated at a force per unit width, the result was equal to 4.27 k/feet.

Summary of Ultimate Load Analysis Results

Both the laboratory test arch and the Brooklyn Bridge arch of Figure 81 and Table 4 were modeled using the proposed methodology presented in this dissertation. A summary of all ultimate load analysis are listed in

Table 7. As can be seen, there is good correlation between the proposed methodology and existing analysis methods. As noted earlier, the British Department of Transport found a +/- 20% range of most analysis methods. The proposed analysis method is well within this range and even more accurate when compared with other mechanism based analysis methods. The best result comparison is with that from Ring 2.0 as both the proposed methodology and the rigid block limit state analysis of Ring 2.0 are both mechanism based analysis methods.

5.2.3. Comparison with Full Scale Load Test

A full scale load test was constructed of the masonry arch bridge at Bridgemill in 1985 (Hendry 1985). The bridge was located near Girven, Scotland. The bridge was constructed in 1869 and had a span of 18.3m (Figure 129). It was tested to failure with a series of hydraulic jacks set up across the cross section of the bridge as shown in Figure 130. The load was applied at quarter point of the span. The ultimate load and load deflection data from the test was provided in the test report (Hendry 1985). Figure 131 show an example of the load deflection plot at the quarter point of the arch span.

Figure 129. Photograph of Bridgemill arch bridge.

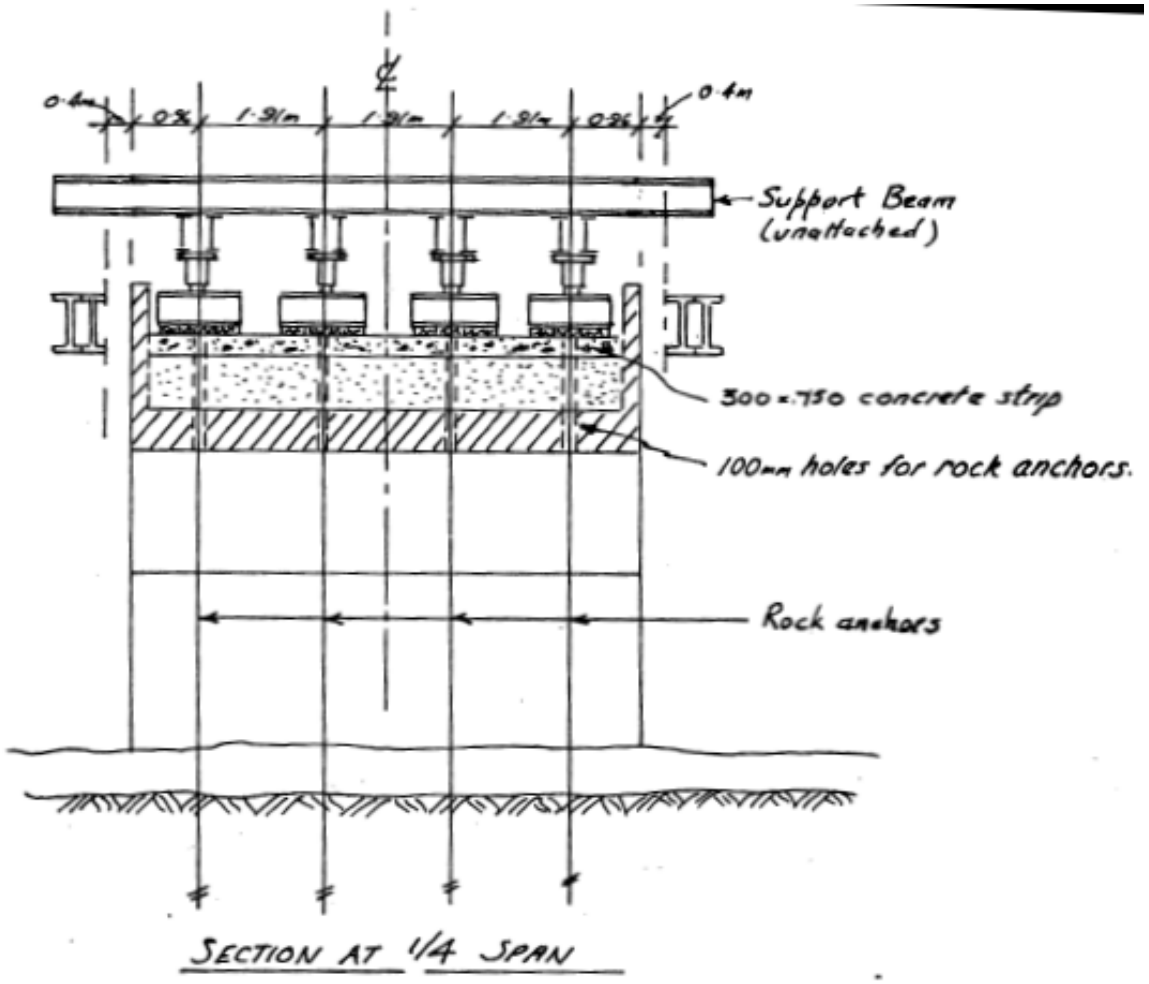

Figure 130. Load test configuration.

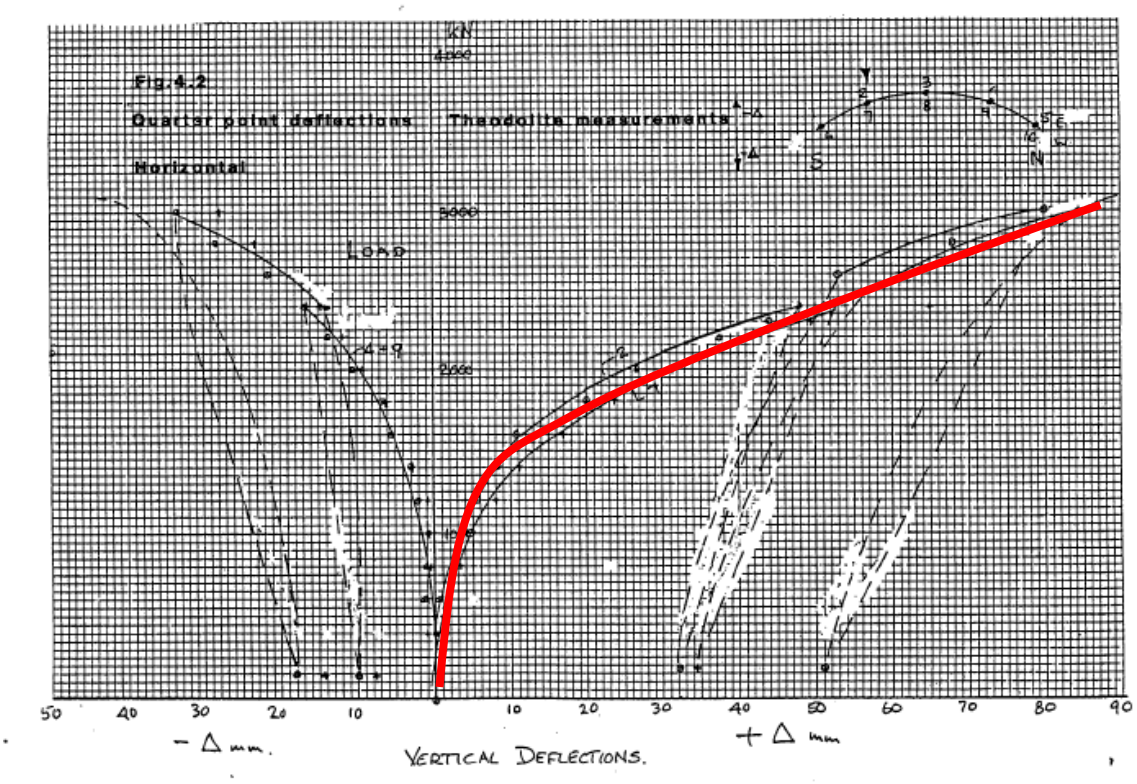

Figure 131. Recorded load deflection data from full scale test.

For comparison with the proposed methodology, a numerical model was created using the process outlined at the beginning of this chapter. A vertical load was incrementally applied at the quarter point span of the bridge and the load deflection plot was calculated. As can be seen from Figure 133, the ultimate load of 34 kips/foot was very near the actual test load of 33 kips/foot. The numerical model was slightly stiffer from a load deflection standpoint, but this was likely due to mortar and masonry deterioration in the over 100 year old bridge. Table 7 shows a comparison between the calculated and actual load test data.

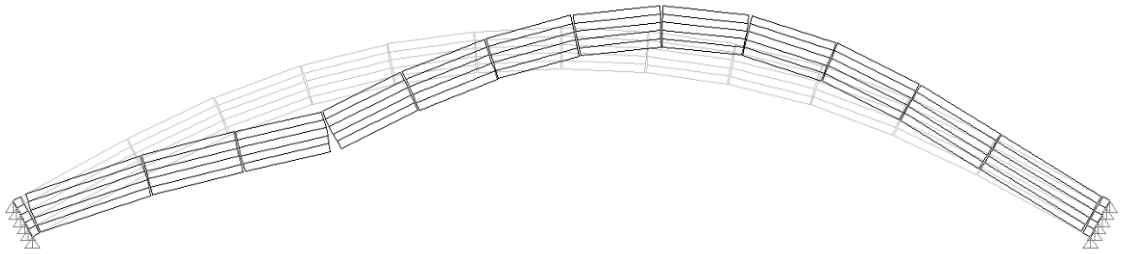

Figure 132. Deflected shape of arch bridge under full load.

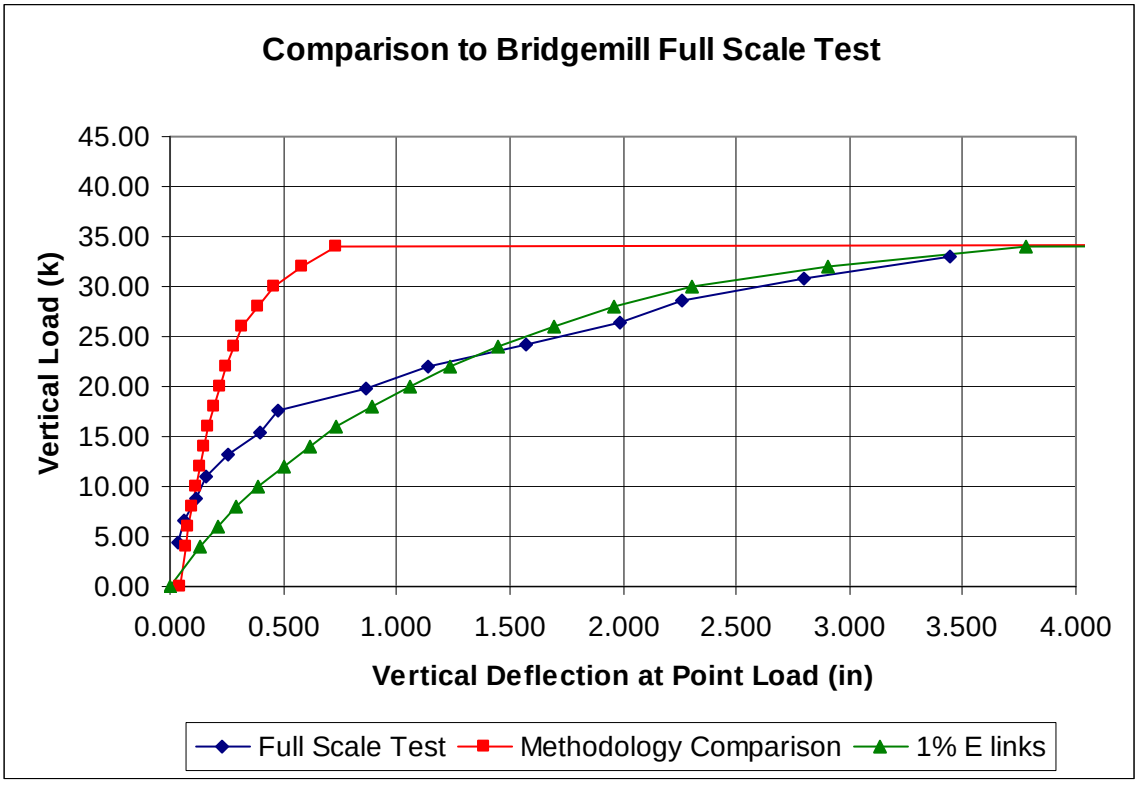

Figure 133. Comparison plot of methodology to actual load test data.

5.2.4. Summary of Load Comparisons

Due to the nature of masonry arches and their construction, British Standards find acceptable calculation methods to have an accuracy of +/- 20% with full scale load tests

and laboratory modeling. The proposed methodology shows good correlation with a full scale load test and other mechanism based analysis methods such as the rigid block, limit state method used in Ring 2.0.

	Proposed Method	Castigliano	MEXE	Ring 2.0	Heyman	Load Test
	k/ft	k/ft	k/ft	k/ft	k/ft	k/ft
Sample Arch	12.00	14.73	10.38	13.61	5.03	
Brooklyn 2ft	4.51	6.10	9.42	4.27	9.82	
Brooklyn 3ft	11.00	13.80	14.05	15.09		
Bridgemill	34.00		16.51		31.15	33.02

* Ring 2.0 does not allow for tapered thickness (Brooklyn 3ft model)

Table 7. Comparison of Ultimate Load Calculations.

5.2.5. Comparison with Pippard Studies

As noted in the introduction, Pippard studied masonry arched using a scaled model with metal fabricated voussoirs. His work in the 1930s still continues to be highly recognized as important research to understanding the structural performance of masonry arches.

One of Pippard's primary studies was based on experiments with a 4' long arch constructed of rigid voussoirs (Pippard 1937). The voussoirs were constructed with machined pieces of steel. Figure 134 shows the test setup used by Pippard.

As discussed earlier, Pippard surmised that an arch with stationary abutments behaves as a two-hinged arch until the point load increases to the point that it creates a third hinge point. Pippard found this hinge point to occur at the extrados of the voussoir joint between the point load and the center of the arch.

To show the transition from a two-hinge arch to a three hinged arch, Pippard applied a point load at voussoir #5. He then plotted the relationship between the increase in magnitude of the point load the corresponding increase in horizontal thrust reactions at the supports (Figure 135). The first section of the plotted data is linear and the slope of 0.485 corresponds with ratio of H/W equal to 0.455 for a two-hinged arch. There is then a transition section of the curve and then the top section of the curve has a slope of 0.720 which corresponds with a ratio of H/W equal to 0.716 for a three-hinged arch.

For verification of the proposed arch modeling methodology, a numerical model of Pippard's test model was created (Figure 136). It was meshed with 15 elements corresponding with the actual number of voussoirs used by Pippard. Each of the meshed elements was divided into four segments with the nonlinear gap elements connecting the adjacent voussoirs. The end conditions were pinned. Figure 137 shows the plot of the resulting data. For comparison to the values calculated see the plot showing the ratio of H/W. A dead load weight factor of 3.0 was used to simulate the dead load weights hung from Pippard's model.

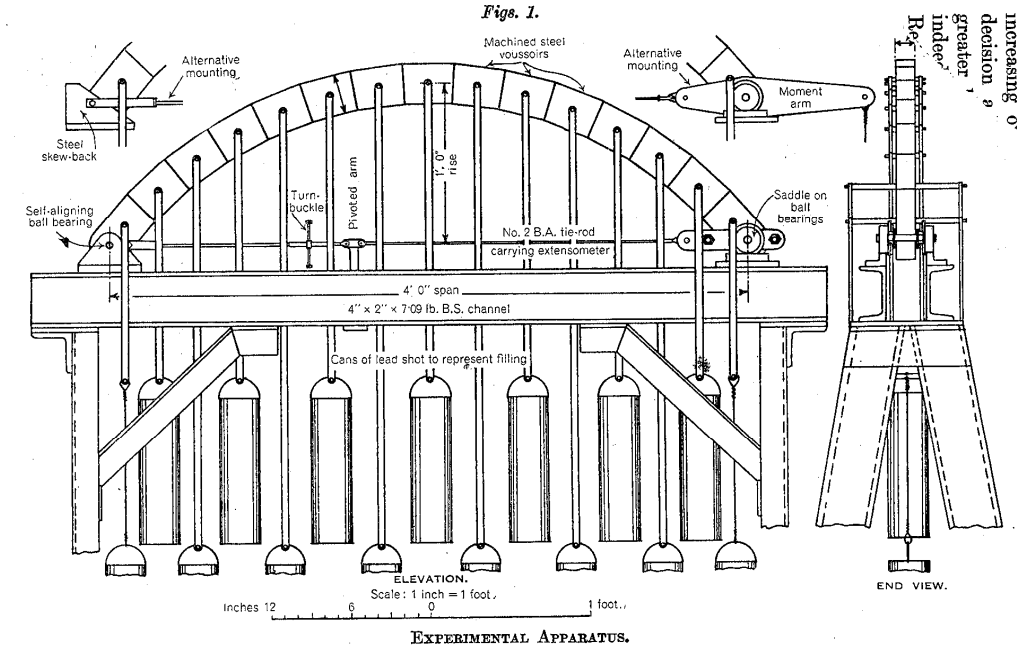

Figure 134. Experimental setup used by Pippard (from Pippard 1936).

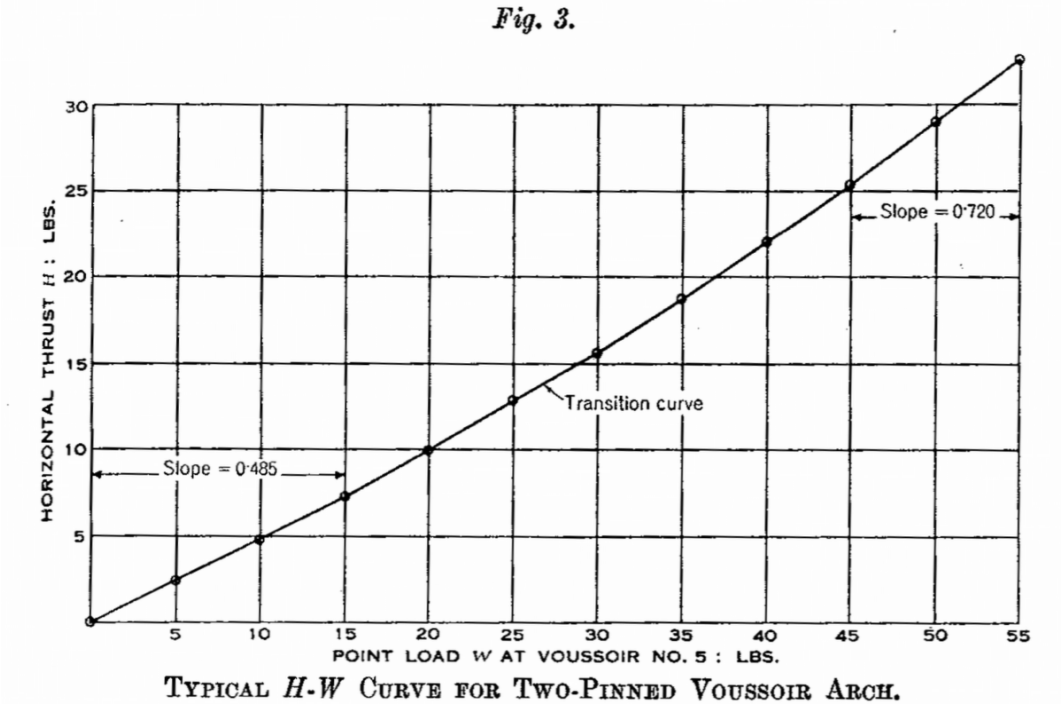

Figure 135. Plotted data by Pippard for the thrust vs. point load relationship (from Pippard 1936).

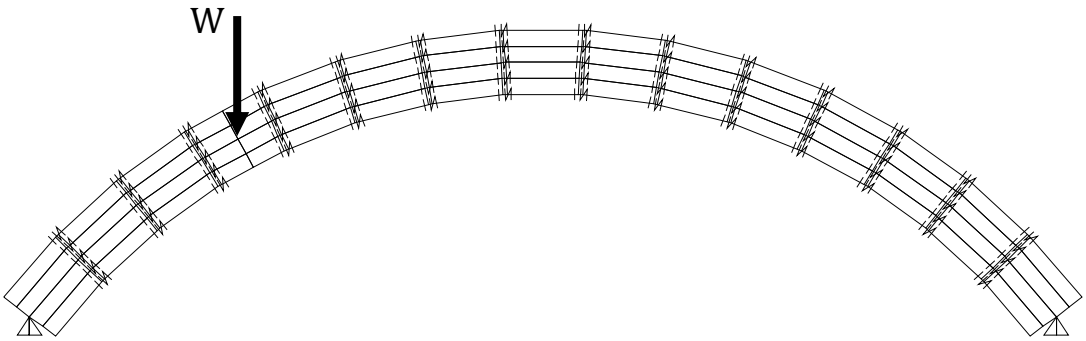

Figure 136. Numerical model constructed to verify Pippard's test.

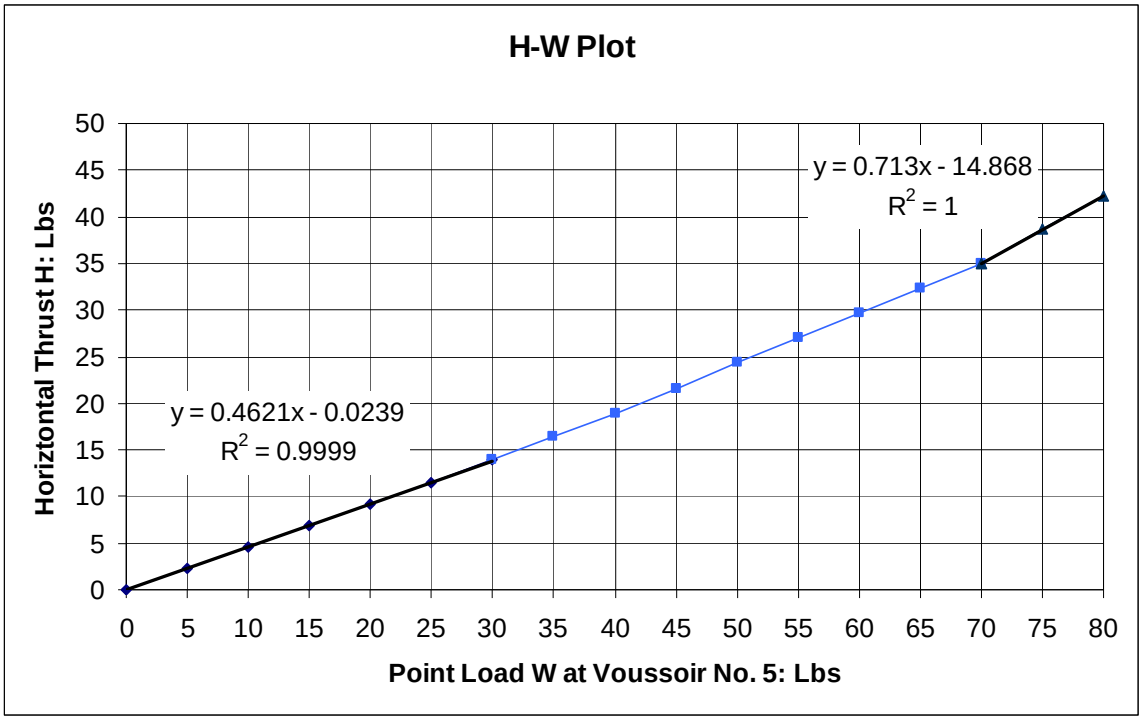

Figure 137. Comparison plot for Pippard H-W plot.

As can be seen for the plot, the ratio of the two-hinge region of the analysis was 0.462. This can be compared to 0.455 calculated by Pippard. At the upper end of the plot in the

three-hinged arch region, an H/W ratio of 0.713 was calculated compared to Pippard's calculated value of 0.716. The above analysis confirms that the numerical model is accurate to both traditional calculation analysis and verified by past experimental work. The only discrepancy between Figure 137 and the work by Pippard was that the three-hinged portion of the plot starts at 70 lbs as compared to 45 pounds in Pippard's plot. This difference is accounted for differences in the dead load weight applied to the model and the experiment. Pippard did not publish the dead loads he used in his experiments and assumptions had to be made on these values.

5.3. Applying the Methodology - Case Study with Brooklyn Bridge SHM Data

The defining motivation for the development of this proposed methodology was to use it as a tool for interpreting and understanding structural health monitoring data from masonry arch bridges. The following is a case study example of how the proposed methodology could be employed for such use.

5.3.1. Tilt of Supporting Walls

As was discussed in the Brooklyn Bridge monitoring chapter, during visual inspection of the longitudinal arch cracking, one of the identified possible causes of the cracks at the crown was movement of the supports. The supports for the Brooklyn Bridge masonry arch spans were thick walls constructed of unreinforced clay bricks.

The east wall of the east arch span abutted the heavy masonry block construction of the cable anchorages. This wall was tied into the massive anchorage structure and it was not expected that any movement of this wall was possible. The tiltmeter data confirmed this. The west wall of the west arch span was adjacent to a steel truss span for a wide roadway. The steel trusses were quite deep and they were supported on stout masonry pilasters. The masonry pilasters essentially acted as a counterfort for the west wall. The tiltmeter readings confirmed that this wall was rigidly held in place and did not move laterally.

The center wall supported both the east and west arch spans. The wall essentially acted as a slender bridge pier. The arches on either side of the support wall were of differing span lengths and there was concern that this wall could move laterally. Vertical cracking in the wall was observed indicating past differential settlement. Such additional settlement could also lead wall rotation which in essence would cause a support movement condition.

Recordings of the tiltmeter at the upper floor of the center wall confirmed that there was in fact some rotation of the wall which correlated with seasonal temperature changes. The tiltmeters on lower floors of the center wall did not record any movement. It was concluded that the floor framing was providing lateral support to these walls and preventing any movement.

The center wall, from the top of the third floor to the bottom of the masonry arch, was approximately 8.3 feet in height (Figure 138). Figure 139 shows a schematic diagram of the center arch pier if it were to rotate. The displacement, delta, is the amount of support movement the arch would experience.

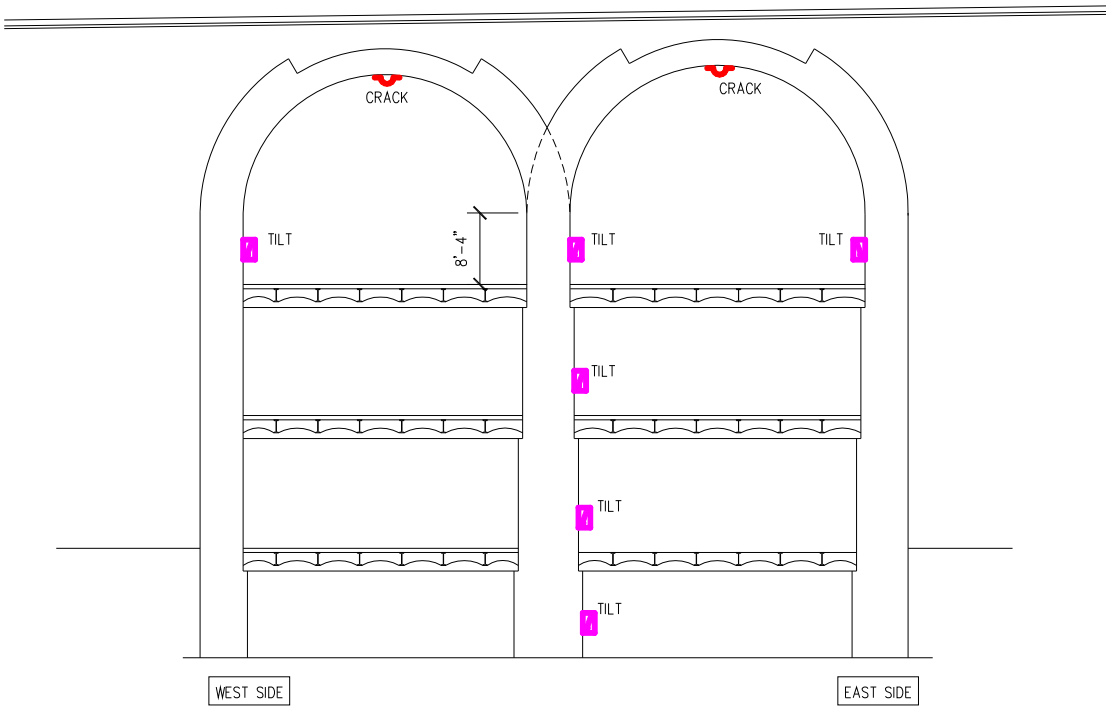

Figure 138. Cross section of arch bridge showing center pier support.

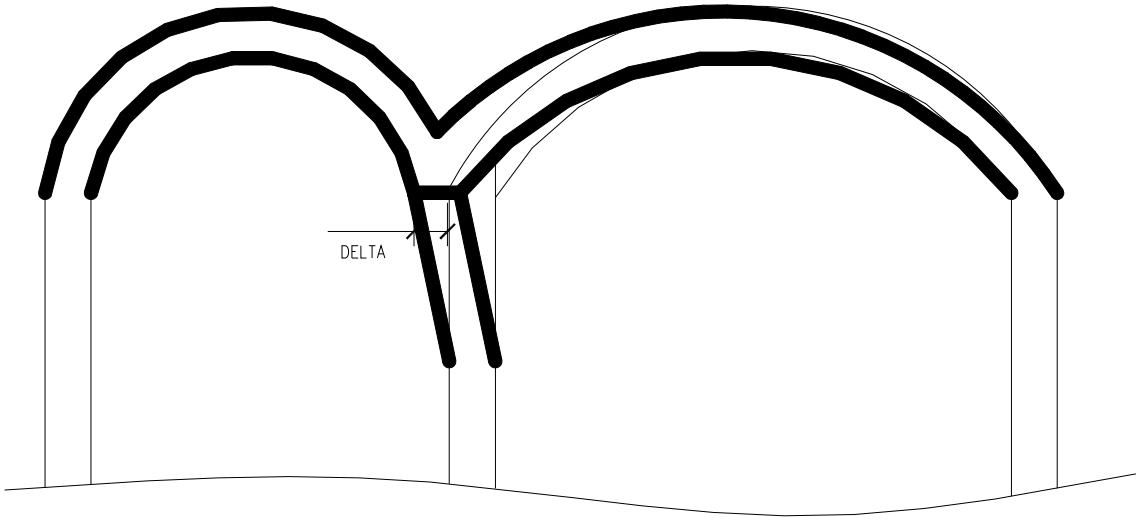

Figure 139. Schematic diagram of arch span showing wall rotation.

If the center supporting wall were assumed to have pinned connections at the top and bottom, it could be schematically drawn as shown in Figure 140. In this case, if a tiltmeter were mounted in the center of the wall, the lateral displacement at the top of the wall could be calculated as:

$$\Delta_{top} = L\left(\sin\theta\right) \tag{40}$$

where,

L = height of the wall

θ = rotation as measured by tiltmeter at midheight of wall

However, because of the thickness of the wall and the floor framing connections on either side of the wall, the actual connections at the top and bottom of the wall would be better represented as a fixed-fixed condition (Figure 141). The derivation to calculate the displacement at the top of the wall based on a measured rotation at the center of the wall is as follows:

$$M(x) = -\frac{6EI(\delta)}{L^2} + \frac{12EI(\delta)}{L^3}x \tag{41}$$

$$\theta(x) = \frac{6\delta}{L^2} + x\left(1 - \frac{x}{L}\right) \quad \text{for } 0 \le x \le \frac{L}{2} \tag{42}$$

$$\theta\left(L/2\right) = 1.5\frac{\delta}{L} \tag{43}$$

$$\delta = \frac{L \cdot \theta(L/2)}{1.5} \tag{44}$$

The maximum rotation in the center wall measured by the tiltmeters during the SHM program was 0.3 degrees, or 0.0052 radians. Based on Equation (44), the maximum lateral support movement for the arch was 0.35 inches.

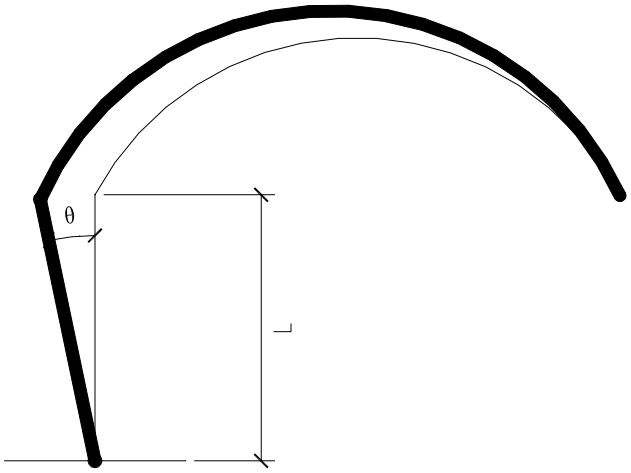

Figure 140. Wall rotation diagram assuming pinned connections at top and bottom of wall.

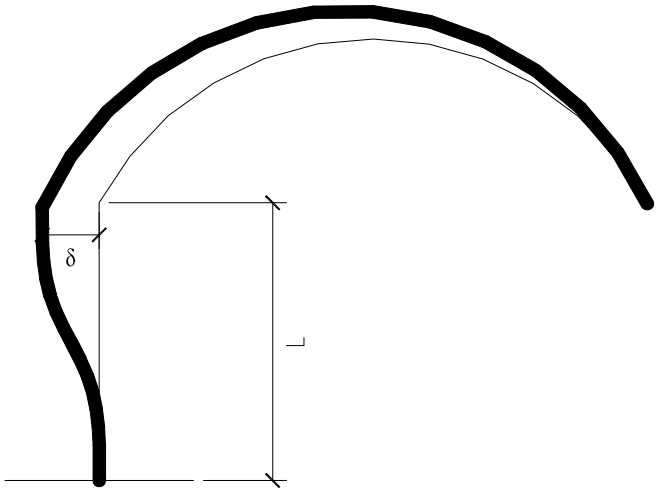

Figure 141. Wall rotation diagram assuming fixed connections at top and bottom of wall.

Using the proposed methodology, the relationship between the crack width opening and the support movement can be plotted (Figure 142). As was seen in the analysis of the laboratory test arches, the plot can be divided into three sections: no hinges, hinge at the crown, and three hinged arch. In the case of the Brooklyn Bridge, we are certain to be in the second stage with a hinge at the crown and it is likely to be in a three-hinged condition.

Using the calculated maximum support movement of 0.35 inches, the expected corresponding crack opening displacement can be calculated to be 0.066 inches. During the SHM program, the maximum crack sensor strain was measured to be nearly 1000 μm, or 0.040 inches. This is slightly less than the predicted value. However, it should be understood that the predicated value is used as an upper limit. Factors such as interaction of the fill and roadway will typical limit the crack opening in the actual

bridge. The intent of the modeling is to understand the approximate crack openings that can be anticipated in an in-service bridge.

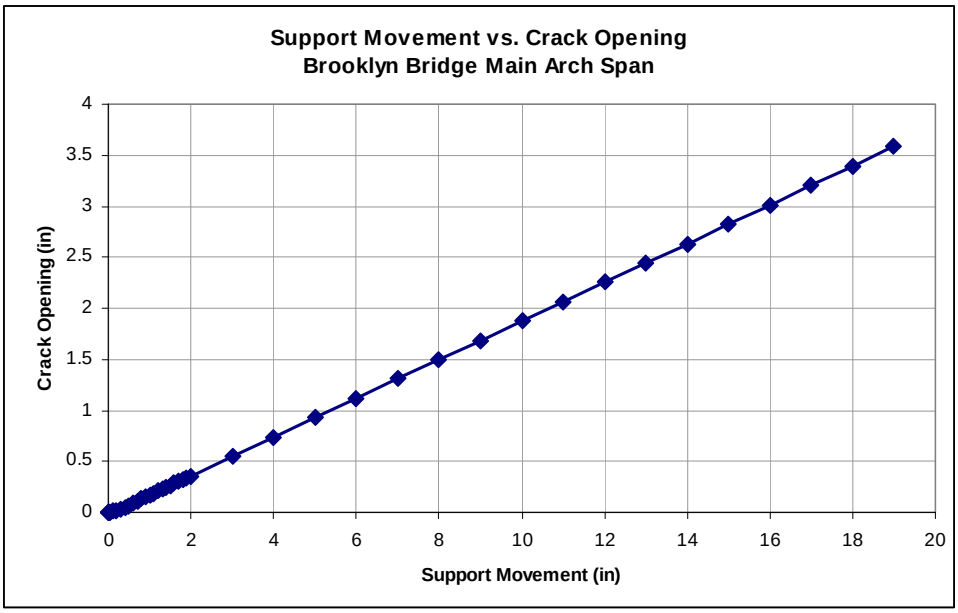

Figure 142. Plot of crack width opening to support movement for the Brooklyn Bridge arch.

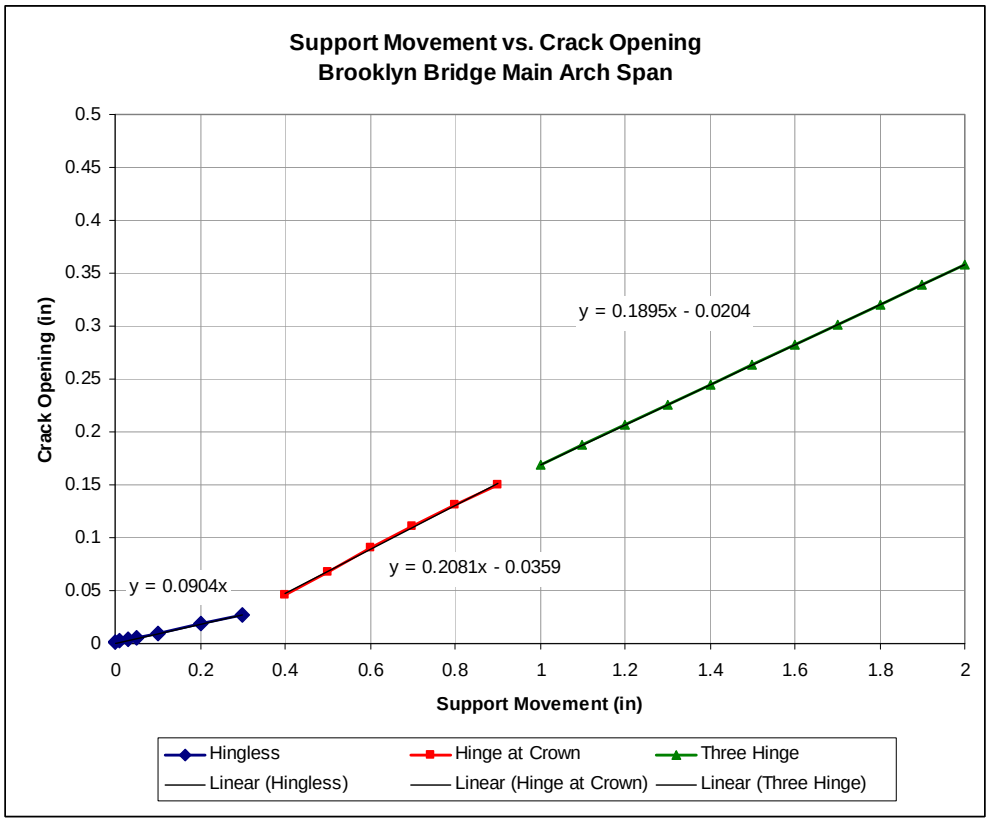

Figure 143. Ratio of crack width to support movement for Brooklyn Bridge arch.

6. CONCLUSIONS

There are numerous in-service arch bridges across Europe, India, and North America. As these bridges age and deteriorate, it is important to be able to safely evaluate them for the allowable loads that they can support. Numerous theories and methodologies have been developed for centuries to calculate the strength of masonry arch bridges. Currently, the two most popular methods are the MEXE method and the rigid block analysis method.

The MEXE method is most popular because of its ease of use. The allowable axle load is calculated from a simple equation using the span length, arch thickness, and depth of fill and then modified using a series of condition factors. It was originally developed for use in World War II to quickly assess bridges for tank loads, but has remained popular for its ease of use and reasonably accurate results. The rigid block method is the other most popular arch analysis method in use today. It is based on a hinge formation and plastic limit state analysis. The contact between arch blocks is modeled with a series of equations that can be solved with linear programming methods. The method has been popularized by recent commercial software.

However, these two methods are not without their shortcomings. The MEXE method has been found to yield unconservative results for bridges with a depth of fill greater than the thickness of the arch. The rigid block method has been found to have better

results for wider range of arch geometries, but requires a proprietary software program. The user is limited to input only the variable specified in the program. Both of the methods do not have the capability to handle non-uniform arch geometries. The proposed methodology yields results similar to these two analysis methods and has been calibrated against full scale load tests while also addressing some of their shortcomings. The proposed method has the following benefits over currently available load analysis methods:

- It can model any arch geometry and any type of loading without specialized computer programming.
- The methodology graphically displays the thrust line and hinge locations of the arch for a given load case.
- Any standard finite element software program can be used to run the analysis without requiring specialized programming.

While all of the above benefits will be helpful to a bridge engineer analyzing an arch bridge, the most significant contribution from the proposed method and the primary motivation for its development is its usefulness in accompanying a structural health monitoring program. SHM systems continue to gain popularity as sensors become more advanced, rugged, and capable and as computing equipment becomes more economical. It is currently possible to deploy a set of sensors on a bridge and monitor them remotely from any location via an internet connection. This can reduce the costs of bridge

maintenance and increase the safety of transportation structures. However, a SHM program is only helpful if the data it provides can be easily and accurately interpreted.

As part of the research work for this study, a structural health monitoring system using fiber optic sensors was designed and installed at the masonry arch approach spans of the Brooklyn Bridge. Cracking was previously observed at the crowns of the two arch spans during routine visual bridge inspections. The structural health monitoring system was installed to provide real-time feedback about the movement of the cracks and other structural components of the bridge span. The proposed methodology calculates acceptable crack opening displacements and predicts the effects of the crack openings on the bridge structure. The analysis results from the proposed methodology were compared to the SHM data to enable an accurate interpretation of the real-time structural condition of the bridge. Prior to implementation, the proposed methodology was verified against scaled masonry arch models tested in the laboratory.

The proposed method consists of creating a mechanism based model can be created in any standard finite element software. From this numerical model, a number of analyses and simulations can be made. Examples include:

- Support settlement and movement of the arch abutments or piers can be modeled. The effects of the settlement on the ultimate strength of the arch bridge

can be determined along the effect of the settlement on the in-service deflections of the bridge.

- Anticipated crack openings can be estimated. This provides a baseline for what can be expected from the sensors mounted on the actual structure. Crack opening displacements can be modeled for temperature changes, support movements, and different loading configurations.
- Maximum alarm criteria for crack sensors and tiltmeters can be modeled to ensure that such limits are not too conservative or unconservative which could hamper the usefulness of the SHM program.

Masonry arch bridges have a non-linear response due to hinge formation and orthotropic building materials. Estimates of strength and deflection as determined by numerical models will never have perfect correlation with field data. However, estimates provided by the proposed methodology provide the user of a structural health monitoring system for arch bridges a strong basis for determining the safe and unsafe levels of movement and crack openings displacement. Also, the movements can be re-modeled into the proposed methodology to determine their effect on the ultimate load carrying capacity of the arch bridge.

CITED LITERATURE

Block, P., Ciblac, T., Ochsendorf, J. (2006): Real-time Limit Analysis of Vaulted Masonry Buildings. Computers and Structures, v 84, n 29-30, p 1841-1852.

Boothby, T. (1995): An Overview of Masonry Arch Bridges in the USA. Arch Bridges: Proceedings of the First International Conference on Arch Bridges, Bolton UK.

Boothby, T. (2001): Analysis of masonry arches and vaults. Progress in Structural Engineering and Materials, 3: 246–256. doi: 10.1002/pse.84

Chettoe, C.S., and Henderson, W. (1957): Masonry Arch Bridges: A Study. Proceedings of the Institute of Civil Engineering, London, UK

CSI (2010): CSI Analysis Reference Manual for SAP200, ETABS, SAFE and CSibridge. Computers and Structures, Inc., Berkeley, CA, USA.

Collingwood, F. (1876): Notes on the Masonry of the East River Bridge. Transactions of the American Society of Civil Engineers, Vol. VI, No. 1, January 1877, p. 7-27

Corradi, M. (1998): Empirical methods for the construction of masonry arch bridges in the 19th Century. Arch bridges: History, Analysis, Assessment, Maintenance and Repair; Proceedings of the Second International Arch Bridge Conference, Venice, Italy, p. 25-36.

Department of Transport (2001a): *The Assessment of Highway Bridges and Structures, Advice Note BA 16/97.* Department of Transport Highways Agency, London, UK.

Department of Transport (2001b): *The Assessment of Highway Bridges and Structures, Design Manual BD 21/01*, part of Design Manual for Roads and Bridges Volume 3, Section 4. Department of Transport Highways Agency, London, UK.

Gilbert, M. and Melbourne, C. (1994): Rigid-block analysis of masonry structures. The Structural Engineer, 72, 21, pp. 356-361.

Gilbert, M. (2001): RING: A 2D Rigid Block Analysis Program for Masonry Arch Bridges. Proc. 3rd International Arch Bridges Conference, Paris, pp. 109-118.

Gilbert, M. (2007): Limit analysis applied to masonry arch bridges: state-of-the-art and recent developments. Proc. 5th International Conference on Arch Bridges, Madeira, p 13-28.

Heyman, J. (1966): The Stone Skeleton. International Journal of Solids and Structures, vol. 2, p. 249-279.

Heyman, J. (1982): The Masonry Arch. Ellis Horwood Ltd, West Sussex, UK.

Heyman, J. (1995): The Stone Skeleton: Structural Engineering of Masonry Architecture. Cambridge University Press, Cambridge, UK

Hughes T.G., Hee S.C., Soms E. (2002): Mechanism analysis of single span masonry arch bridges using a spreadsheet. Proceedings of the Institution of Civil Engineers; Structures and Buildings, 152 (4) p. 341-350

ICE (2008): ICE Manual of Bridge Engineering, 2nd Edition. Thomas Telford Ltd., London, UK

LimitState Ltd. Ring Theory & Modeling Guide, Version 2.0k. Sheffield, UK

Livesley, R. (1978): Limit Analysis of Structures Formed from Rigid Blocks. International Journal for Numerical Methods in Engineering, 12: 1853–1871. doi: 10.1002/nme.1620121207

McKibbons, L., et. al. (2006): Masonry Arch Bridges: Condition Appraisal and Remedial Treatment. CIRIA C656, London, UK.

Mufti, A., Bakht, B., Jaeger, L (1996): Bridge Superstructures New Developments. National Book Foundation, Pakistan.

New York City Department of Records (1867-1938). Original construction and subsequent alteration plans for the Brooklyn Bridge. Microfilm.

Ochsendorf, J. (2006): The masonry arch on spreading supports. Structural Engineer, v 84, n 2, p. 29-35.

Page J. (1990): Assessment of Masonry Arch Bridges. Proceedings of the Institution of Highways and Transportation National Workshop, Leamington Spa, March 1990.

Page, J. (1993): State of the Art Review – Masonry Arch Bridges. Transportation Research Laboratory, Department of Transport, London, UK

Pippard, A.J.S., Tranter, E., and Chitty, L. (1937): The Mechanics of the Voussoir Arch. Institution of Civil Engineers - Journal, n 7, p 4-26.

Pippard, A.J.S. (1948): The Approximate Estimation of Safe Loads on Masonry Bridges. Civil Engineer in War, Vol. 1, The Institution of Civil Engineers, London, UK, p. 365-372.

Talebinejad I., Fischer C. and Ansari F. (2001): Simplified Technique for Remote Monitoring of Deflection in Arch Structures. *Journal of Experimental Techniques,* Accepted, 2011

Talebinejad I., Fischer C. and Ansari F. (2009): Serially Multiplexed FBG Accelerometer for Structural Health Monitoring of Bridges. *Journal of Smart Structures and Systems*, 5 (4), pp 345-356.

Wang, J. and Melbourne, C. (2010): Mechanics of MEXE Method for Masonry Arch Bridge Assessment. Proceedings of the Institution of Civil Engineers; Engineering and Computational Mechanics, 163 (3) p. 187-202.

VITA

NAME:	Chad Ryan Fischer
EDUCATION:	B.S., Civil Engineering, University of Illinois at Urbana-Champaign, 1999
	M.S., Civil Engineering, University of Illinois at Urbana-Champaign, 2000
PROFESSIONAL:	Senior Consultant, Engineering Systems Inc., Aurora, Illinois, 2001-2011
TEACHING/ RESEARCH:	US Army Corps of Engineers, Champaign, Illinois Research Assistant, 1999-2000
	University of Illinois at Urbana-Champaign, Illinois Teaching Assistant, 1999-2000
LICENSES:	Registered Structural Engineer (S.E.) State of Illinois, 081-006193
	Registered Professional Engineer (P.E.) State of Illinois, 062-057501 Comm. of Penn. PE075699 State of Indiana, PE10708865 State of Wisconsin, 38908 State of Michigan, 6201055349 State of South Carolina, 28727
HONORS:	ASCE 2003 New Face of Civil Engineering
	2002 ASCE New York State Council Outstanding Civil Engineering Achievement Award – "World Trade Center Disaster Site Recovery"
PROFESSIONAL MEMBERSHIP:	American Society of Civil Engineers (ASCE)
	National Council of Structural Engineers Association (NCSEA) -Structural Engineers Emergency Response (SEER) Committee Secretary
	Structural Engineers Association of Illinois (SEAOI)
	American Institute of Steel Construction (AISC)

International Society for Structural Health Monitoring of Intelligent Infrastructure (ISHMII)

PUBLICATIONS:

Talebinejad I., Fischer C. and Ansari F., "Numerical Evaluation of Vibration Based Methods for Damage Assessment of Cable Stayed Bridges", Journal of Computer-Aided Civil and Infrastructure Engineering, In Press, 26 (3), 2011

Talebinejad, I., Fischer, C., and Ansari, F. "Serially Multiplexed FBG Accelerometer for Structural Health Monitoring of Bridges." Smart Structures and Systems, Volume 5, Number 4, July 2009.

Talebinejad I., Fischer C. and Ansari F. "Low Frequency Fiber Optic Accelerometer for Civil Structural Health Monitoring." 16th SPIE Annual International Symposium on Smart Structures/NDE, San Diego, CA, March 9-12, 2009.

Talebinejad, I., Fischer, C., et. al. "Structural Health Monitoring of the Lingotto Cable-stayed Pedestrian Bridge with Optical Fiber Sensors." Proceedings of the Third International Conference on Structural Health Monitoring of Intelligent Infrastructure, Vancouver, British Columbia, Canada, November 13-16, 2007.

Zhang, G., Zhang, Z., and Fischer, C. "Structural Health Monitoring of a Long-span Cable-stayed Bridge." Journal of Intelligent Material Systems and Structures, Volume 18, August 2007

Morin, C.R., and Fischer, C.R. "Kansas City Hyatt Hotel Skywalk Collapse." Journal of Failure Analysis and Prevention, Volume 6(2), April 2006.

Fischer, C.R., and Wojnowski, D.A. "Roof Failure Due to Snow: The Implications of Improperly Applying Code Provisions." Forensic Engineering - Diagnosing Failures and Solving Problems, Proceedings of the 3rd International Conference on Forensic Engineering, London, UK, November 10-11, 2005.

Morin, C.R., and Fischer, C.R. "Historical Failures: Kansas City Hyatt Hotel Skywalk Collapse." Proceedings of the 2005 Materials Science & Technology (MS&T) Conference and Exhibition, Pittsburgh, PA, September 26, 2005

Kenner, M.T., Wilkinson, J.A., Fischer, C.R. "Effect of Boundary Conditions on the Modal Analysis of a Staircase." ABAQUS Users' Conference Proceedings, Boston, MA, May 2004.

Domel, Fischer, et. al. "SEERPlan Manual - Structural Engineers Emergency Response Plan." National Council of Structural Engineers Association, August 2003.

Wilcoski, J., Fischer, C., et. al. “Alternative Shear Panel Configurations for Light Wood Construction: Development, Seismic Performance, and Design Guidance.” Engineering and Research Development Center, ERDC/CERL TR-02-12, April 2002.